CZECH TECHNICAL UNIVERSITY IN PRAGUE

Faculty of Civil Engineering
Department of Concrete and Masonry Structures

Non-linear analysis of slender masonry structures

DOCTORAL THESIS

Marek Vokál

Doctoral study programme: Civil Engineering

Branch of study: Building and Structural Engineering

Doctoral thesis tutor: Prof. Ing. Alena Kohoutková, CSc., FEng.
Ing. Michal Drahorád, PhD.

Prague, 2022

Poděkování

Děkuji všem, kteří mi studium umožnili. Jedná se především rodinu, katedru Betonových a zděných konstrukcí, jejímž hlavním hrdinou je z pohledu tého práce Ing. Michal Drahorád, PhD. a firmu Pontex, spol. s r.o. Děkuji Tomáši Hejdovi a Petru Olšákovi za zpracování šablony pro závěrečné práce na ČVUT v prostředí LaTeX.

Declaration

I hereby declare that this doctoral thesis is my own work and effort written under the guidance of the tutors. All sources and other materials used have been quoted in the list of references.

In Prague, 1. March 2022

Abstract

This thesis focuses on ways of modelling of unreinforced slender masonry elements that are susceptible to loss of stability. An algorithm for assessment of slender masonry elements was proposed and implemented. The algorithm is based on a beam model with material and geometric non-linearity. The results of modelling are used for masonry arch bridges and slender masonry columns. There is a lack of literature and methods on the topic of assessment of existing structures using the input parameters that can be stated by the real diagnostic survey, i.e., the diagnostic survey that does not damage the structure too much and has adequate costs. The current literature is based on theoretical parameters, such as real tensile strength, real stress-strain diagram, biaxial stress diagram of material, fracture energy, etc. The proposed algorithm and the thesis, in general, are based on usually available input parameters; therefore, it also applies for the practical design of structures in accordance with the current standards. The thesis also comments on the approach of standards and proposes its improvements to be able to approximate the real behaviour of masonry elements. The assessment of slender columns is affected by the 3D effects, which the literature describes insufficiently. The design standards, for example, do not deal with columns subjected to biaxial bending. The algorithm consequently focuses on the columns loaded in 3D. In addition, in today's literature, there is no evaluation of the influence of the stress-strain diagram used on the behaviour of slender columns; no recommendations on use of the stress-strain diagram are given. At the ultimate limit state, the standards recommend only rigid-plastic check which has been in this thesis proven to be the most inadequate check among the compared checks. A case study of a set of columns of different slenderness is carried out, and the results are plotted; results of six various stress strain diagrams are compared. Also, a parametric study was carried out on a set of masonry vault bridges, and variable arch spans, rises, depths of backfill and others were compared. The sensitivity analysis of the input parameters of the vault bridges on the final load carrying capacity is carried out. Because the current standards minimally deal with the assessment of masonry arch bridges, the thesis also focuses on this topic.

Keywords: masonry, brick columns, no-tension material, slenderness, second-order analysis, vault bridge, backfill, non-linearity, load carrying capacity, bridge assessment, limit states, finite element analysis, historical heritage

Supervisor: Prof. Ing. Alena Kohoutková, CSc., FEng.
Thákurova 7,
166 29 Praha 6 - Dejvice

Abstrakt

Práce hodnotí a porovnává různé způsoby modelování nevyztužených štíhlých zděných konstrukcí, tedy konstrukcí náchylných na ztrátu stability. Byl navržen a implementován algoritmus pro posuzování štíhlých zděných konstrukcí. Jeho jádrem je prutový model s materiálově a geometricky nelineárním chováním. Výsledky výpočtů s tímto přístupem jsou použity pro hodnocení klenbových konstrukcí a zděných sloupů. U stávajících konstrukcí v současnosti chybí literatura a metody vycházející především ze vstupních parametrů, které je možné získat běžným diagnostickým průzkumem, aniž by byla konstrukce nadměrně poškozena nebo aniž by byly vyžadovány nepřiměřené náklady. Současná literatura vychází z teoretických parametrů, jako například tahová pevnost malty v konstrukci, skutečný pracovní diagram, pracovní diagram při dvouosém namáhání, lomovou energii materiálu a podobně. Algoritmus a přístup této práce vychází pouze z dostupných parametrů, díky tomu může sloužit i pro praktické návrhy a posouzení, které podléhají soustavě norem. Z tohoto důvodu se tato práce kromě navrhovaného přístupu maximálně snaží přístup norem objektivně zhodnotit a podat návrhy pro jejich zlepšení. Z hlediska štíhlých sloupů vstupují do výpočtu i prostorové 3D účinky, které jsou v dnešní literatuře postiženy nedostatečně. Současná norma kupříkladu sloupy zatížené ve dvou rovinách (obecně ve 3D) vůbec neřeší, proto se algoritmus pro řešení sloupů soustředí zejména na tuto problematiku. Rovněž se v dnešní literatuře nikde nevyskytuje hodnocení vlivu užitého pracovního diagramu na chování štíhlých sloupů a doporučení, který pracovní diagram použít. Norma uvádí v mezním stavu únosnosti pouze posudek s pracovním diagramem tuho-plastickým, který je v této práci ukázán jako nejméně vhodný. V této práci byla provedena parametrická studie sloupů o různých štíhlostech a výsledky jsou prezentovány v grafech, dále byla provedena studie vlivu šesti různých pracovních diagramů na chování štíhlých sloupů. Stejně tak bylo analyzováno chování klenbových zděných mostů různých rozpětí, tlouštěk násypu a dalších parametrech. Byla provedena citlivostní analýza vlivu jednotlivých vstupních parametrů na výslednou zatížitelnost klenbových mostů. Protože se normy jen minimálně zabývají posouzením zděných mostů, byly v práci řešeny i způsoby posouzení zděných mostů.

Klíčová slova: zděné konstrukce, sloup, materiál bez tahové pevnosti, štíhlost, výpočet podle teorie 2. řádu, klenbový most, násyp, nelinearita, zatížitelnost, hodnocení mostu, mezní stavy, metoda konečných prvků, kulturní památka

Překlad názvu: Nelineární analýza štíhlých zděných konstrukčních prvků

Kontakt: marek.vokal@gmail.com

iii

Contents

Figures

vii

ix

x

Tables

Part I

Introduction and goals

▋ State of the art

The state of the art is divided into four parts. Material behaviour and properties see in Section 1.1, methods of analysing the columns in 2D see in Section 3.2, the columns in 3D see in Section 4.2 and the methods of analysing vaults see in Section 6.

▋ General introduction

The masonry elements connected by the mortar is one of the oldest building materials. Many historic buildings, listed as a cultural heritage, are still in use. Bridges usually carry much more load than at the time of their design. The traffic load is still increasing. For this reason, we must still analyse the historic structures and the behaviour of the historic masonry. Proper assessment of structures is one of the principles of sustainable development and has an impact on the economics of construction; the portion of masonry structures is large. The primary usage of masonry is for compressed members. Real masonry structures are always also loaded by imperfections or some lateral load. Hence, the structures are loaded by a combination of normal compressive force and bending moment (except for some special cases, such as infill walls). For the case of a slender member, the slenderness of the member plays an important role. The behaviour of the structure is impacted in several ways: geometric and material non-linearity.

This thesis aims to describe the behaviour of slender masonry unreinforced elements, implement a new method for handling the slender masonry elements, offer existing calculation methods, compare its results, show its advantages and disadvantages, and recommend the real-time ways for assessing the slender masonry structures. The methods used are reliable but "simple" and not complex too much - the 3D solid elements with non-linear behaviour representing each masonry unit and mortar separately, taking into account moisture, climatic effects, and construction stages (time-depending analysis) are not used in this thesis. For the case of assessing the existing structures, homogenization approaches validated with small-scale tests and engineering judgement must provide sufficient and reliable input data for the models without the need for large-scale destructive experiments, which are not feasible. The chosen material model is in this thesis considered homogenized because the detailed micro-modelling demands input parameters which are almost impossible to obtain in the case of existing structures. This thesis concentrates on methods that do not require theoretical parameters such as the real tensile strength of the structure, the real stress-strain diagram, the biaxial stress diagram of the material, and the fracture energy. These parameters cannot be stated by the diagnostic survey with the required precision and the complex analysis is therefore impracticable.

The study of a set of certain structures is presented to show the importance of dealing with several input parameters. Finally, recommendations are given for the calculations and scope of the work of a diagnostic survey.

The newly proposed simplified method uses beam elements considering both material and geometric non-linearity. Therefore, it includes all the impacts of the behaviour of slender masonry columns and offers a sufficient realistic simulation for the majority of vault bridges.

In most cases, the material behaviour is considered non-linear, mainly because of the very limited tensile strength of the masonry. In this thesis, the zero tensile strength is considered. In compression, mostly the linear behaviour is assumed. The impact of considering six various stress-strain diagrams is also shown.

The thesis is divided into two parts. In the first one, the columns are handled. In the second one, vaults are analysed.

Masonry columns

At first, the 2D column problem is handled, the importance of considering both geometrical and material non-linearity is shown. For example, the method specified in the current standard [PL07] fails and leads to an overestimation of the impact of the stability problem (leading to conservative results). This thesis aims to analyse the real behaviour of slender masonry columns under compression and to develop the simplified method for their design and assessment, which can also be used in accordance with the applicable standards; this simplified method was developed using a MATLAB® algorithm that takes into account the phenomena mentioned above: the material and geometric non-linearity.

Then, the solution to the 2D problem was extended to the solution of the 3D problem. The motivation is to address the realistic three-dimensional aspects of the problem which is not described sufficiently in the literature and the standard omits it completely. Recently designed masonry structures are, considering their arrangement and resistance, usually designed as a wall, which strongly emphasize the existing standards (especially [PL07]). This standard is conservative and assumes the rigid-plastic stress-strain diagram which is shown to be unreal.

The algorithm implemented uses non-linear beam elements. Six various stress-strain diagrams for the behaviour of masonry in compression were implemented; impact of the stress-strain diagram used is shown. The study of a set of columns of various heights was carried out and the results were compared. Then, the results of the experiment were taken from other authors; these results were compared with the result of modelling. The results are also compared to different calculation methods and current standards.

The choice of stress-strain diagram, use of material and geometric non-linearity are shown to have a high impact on the resulting behaviour.

Masonry vaults

The main motivation is to provide "simple", robust, and reliable methods that can be used also for practical design and require only the parameters that can be obtained. This thesis also compares available methods and shows the main disadvantages of the most commonly used model - the linear beam model which is unreal and mainly conservative. See the motivation for the analysis also in Section 5.

In this part, the new method is described (using non-linear beam elements). The results are compared with other methods: the linear method using beam elements, planar

elements with linear and non-linear behaviour, and equilibrium of rigid slabs were used. The comparison was made for a set of masonry arch bridges of various spans, the height of the backfill, and other input parameters. The results of the modelling were calibrated and compared to the in-situ tests of the Legion Bridge; where the static load test was performed, and the comparison with the original static analysis (graphical method) was also carried out. The sensitivity of the input parameters for calculating the load carrying capacity of the masonry arch bridges is carried out.

Mainly the 2D case of vaults is handled which is sufficient for the overwhelming majority of vault bridges. The vault bridges that are skew such that the skewness must be handled see in [oR17] and [FSB17].

As an example of the use of the mentioned methods, the Cheb Bridge in Karlovy Vary was assessed in detail. A diagnostic survey was used as a basis for assessing the load carrying capacity (as well as for the case of the Legion Bridge).

Part II

Masonry - Material properties, behaviour and methods of assessment

Chapter 1

Material behaviour and properties

1.1 Material modelling - State of the art

Masonry is highly heterogeneous, anisotropic material with a strongly non-linear constitutive response. The development of accurate and efficient numerical procedures to study masonry structural response is still a challenging task related to the assessment of the safety and reliability of masonry structures, especially the old ones. Although detailed material modelling is not the focal point of this thesis, a basic overview of masonry modelling methods is provided.

The basic approaches of material modelling are taken from the article [Lou13]:

- Detailed micro-modelling in which units and mortar in the joints are represented by continuum elements whereas the unit-mortar interface is represented by discontinuous elements,

- simplified micro-modelling in which expanded units are represented by continuum elements whereas the behaviour of the mortar joints and unit-mortar interface is lumped in discontinuous elements,

- macro-modelling in which units, mortar and the unit-mortar interfaces are smeared out in a homogeneous continuum.

The way of detailed micro-modelling is described, for example, in [RKR$^+$19]. The simplified micro-modelling is explained, for example, in [Esh57], where the close-form solution for the problem of ellipsoidal inhomogeneity within an infinite matrix is shown. The model of article [BRR99] relies upon the exact solution after Eshelby and describes brickwork as a mortar matrix with insertions of elliptic cylinder-shaped bricks. For an example of the masonry arch bridge modelling, the paper [PeD07] can be referred. The micro-modelling method requires a high computational effort; thus, it is typically adopted for simple masonry elements, for the masonry non-linearity, local response, and details. For this reason were, for example of the thesis [Boe15], all the implemented materials assumed to be homogeneous and isotropic and a Smear Crack, even when modelling the reinforcement of the masonry. The simple element (wall of dimensions $67.5 \times 55 \times 10$ cm) was examined experimentally and mathematically for example in [SAS17], or [MLGB13] (element of dimensions $120 \times 120 \times 70$ cm). Micro-modelling is not discussed in this thesis.

The methodology of mesoscale modelling is described, for example, in [MI11], further experiments were carried out in the article [CMAI18]. In this approach, the mortar and brick–mortar interfaces are modelled by 2D 16-noded zero-thickness non-linear interface elements. Elastic solid elements represent the masonry units. The data-fitting is done by minimising a functional representing the discrepancy between experimental and numerical data. In the article [SSZ$^+$08] two specific approaches to the derivation of macroscopic (effective) fracture energy needed in full-scale macroscopic simulations were examined. The first approach exploits the well-known elements of the first-order homogenization in conjunction with the statistically equivalent periodic unit cell, while the second approach draws on the numerical representation of standard laboratory tests proposed for the determination of size-independent fracture energy for quasi-brittle materials, including concrete and masonry structures. A comparison of the results suggests good agreement between individual approaches.

For the purpose of analysis and the structural design, the material in this thesis is homogenized appropriately to preserve its properties in relation to the real behaviour of the structure modelled. The method of Eurocode is used (see [PL07]) which is according to [MLT06] called "yield line theory" and it is based on laboratory tests (e.g. [GDE85] and [SMC95]) conducted on the brick masonry walls subjected to lateral loads, showing that failure takes place along a well-defined pattern of lines. Other homogenization techniques are described in the paper [LMTZ07] which addresses many different homogenization methods available in the literature, showing their advantages and disadvantages. The strategy employed in [ZNSS08] is based on the well-established first-order homogenization schemes, e.g. [Ant95]. In the article [ZNSS08], which concentrates on the Charles Bridge in Prague, the non-linear mechanical behaviour of the masonry was modelled using the CC3DNonLinCementitious plastic-fracturing constitutive model available in ATENA 3D. According to article [ZNSS08], computational homogenization approaches, when carefully validated with small-scale tests and engineering judgement, can provide a reasonable procedure for feeding material models with reliable data without a need for large-scale destructive experiments. In the thesis [Laf17], special modelling of replacing the damaged stone units of Charles Bridge is done using both micro modelling and homogeneous model.

1.2 Compressive strength of masonry - State of the art

There are many possibilities of calculating the strength of masonry from the strength of masonry units and mortar. The authors of [PG09] presents a list of 34 models for the maximum masonry compression strength ("most models are based on simple empirical investigations and are usually strongly related to the special conditions of the investigated masonry type").

The publication [Ohl86] proposed an approach adopted also by [oR11]; the strength can be calculated as follows:

$$f_k = 0.5 f_m + \frac{a.f_b - f_m}{2 + \frac{b.h_f f_b}{2 h_s R_{st}}}, \tag{1.1}$$

where:

- h_f is the thickness of the joint,

- h_s is the thickness of the masonry unit,

- a, b are coefficients according to Table 9, source [oR11].

The model according to DIN 1053-1 (1996) and DIN 1053-100 (2004) has a simple application since only two tables have to be used (see the tables, for example, in [PG09]).

The method of current standard [PL07] comes out of the group of models called "Empirical exponential models", see the following section.

■ 1.3 Compressive strength of masonry - used equations

The methods used in this thesis can be used independently of any standard; in order to illustrate and demonstrate the examples and because of the comparison with other bridges, current standards are used and the following formula is used for the characteristic compressive strength of the masonry in acceptance with Eurocodes [PL07]:

$$f_k = K_z f_b^{\alpha_m} f_m^{\beta}, \tag{1.2}$$

where:

- f_k is the characteristic compressive strength of the masonry,

- K_z is coefficient depending on the masonry type and elements, for the cases in this thesis equals 0.45 (see Tab 3.3 of [PL07]; in this thesis are used clay and natural stone masonry units),

- α_m is coefficient depending on the type of joints and mortar, for the cases in this thesis equals 0.7 (unreinforced masonry, general purpose mortar),

- β is coefficient depending on the type of the mortar and composition, for the cases in this thesis equals 0.3 (general purpose mortar),

- f_b average normalised compressive strength of the masonry units,

- f_m average compressive strength of the masonry mortar; the minimal value of f_m is 0.1 MPa according to [ÚN14].

The design compressive strength is calculated as follows (according to [ÚN05c] and [PL07]):

$$f_d = \frac{f_k}{\gamma_M}. \tag{1.3}$$

γ_M can be according to [ÚN14] calculated as:

$$\gamma_M = \gamma_{M1}\gamma_{M2}\gamma_{M3}\gamma_{M4}, \tag{1.4}$$

where:

11

- γ_M – partial safety factor of the masonry, can be stated according to previous equation or paragraph 2.4.3 of [PL07],
- γ_{M1} – constant coefficient - the basic value of the safety factor is 2 (for the case of clay masonry units with general purpose mortar; in other cases, it should be assessed individually depending on the way of obtaining the material characteristics),
- γ_{M2} – constant coefficient to take into account the level of brickwork; $0.85 \leq \gamma_{M2} \leq 1.2$; value 0.85 is for masonry with perfect brickwork,
- γ_{M3} – constant coefficient for the consideration of moisture of the masonry; $1 \leq \gamma_{M3} \leq 1.2$; value 1 is for dry masonry,
- γ_{M4} – constant coefficient for the considering cracks in the masonry; $1 \leq \gamma_{M4} \leq 1.4$; value 1 is for masonry without cracks.

The values of these coefficients can be seen in [ÚN14]. See the example of assessing γ_M coefficient in Section 11.2.3.

The stress-strain diagrams, which are considered in this thesis, are given in following Section 1.6.1, and 2.

1.4 Shear strength of masonry

The shear strength consists of two components: initial shear strength under zero compressive stress and a contribution due to the design normal stress multiplied by the coefficient of friction (Mohr-Coulomb failure criterion). This is expressed by Eq. 2.2.

1.5 Tensile strength of masonry

The tensile strength of masonry is in this thesis considered zero. See the details in Section 1.6.1. See the discussion on this topic and the literature review for the case of vault bridges in Section 5.

1.6 Deformation properties of masonry

1.6.1 Stress-strain relationship

Masonry is in this thesis considered a homogeneous material. It is assumed that the dimensions of the masonry elements and the joints between them do not significantly affect the distribution of stress in a masonry member. The check of the structure is then carried out only in the weakest cross section, i.e., in the joints of the brickwork. It is assumed that if the structure fulfils the verification in the joints, it fulfils the verification in all other cross sections.

The real stress-strain diagram of masonry in compression, as can be seen in [MGF14], shows a non-linear behaviour, see also Figure 1.1.

Figure 1.1: Stress-strain diagram of masonry in compression – experiments and curves which try to fit it.

The stress-strain diagrams were described, for example, by Hendry and Khalaf [HK01], Augenti and Parisi [AP10]. In Figure 1.1, Sargin's curve describing concrete behaviour is also displayed according to [Sar71].

The behaviour of masonry columns considering various stress-strain diagrams was studied in Section 4.3.5; six used diagrams see in Fig. 4.7.

This thesis assumes that the material reacts only to the pressure, and tensile stress leads to cracking and its opening. This is illustrated by Figure 1.2. If subsequently (e.g., in another load combination) the tensile stress in the cross section vanishes, the cracks will close, and the cross section will act as complete again. Other authors often chose the same approach; the no-tension material with the linear stress-strain law for compression is used, for example, in [TB77], [FF80], and [LLM93].
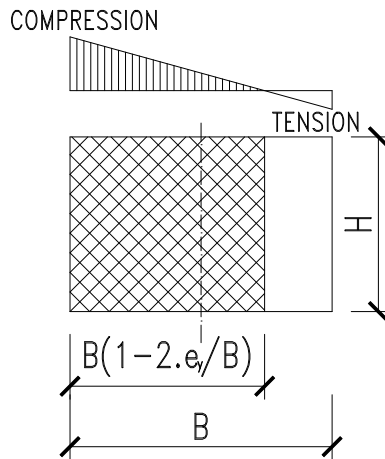
Figure 1.2: Changes of cross section properties in dependence on load.

Idealized stress-strain diagrams of the material for the individual limit states in accordance with [PL07] are shown in Section 2. Stress-strain diagrams are considered linear (at the SLS – serviceability limit state), or linearly-plastic (at the ULS - ultimate limit state). See more possibilities of diagrams in Section 4.3.5.

13

1.6.2 Modulus of elasticity

In this thesis, the modulus of elasticity is mostly considered $E = K_E f_k$, where K_E has a recommended value 1000 according to [PL07]. For the case that the existing structure was assessed and the diagnostic survey was available (such as the case of the Legion Bridge; Section 10.3.3), the modulus of elasticity of the masonry units was taken from the tests. According to [oR17], the modulus of elasticity of masonry is lower due to the fact that the modulus of elasticity of masonry units is combined with the impact of the mortar:

$$E_{cm} = 5000 + 300 f_b. \tag{1.5}$$

The example of use of this equation see in Section 11.2.5.

1.6.3 Shear modulus

According to [PL07], the shear modulus, G, can be taken as 40 % of the elastic modulus. This approach is adopted in this thesis.

Chapter 2

Limit states – methods of assessment

A limit state is a condition of a structure beyond which it no longer meets the relevant design criteria. In Europe, the limit state design is enforced by the Eurocodes. For this reason, the limit state criteria are in this thesis used to assess the masonry structures. Furthermore, the applicability of these criteria is also discussed.

2.1 Ultimate limit state

At the ultimate limit state (ULS), the behaviour of the structure just before the collapse is investigated. The load factors according to the appropriate standard (EN 1990 - [ÚN05b]) are considered for the determination of the bearing capacity. Generally, plastic hinges are assumed to be fully developed in the structure. The main assumption of the calculation is that the function of strain is linear (plane sections remain plane). The second assumption is that the stress in the cross-section is derived from the stress-strain diagram. The details on masonry arch bridges behaviour see also in [Dra13] and [VD18]. The resistances for axial and shear forces at the ULS can be written according to [PL07] as:

$$N_u = N_{Ed} \leq N_{Rd} = f_d B \left(H - 2e_u \right), \tag{2.1}$$

$$V_{Ed} \leq V_{Rd} = \left(f_{vk0} H + 0.4 \sigma_d \left(H - 2e_u \right) \right) B / \gamma_M, \tag{2.2}$$

where:

- f_d is the design strength of the masonry in compression, calculated according to Equation 1.3,
- f_{vk0} is the characteristic value of the initial shear strength at normal stress equal to 0,
- B, H is the width or height of the cross section, respectively,
- e_u is the eccentricity of the resultant axial force in the cross section at the ultimate limit state; $e_u = M_{Ed}/N_{Ed}$,
- σ_d is the design compressive stress in the compressed area at the ultimate limit state (uniformly distributed, see Figure 2.1),

- ▪ 0.4 is the coefficient of friction in the masonry joint, in this thesis denoted μ, see the study on this parameter in Section 7.2.2 and 8.2.3,
- ▪ γ_M is the factor of the material according to Equation 1.4,
- ▪ $N_u = N_{Ed}$ is the design value of applied normal force,
- ▪ N_{Rd} is the design normal resistance force,
- ▪ V_{Ed} is the design value of applied shear force,
- ▪ V_{Rd} is the design shear resistance force,
- ▪ M_{Ed} is the design value of applied bending moment.
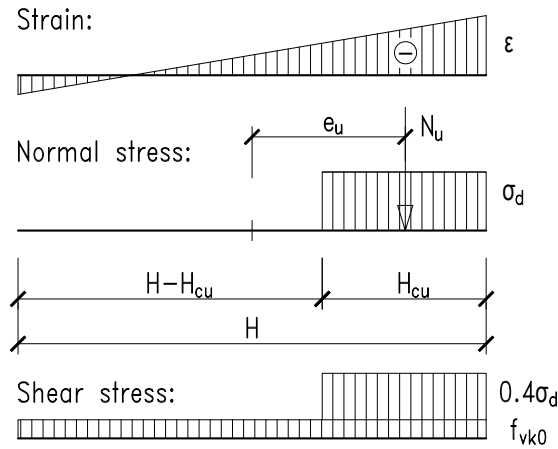
Figure 2.1: Stress distribution of the masonry cross section at the ultimate limit state.

2.2 Serviceability limit state

The serviceability limit state (SLS) describes the behaviour of the structure under ordinary operating conditions. Fulfilling the requirements of the serviceability limit state provides the required properties and behaviour of the structure throughout its lifetime. In terms of the serviceability limit state, crack width and structural stress under operating load are verified (load factor equals to 1.0). In terms of vault structure verification, it is necessary to verify the maximum axial stress in the cross section and the height of the compressed area of the cross section (see [HD08] and [PL07]). The elastic behaviour of the structure is considered with a linear distribution of axial stress in the compressed area of the cross section. The tensioned part of the section is excluded for stress determination (see Figure 2.2).

$$\sigma_{n,max} = \frac{N_{Ek}}{3B\left(H - 2e\right)} \leq 0.45 f_k \tag{2.3}$$

$$H_c \geq \frac{H}{2} \longrightarrow e \leq \frac{H}{3} \tag{2.4}$$
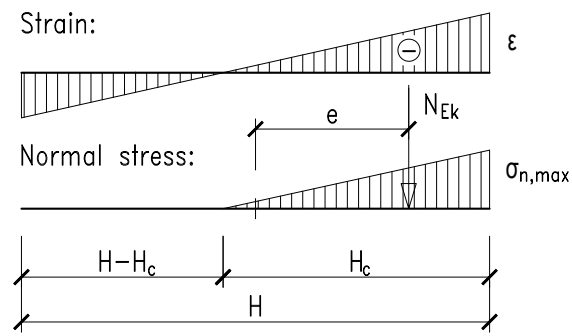
Figure 2.2: Stress distribution of the masonry cross section at the serviceability limit state.

$$e = \frac{M_{Ek}}{N_{Ek}} \tag{2.5}$$

where:

- M_{Ek} is the characteristic value of applied bending moment,
- N_{Ek} is the characteristic value of applied normal force.

See the graphical expression of the criteria of limit states in Figure 8.1.

Part III

Slender columns

Chapter 3

Slender masonry columns in 2D

The content of this chapter is taken mainly from the article [VD17].

3.1 Introduction

Stability analysis is one of the most studied problems in civil engineering. One reason is that the research is quite complex due to the many phenomena that need to be included. For example, the method specified in [PL07] fails and leads to an overestimation of the impact of the stability problem (leads to conservative results).

Recently proposed masonry structures are, considering their arrangement and resistance, usually designed as a wall, which strongly emphasizes the existing standards (especially [PL07]). However, this is insufficient for the slender masonry column because the behaviour of a wall is quite different to the behaviour of the column. See the discussion on this topic also in Section 4.1. The standard also does not take into account the impact of masonry elements composition regarding the structures constructed before the acceptance of EN.

The current research aims to analyse the real behaviour of slender masonry columns under compression and to develop the simplified methods for their design and verification in combination with the applicable technical regulations. Accurate modelling methods have to consider the non-linear stress-strain diagram of masonry, changes in the cross section characteristics due to the development of cracks, and the geometric non-linearity of the problem. Only one non-linearity was considered in the analysis in the first analysis methods, e.g., the linear stress-strain diagram in compression with zero tensile strength. Today, the most common option is modelling using the finite element method. There are many other methods, see Section 3.2.

The object of this chapter is to develop a MATLAB® algorithm that takes into account the phenomena mentioned above, i.e., the material and geometric non-linearity, including changing the centroid position and mechanical properties of the structure due to the development of the cracks. The prismatic beam loaded in the plane of the main inertia is considered in the analysis.

3.2   Methods of modelling - state of the art

One of the main analysis assumptions is the assumption of the chosen material model. See this topic in Section 3.3.2.

This section lists the methods of the load-bearing capacity assessment of unreinforced masonry columns (such as the buckling load).

3.2.1   Analytical solutions

Stability analysis of a theoretically straight column with linear behaviour

Euler's critical load for the theoretically straight column:

$$F_{cr} = \frac{\pi^2 EI}{L_{cr}^2},$$ (3.1)

where:

- F_{cr} – is critical load, for which the column buckles,

- EI – is bending stiffness,

- L_{cr} – is critical length.

The critical length depends on the boundary conditions - see Fig. 3.1. For the masonry column, only full restraint or free end boundary conditions are applicable.
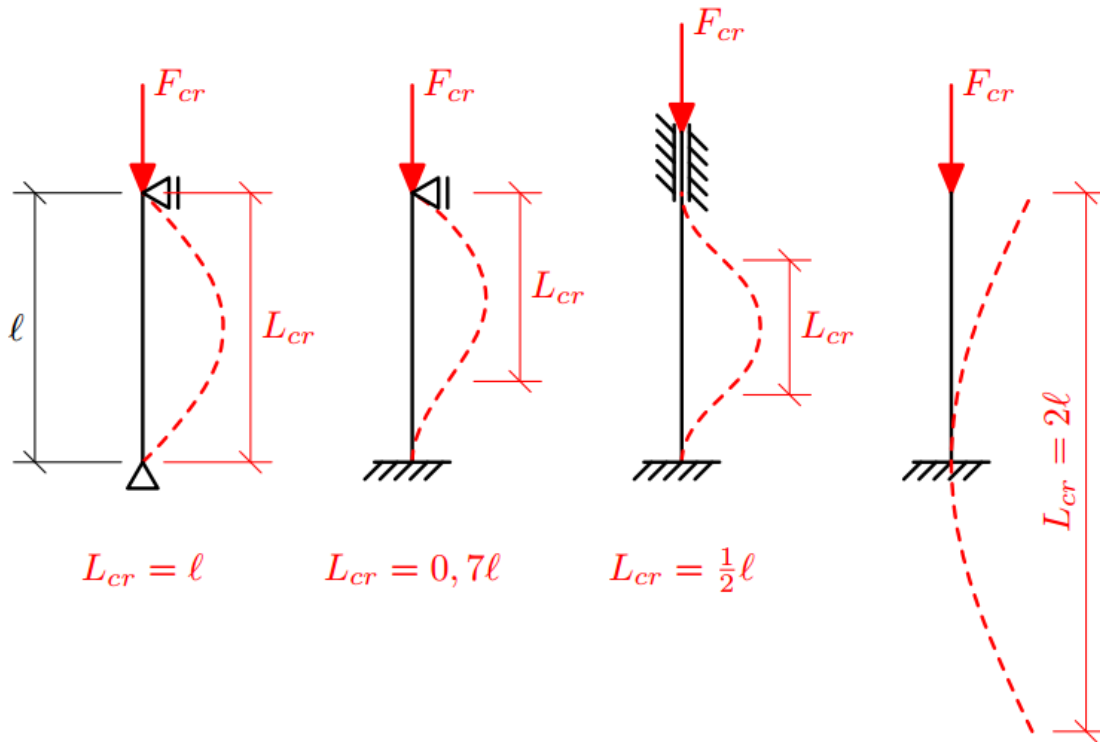
Figure 3.1: Buckling shapes and critical lengths for various boundary conditions.

In the algorithm, the buckling shapes according to Fig. 3.1 are used in the form of the prescribed initial shape of a column (called initial imperfection); see below.

■ Stability analysis of beam with initial imperfections with linear behaviour

The model geometry is based on the real layout and dimensions of the analysed structure. A crucial input data is the maximum estimated value of the initial imperfection of the structure, which is defined by the principles which are set out in [fS07] by:

$$e_0 = max(L/450; H/30; 20)mm, \tag{3.2}$$

where:

- e_0 – maximal initial displacement,
- H – is width of cross section in the direction of buckling and
- L – is effective length, for beam column it is the distance of supports in the analysed direction.

The maximal imperfection values are derived from the standard [ifs95], which is applicable for the design of new structures. For the case of existing structures, the shape and values of maximal imperfections should be measured in-situ. The initial shape of the structure (imperfection) is determined on the basis of the expected buckling shape. Given the nature

23

of masonry as a material with relatively small strength, the buckling shape is considered sinusoidal or part of the sine function in any "span" of a column, i.e., between the supports. The functions used for the approximation of the initial shape of the structure are shown in Fig. 3.2. In the case of unequal length of "spans", approximation functions have to be selected individually for each "span" (there is also a condition that the derivative of shapes of imperfect beam axis is continuous).
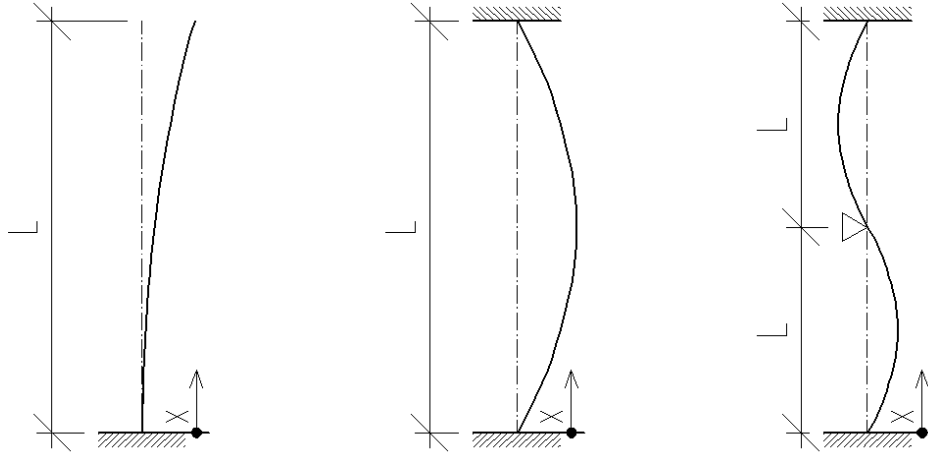
Figure 3.2: Initial shape of the imperfect column. Left: cantilever beam, middle: simply supported beam, right: the beam which is supported on both sides by hinges and has a hinge support in the middle of height.

The function of initial imperfection y_0 can be for the middle and right parts of Figure 3.2 described as:

$$y_0 = e_0 sin\left(\pi x/L\right), \tag{3.3}$$

the left part of the figure (the cantilever beam) can be described by the equation:

$$y_0 = e_0 sin\left(\pi/2 + \frac{\pi x}{L}\right)/2 + e_0/2. \tag{3.4}$$

The general equations for the solution used for the algorithm presented are the same as in the 3D case; see Section 4.3.3.

▪ Stability of a column with material non-linear behaviour

Most analytical simulations are based on the solution to the governing differential equation derived with reference to the cracked [Yok71] or the partially cracked member [CA72]. Mainly, the beam model is used.

The method of calculation of axial and bending tangent stiffness properties for an un-cracked and cracked masonry section with parabolic stress–strain law in compression was proposed by [SR84].

■ 3.2.2 Numerical solutions

The solution of the differential equation at the deformed state of the masonry member see in [Kyu01] for an example of a cantilever beam element. The author used the numerical integration procedure - Butcher's fifth-order Runge–Kutta method.

In the article [Mur08], the integro-differential problem has been formulated and solved numerically with the finite difference method (FDM). The precision of the finite difference results is assessed by comparison with the results obtained using of the 4th-order Runge–Kutta method and the Collocation method.

A comprehensive finite element model was presented for the combined material, and geometric non-linear analysis of slender unreinforced masonry walls in [LSS04]. The material tensile strength is considered; an exponential stress-strain relationship is adopted for the compressive region, and its smooth linear extension is used for the tensile area. The numerical results were compared with the experimental results and with the analytical results in published technical papers.

The arc length method is a powerful numerical technique for solving systems of non-linear equations. This technique was used in [MSS05].

■ 3.3 Material properties

■ 3.3.1 In general

Masonry as a construction material is highly heterogeneous, consisting of separate masonry elements (bricks, blocks, etc.) and joints filled with a binder (mortar) usually of significantly lower strength and stiffness. The lower strength and stiffness of the mortar ensure a uniform transfer of a load between the masonry units, even in places of local stress concentrations (i.e., where the asperity or roughness of the masonry elements occurs). High mortar strength and stiffness increase the strength of the entire composite material. Still, in areas of local asperities or roughness, undesired crushing of masonry elements would occur with a consequent risk of failures.

■ 3.3.2 Masonry material model

In practical terms, a 3D discrete element model of the structure, which considers the individual elements and their behaviour, is unusable, particularly with regard to the complicated determination of the input data, its calculation, and evaluation of the result. Therefore, for analysis and the structural design, the material is usually homogenized appropriately to preserve its properties concerning the real behaviour of the modelled structure. A consistent approach is chosen in this study. Masonry is considered a homogeneous or homogenized material. See also Section 1.

3.4 Mechanical modelling of masonry columns

The above-described material model causes significant changes in geometry and stiffness of the structure being modelled depending on the applied load. The widening of the cracks in the masonry and the geometrical non-linearities leads to non-linear solution of the whole problem. The principle of modelling of cross sections and individual elements, changes in the stiffness and the geometry of the structure caused by the applied load are shown in Fig. 3.3 and 1.2. It may be seen that tension in the part of the cross section makes this part excluded (see also 1). As a result, the cross section area decreases and the centroid moves; the move of centroid is denoted δ, its unit is [m]. The move δ of the centroid has a positive effect on the load eccentricity (the bending moment decreases). Still, the cross section is getting smaller, which has a negative impact on the stresses (the stress increases).
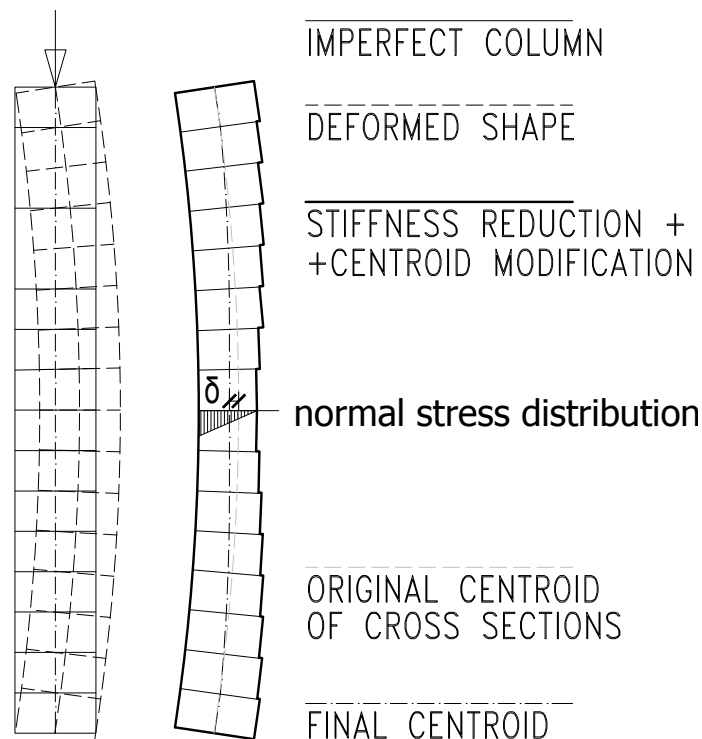
Figure 3.3: Changes of cross section and geometry of structure due to excluding the tensioned parts.

3.4.1 The method of calculation - MVo code (see also Section 4.3.3)

1. **First step**

   a. Dividing of the column to partial beam elements, calculate their stiffness.

   b. Elastic analysis with the full cross section.

   c. Calculation of stresses in the cross section of each element and determining whether the excluding of the tensioned part of the cross section executes, or the cross section remains full.

   d. Calculation of the matrix "prop" – the matrix of the height, the area, the moment of inertia, and the stiffness of the cross section in each step of the calculation.

2. **Second and every other step**

   a. Calculation of δ - move of a cross section of each element (from matrix "prop" from the last step).

   b. Calculation of matrix K (global stiffness matrix) with the new cross section properties and changed geometry.

   c. Calculation of matrix K_G (global geometric stiffness matrix).

   d. Calculation of vector r_d (vector of displacement) with changed geometry and new matrix K.

   e. Calculation of stresses in the new cross section and determination, whether the new cross section becomes even smaller or it grows bigger again.

   f. Filling of the matrix "prop".

   g. Checking the condition of convergence – see Equation 4.19.

■ 3.5 Example 1

The column hinged on both sides with the square cross section $B \times H = 0.4 \times 0.4$ m with the height of 4.2 m was chosen. Its initial imperfect shape was chosen according to Section 3.2.1, initially inclined right. The axial load on the column was 770 kN and the bending moments at both ends 39 kNm. These moments were chosen so that they enlarge the moment from imperfection. The final deflection and internal forces can be seen in Fig. 3.4: Left top - final shape and lateral deflection (see also Fig. 3.5), right top – lateral deflection of the middle of the column in each step of the calculation, left bottom – shear force in the final step, right bottom – the bending moment in the last step. In Fig. 3.6 can be seen the final shape of column (function of thickness H) when excluding the tensioned zones. All this is for the case that cross section reduces, and the calculation converges to equilibrium.
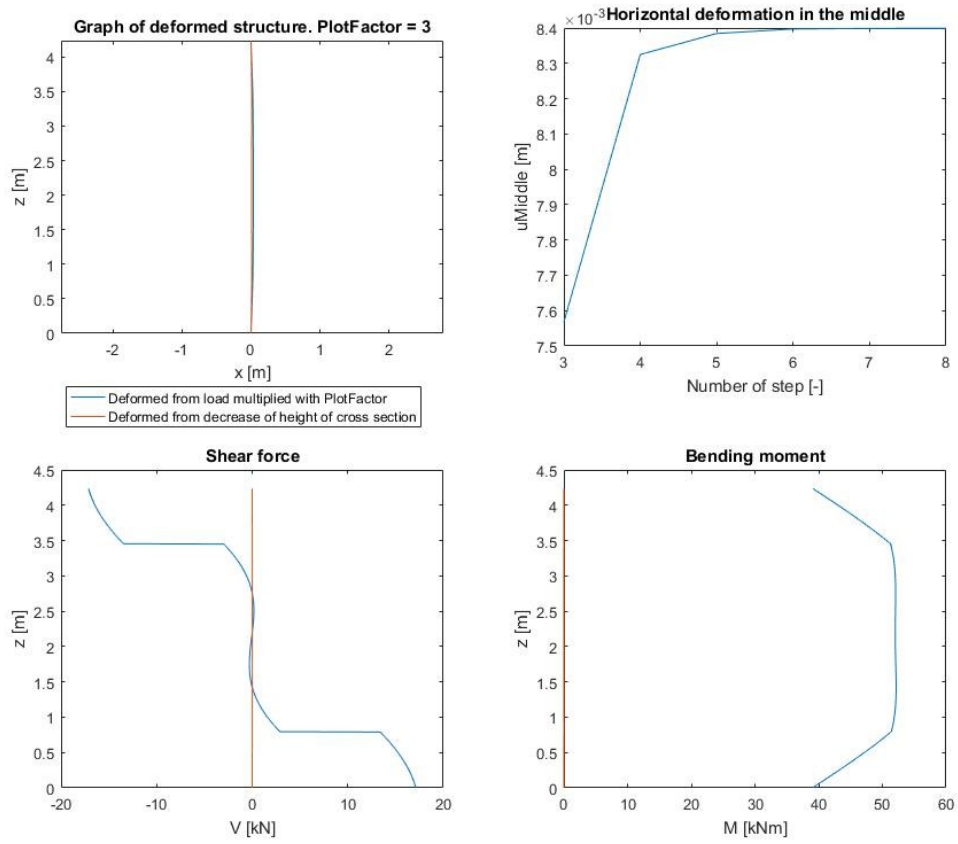
Figure 3.4: The results of modelling - Example 1.
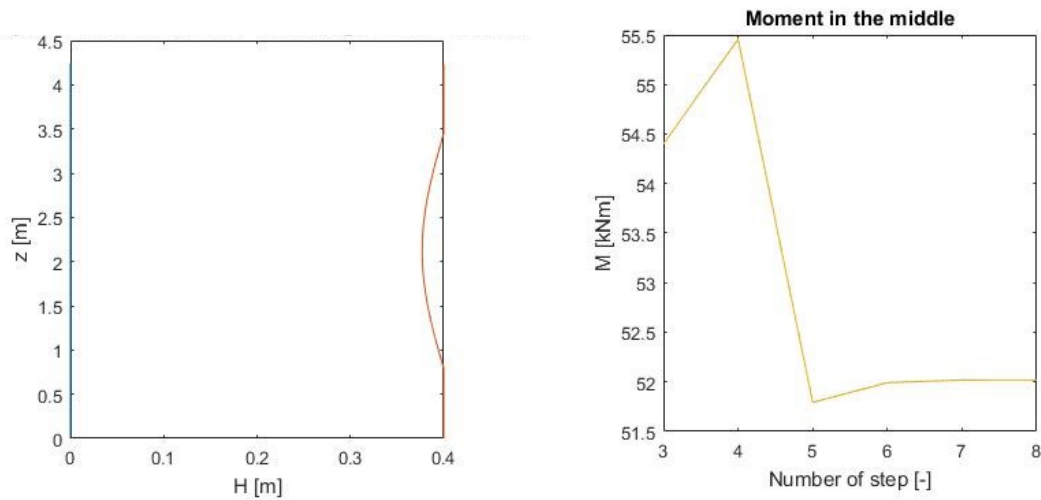
(a) : The final height of the cross section at the final step.

(b) : The bending moment in the middle of the height of the column in each step of calculation.

Figure 3.6: The results for the case that the cross section reduces and the calculation converges to equilibrium.
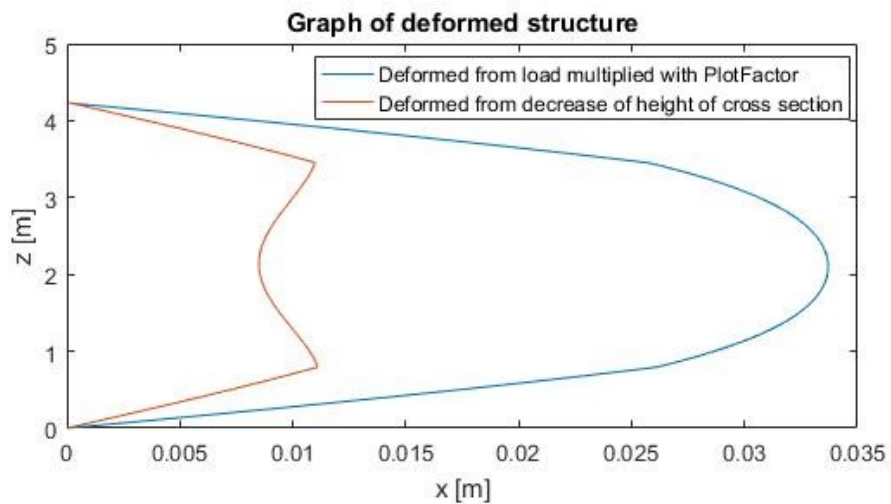
Figure 3.5: The final shape of central line and lateral deflection of this structure, non-proportional plot. The results for the case that cross section reduces and the calculation converge to equilibrium.

The load in the above example was chosen to show the impact of the material non-linearity. If the load is higher than the critical load, the lateral deflection grows excessively large. In such a case, the calculation stops after a few steps; see Figure 3.7.

29
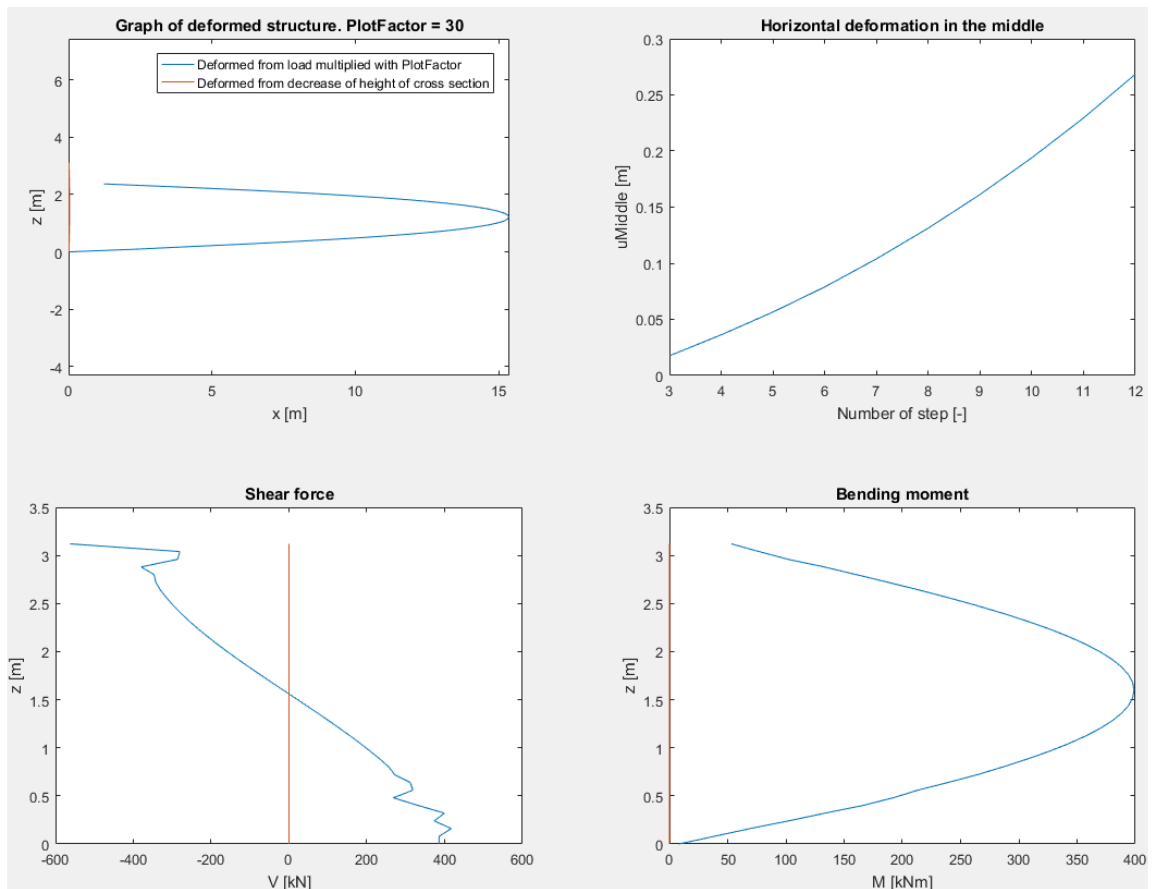
Figure 3.7: Lateral deflection of the middle of the column in each calculation step. The results are shown for the case that the cross section is reduced and the calculation did not converge.

The last possible case is that the column cross section does not reduce because the tension did not occur. So the calculation is carried out only with the assumption of the linear behaviour of the material. The result can be seen in Figure 3.8.
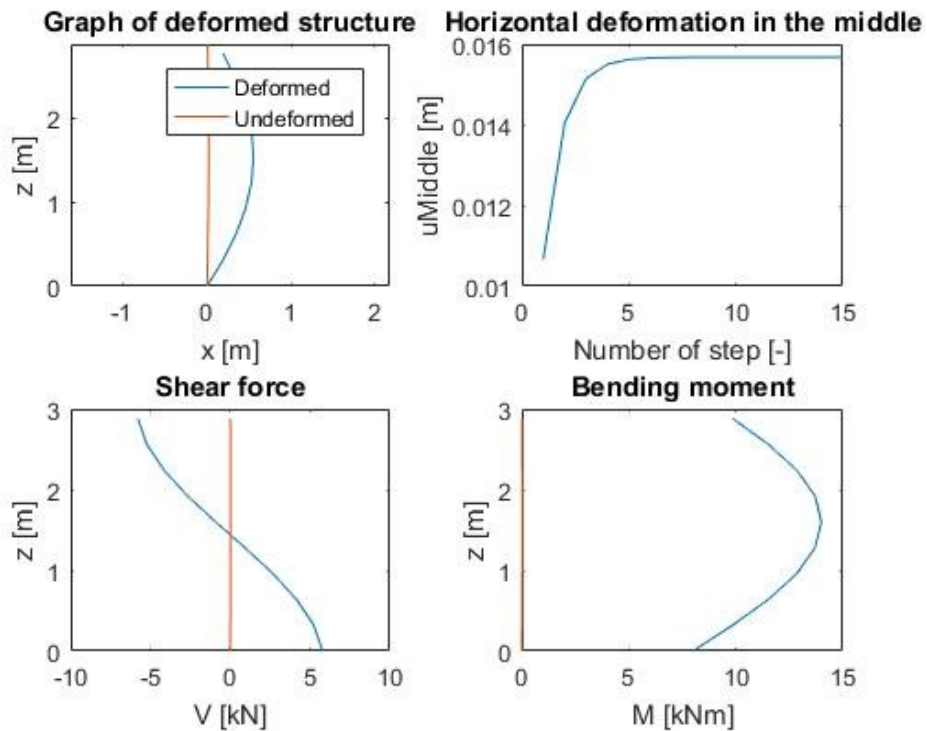
Figure 3.8: Left top - final shape and lateral deflection, right top – lateral deflection of the middle of the column in each step of calculation, left bottom – shear force in the final step, right bottom – bending moment in the final step. All this is for the case, that the cross section does not reduce and the calculation converges to equilibrium.

3.6 Example 2

The column fixed at both ends with the square cross section $B \times H = 0.4 \times 0.4$ m with the height 8.2 m was chosen. Its initial imperfect shape was chosen 0.18 m, initially inclined right. The axial load on the column was 770 kN. The final deformation and the internal forces can be seen in Fig. 3.9. In Fig. 3.10 can be seen the final shape of column (function of thickness H) when excluding the tensioned zones.
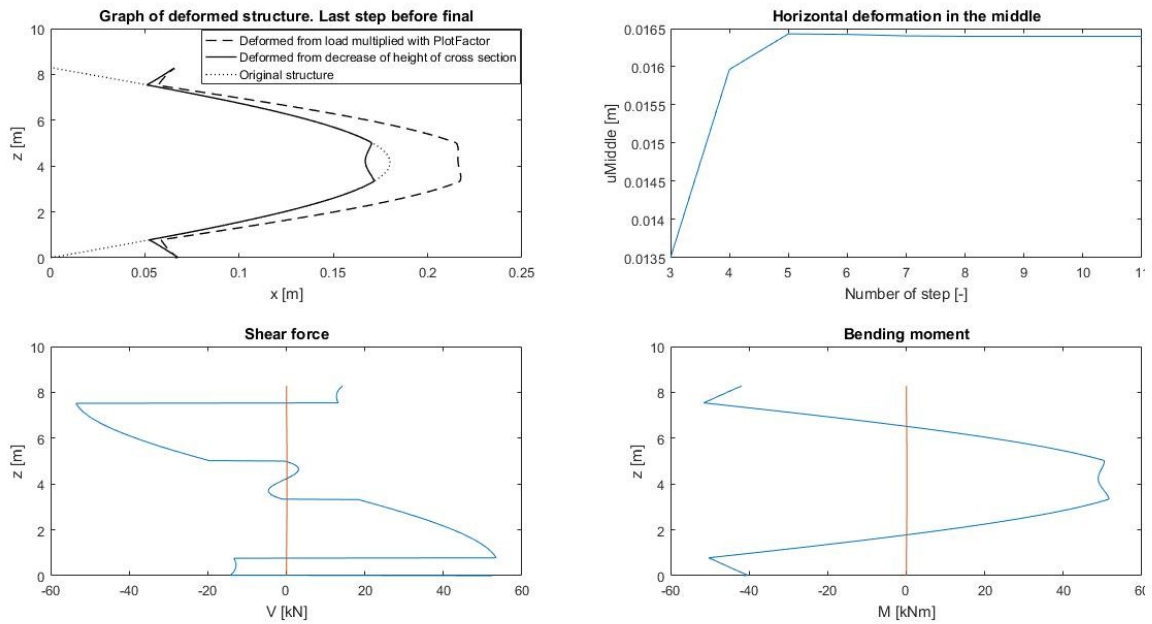
Figure 3.9: Left top - final shape and lateral deflection, non-proportional plot, right top – lateral deflection of the middle of the column in each step of the calculation, left bottom – the shear force in the final step, right bottom – the bending moment in the final step. All this is for the case that the cross section reduces and the calculation converges to equilibrium.

■ 3.7 Conclusions

An algorithm that can solve non-linear stability analysis of slender columns loaded in the plane of the main moment of inertia was implemented in the program MATLAB®. The program allows us to analyse these structures till their failure. The comparison of the results of the developed algorithm with other calculation methods can be seen in Section 4.4.3.
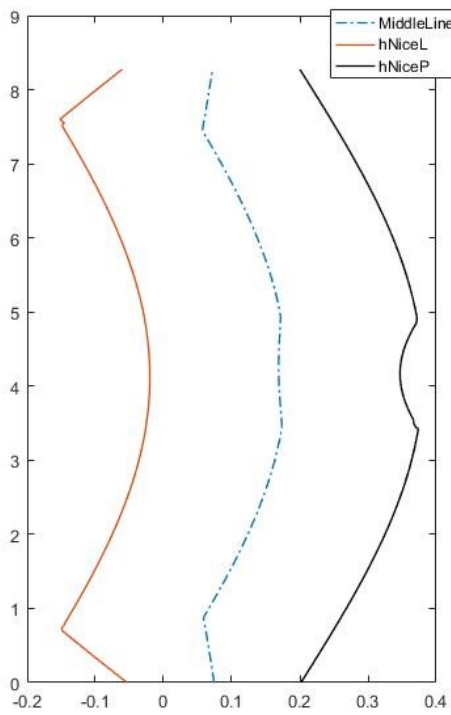
(a) : The final height of cross section at the final step.
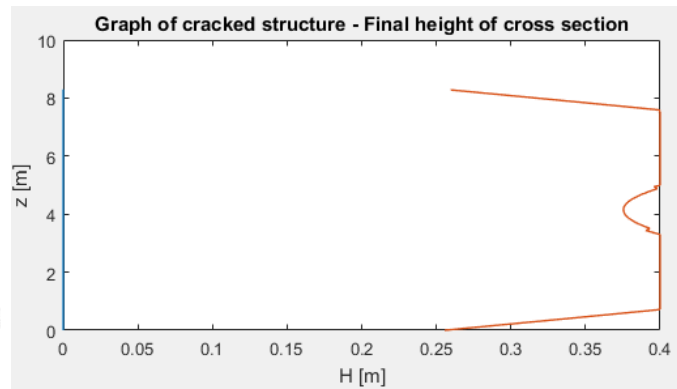
(b) : The final shape of the column – without excluded tensioned parts of the cross section.

Figure 3.10: The results for the case that the cross section reduces and the calculation converges to equilibrium.

Chapter 4

Slender columns subjected to biaxial bending combined with compressive normal force

The content of this chapter is taken mainly from the article [VD21].

4.1 Introduction

In general, all structures are loaded in all three directions, and all material behaviour is described by the non-linear behaviour. In practical structural design, the stiffness of an element usually allows the minor load effect to be neglected and to consider the element loaded in one direction only. It is not suitable for cases, for which $M_y > 0.1M_z$ (or $M_z > 0.1M_y$), such as columns in the corner of the building, where load by wind can occur in two directions or for example of a high bridge pier, where the transverse wind load cannot be neglected. The impact of the biaxial bending loading combined is even higher in the case of slender columns.

According to the current code of masonry structures ([PL07]), the rectangular cross section loaded by a combination of normal force and one bending moment (which results in a smaller, again rectangular cross section according to Section 1.6.1 and 3) can be considered. This is not sufficient for the case of biaxial bending moments, which can lead to a skew neutral axis and a trapezoidal or general polygon-shaped cross section; neutral axis impacts the calculation at the level of cross section. The approach that all members are designed as a wall does not reflect the behaviour of column member which impacts the whole structure. The standard [PL07] also assumes that the columns are used mainly in combination with a stiff ceiling, which is not the case of many existing (often historic) columns.

The general stress diagram arising from biaxial bending is shown in Figure 4.1 for the case of the linear stress-strain diagram (used in SLS) and in Figure 4.2 for the case of the rigid-plastic diagram (used in the ULS). The stress-strain diagram for the SLS is doubtless linear for the compression, but for the ULS, there are many options. The [PL07] recommends a non-linear relation, even though it does not recommend which relation should be used. Another possibility is to use an elastic - ideal plastic. The equation for the check of the design value of resistance normal force arises from the rigid-plastic diagram, which is also used in this chapter. See all the diagrams used in Section 4.3.

Figure 4.1: The general stress diagram of a rectangular cross section - at the SLS.

Figure 4.2: The general stress diagram of a rectangular cross section at the ULS – for example of rigid-plastic stress-strain diagram.

4.2   Methods and literature review

Biaxial bending is mentioned in a few masonry standards throughout the world. In case that the biaxial bending is mentioned, the verification is very conservative. For example of the British standard – [BSI05], the slenderness ratio λ_s is limited by the value of 27 (in this case study, columns of ratio λ_s up to the value of 300 are analysed). All the methods consider only the rectangular shape of the cross section. In general, methods can be divided by (each method has its shortcut):

- Consideration of material non-linearity for calculation of internal forces.
  - Yes (M)
    - Linear stress-strain diagram (L)
    - Rigid-plastic diagram (R)
    - Non-linear diagram (N)
  - No (-)

- Consideration of geometric non-linearity for calculation of internal forces.

- Yes (G)
- No (-)

■ Method, how is the check done.

- Effective area – rectangular shape, 1 coefficient for impact of buckling (B1)
- Effective area – rectangular shape, 2 coefficients for impact of buckling (B2)
- Effective area – general shape according to B. Das [Das18], 1 coefficients for impact of buckling (D)
- Fully non-linear calculation, controlling the strain and stress of material (S)

For example, the method proposed by this thesis is ML,R,N GB1,D,S method ("," means multiple options). The order of characters in the shortcut corresponds to the items in the list above. For example, the method of EC6 [PL07] is -RGB?, see the following chapter.

■ 4.2.1 Methods according to EC6 [PL07]

According to [PL07], only the wall should be verified. The standard does not deal with biaxial bending. The eccentricity of the load occurs only in one direction (in the direction of smaller stiffness). The design normal resistance force (see also equations in Section 2) must fulfil the following condition:

$$N_{Ed} \leq N_{Rd} = \Phi B H f_d, \tag{4.1}$$

$$\Phi_i = 1 - 2\frac{e_i}{B}, \tag{4.2}$$

for check at foot and head of column, and

$$\Phi_m = A_1 e_{nl}^{\frac{-u^2}{2}}, \tag{4.3}$$

$$A_1 = 1 - 2\frac{e_{mk}}{B}, \tag{4.4}$$

$$u = \frac{\lambda - 0.063}{0.73 - 1.17 e_{mk}/B}, \tag{4.5}$$

$$\lambda = \frac{h_{ef}}{B}\sqrt{\frac{f_k}{E}}, \tag{4.6}$$

for check in the midspan of columns height, where:

- N_{Ed} – design value of applied normal force,
- N_{Rd} – normal resistance force,

Figure 4.3: Shape of the cross section due to the load with eccentricity in one direction.

- Φ – capacity factor according to slenderness, Φ_i at the top or bottom of the column, Φ_m in the midspan ,
- B – width of a section,
- H – thickness of a section,
- f_d – design masonry normal strength according to Equation 1.3,
- f_k – characteristic masonry normal strength according to Equation 1.2,
- E – modulus of elasticity of masonry,
- h_{ef} – critical (buckling) length,
- e_{nl} – the base of the natural logarithm,
- e_{mk} – sum of eccentricities from the load, initial imperfection and creep in the midspan of the column,
- e_i – sum of eccentricities from the load, initial imperfection and creep in the head or foot of the column.

This relation considers bending only in one plane, at the ultimate limit state. The serviceability limit state is not handled, no relationship is given. It is generally noted that overstressing or damage shall be avoided.

▪ 4.2.2 JÄGER, W. Mauerwerk-Kalender

The reduced shape of the cross section according to [Jä13] can be seen in Figure 4.4.

According to [Jä13], the following relation should be used:

$$N_{Rd} = \Phi_{iy}\Phi_{iz}BHf_d, \tag{4.7}$$

Figure 4.4: Method which uses effective area – rectangle shape (shortcut B).

$$\Phi_{iy} = (1 - 2\frac{e_y}{B})e_{nl}^{\frac{-u_y^2}{2}}, \tag{4.8}$$

$$\Phi_{iz} = (1 - 2\frac{e_z}{H})e_{nl}^{\frac{-u_z^2}{2}}, \tag{4.9}$$

where:

- u_y and u_z can be calculated according to the previous section.
- e_y and e_z – the sum of eccentricities of the load, initial imperfection, and creep in the midspan of the column in the direction of axis y and z, respectively.

It is -RGB2 method. The equations consider the rigid-plastic stress-strain diagram and multiply two buckling coefficients (capacity factors), which is very conservative.

■ 4.2.3   Valentin Förster [Fö17]

The method shortcut is -R-B1. The article [Fö17] states that:

$$N_{Rd} = min(\Phi_{Rd,y}B_{red}Hf_d; \Phi_{Rd,z}BH_{red}f_d), \tag{4.10}$$

$$B_{red} = (1 - 2\frac{e_y}{B})B, \tag{4.11}$$

$$H_{red} = (1 - 2\frac{e_z}{H})H, \tag{4.12}$$

where:

- $\Phi_{Rd,y}$ – slenderness reduction factor in direction of axis y according to the previous section,

- $\Phi_{Rd,z}$ – slenderness reduction factor in direction of axis z according to the previous section.

This method is based on the use of the load-bearing capacity of exclusively uniaxially eccentrically loaded compressed members to calculate the load-bearing capacity of biaxially eccentrically loaded compression members. It uses the rigid-plastic stress-strain diagram and only one coefficient of buckling.

■ 4.2.4 Cais, J. and Das, B.: the skew shape of compressed area

Skew shape (shortcut -R-D) using a rigid-plastic stress-strain diagram according to [Das18] and [Cai57] proposed for the check of stress in the soil under the shallow rectangular foundations gives us the following relations:

$$N_{Ed} \leq N_{Rd} = \Phi A_{eff} f_d, \tag{4.13}$$

$$A_{eff} = \lambda_D \beta / 2, \tag{4.14}$$

$$\lambda_D = 3/2 - 3\epsilon_x, \tag{4.15}$$

$$\beta = 3/2 - 3\epsilon_z, \tag{4.16}$$

$$\epsilon_z = e_z / H, \tag{4.17}$$

$$\epsilon_x = e_x / B, \tag{4.18}$$

where:

- B – width of a section,
- H – thickness of a section,
- e_x – eccentricity in the direction of dimension H,
- e_z – eccentricity in the direction of dimension B.

These relationships are valid only for the case that the effective area has a triangular shape; see Figure 4.5. In other cases, the calculation is much more complicated; see [Das18].

Figure 4.5: Shape of the effective compressed area according to [Das18].

■ 4.2.5 ACI – standard of American concrete institute

The method of ACI [ms13] is described in Section 4.4.2.

■ 4.3 Method used in this chapter

■ 4.3.1 Assumptions of analysis

On the cross section level, the local axes are used: y_loc and x_loc. For the formation of the global stiffness matrix, the global axes are used: x_g and y_g. Because the material cannot be carried by the tension, cracks open and the loaded part of the cross section, which carries the load, changes its shape. As a consequence, the centroid of the cross section moves. The centroid can, in general, move in both horizontal directions, in the plane of cross section (according to Figure 4.6 in the direction of y_loc and x_loc). The behaviour of the slender column, when considering the material non-linearity, can be described by Figure 3.3.

Depending on the magnitude of the acting bending moments, the neutral axis can be skewed or, in a particular case, perpendicular to one of the axes y_loc and x_loc of the local coordinate system. The special case, for which the neutral axis is parallel to one of the axes and the imperfection in the perpendicular direction is considered zero, is discussed in Chapter 3 and article [VD17].

In general, the following shapes of a cross section can occur:

1. Rectangular shape in case of occurrence of one bending moment – M_{y_loc}.

2. Rectangular shape in case of occurrence of one bending moment – M_{z_loc}.

3. General polygon shape which was created by cutting of a triangle.
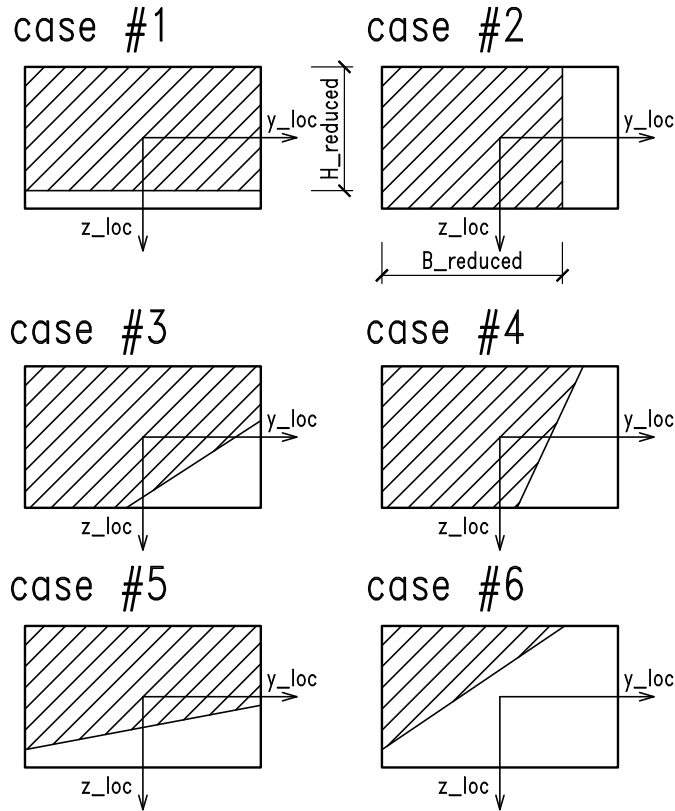
Figure 4.6: Cases which can occur in the structure.

4. Trapezoidal cross section, where the edge B is reduced (see B, H in Figure 4.3).

5. Trapezoidal cross section, where the edge H is reduced.

6. Triangular shape.

In the proposed algorithm, all cases are covered. If $M_{z\_loc} < 0.1 M_{y\_loc}$, case # 1 can be used and if $M_{y\_loc} < 0.1 M_{z\_loc}$, case # 2 can be used. Case # 6 usually results in the collapse of the structure for the case of a slender column (see the conclusions of this chapter). However, it can occur in the case of a short column loaded by force with large eccentricities. In this chapter, the approach to the interaction of mortar and the masonry units is chosen the same as in the current code [PL07] – the masonry is homogenized in a suitable manner. See the details of homogenization in Section 1.

The whole column is considered as a beam of the same material, uniform strength and uniform modulus of elasticity of masonry. The shape of the cross section depends on the resulting strain diagram for the appropriate cross section in the i-th step of the calculation. The tensioned part of the cross section is excluded. The column has an eccentricity (imperfection) in both directions y_loc and z_loc. In general, the imperfection in the direction y_loc can be independent of the imperfection in the direction z_loc. The imperfection of sin function shape is considered. The buckled shape or eigenvector is described in [TG61].

As boundary conditions, both the top and the bottom of the column are considered hinged; at the bottom, all translations are fixed; at the top, horizontal translations are fixed, and vertical translation is free (a simply supported beam).

∎ 4.3.2 Developed algorithm - MVo code

The algorithm considers in each step the material non-linearity and geometric non-linearity. The geometric non-linearity is solved by second-order analysis. The solution is sought iteratively; the calculation stops if the error is less than the chosen precision of the calculation. As an error, the difference between the two deformations in the midspan of the column in the following two steps is chosen:

$$\epsilon = abs(r^i_{d,Nel/2} - r^{i-1}_{d,Nel/2})) < \epsilon_{chosen}, \tag{4.19}$$

where:

- Nel – number of elements,
- $Nel/2$ means the midspan of the column,
- r_d see below in the next section,
- i – number of step,
- ϵ_{chosen} – chosen error in metres. In the algorithm, 10e-07 is used.

The beam representing the column is divided into smaller elements which have the prismatic shape – the cross section is constant over the elements length. For demanded precision, the usual number of elements is between 128 and 512. The solution is carried out in the following steps:

1. Finding the linear solution in the first step, calculating of internal forces.

2. Finding the neutral axis of each element, forming the updated matrix of cross section properties with reduced moments of inertia I_y, I_z, I_{yz}, area and move of centroid due to material non-linearity.

3. Updating the geometry of the column, finding the solution to the set of new equations, going to step 2, and repeating it until the error is lower than the chosen precision of the calculation. The case for which error is growing and does not converge means collapse of the structure.

∎ 4.3.3 General equations for the solution

Analysis of frame buckling by the stiffness method generally reduces according to [Lep14] and [BC10] to linear matrix equation:

$$K(\mu_k)r_d = f, \tag{4.20}$$

where:

- r_d is the column matrix of small generalized displacement increments from the initial state,
- f is column matrix of the associated small generalized force increments,
- K is matrix of incremental stiffness coefficients and
- μ_k is the parameter of initial loads, that are independent of f.

Equation 4.20 represents a matrix eigenvalue problem of nonstandard type because the coefficients of K depend on μ_k non-linearly, and μ_k appears not only in diagonal terms. To get rid of this non-linearity, columns are subdivided into three or more elements (in this chapter, the number of elements is between 128 and 512). The linear part of Taylor expansion is used; we obtain a nonstandard linear eigenvalue problem:

$$(K - K_G)r_d = 0, \tag{4.21}$$

where: K_G – geometric stiffness matrix. The iterative solution begins with the equation:

$$Kr_d = f + f_{ekv}, \tag{4.22}$$

where:

$$f_{ekv} = K_G r_d. \tag{4.23}$$

▪ 4.3.4 Equations used for the solution and the step-by-step solution

In first step

$$Kr_d^0 = f, \tag{4.24}$$

From which we obtain r_d^0, N^0, K_G^0, where:

- r_d^0 – initial displacement vector from the first step,
- N^0 – initial normal force from the first step,
- K_G^0 – geometric stiffness matrix which is calculated from the initial normal force and is used in the next step.

In i-th step of iteration:

$$Kr_d^{i+1} = f + K_G^i r_d^i, \tag{4.25}$$

Convergence criterion: see Equation 4.19. For the both-end-hinged beam in 2D, the matrix K_G has the form:

$$K_{G,2D} = \frac{N}{L_e} \begin{bmatrix} 0 & 0 & 0 & 0 & 0 & 0 \\ 0 & 1 & 0 & 0 & -1 & 0 \\ 0 & 0 & 0 & 0 & 0 & 0 \\ 0 & 0 & 0 & 0 & 0 & 0 \\ 0 & -1 & 0 & 0 & 1 & 0 \\ 0 & 0 & 0 & 0 & 0 & 0 \end{bmatrix}. \tag{4.26}$$

For the both-end-fixed beam in 2D, the matrix K_G has the form:

$$
K_{G,2D} = \frac{N}{30L_e}
\begin{bmatrix}
0 & 0 & 0 & 0 & 0 & 0 \\
0 & 36 & 3L_e & 0 & -36 & 3L_e \\
0 & 3L_e & 4L_e^2 & 0 & -3L_e & -L_e^2 \\
0 & 0 & 0 & 0 & 0 & 0 \\
0 & -36 & -3L_e & 0 & 36 & -3L_e \\
0 & 3L_e & -L_e^2 & 0 & -3L_e & 4L_e^2
\end{bmatrix}.
\tag{4.27}
$$

For the both-end-fixed beam in 3D, the matrix K_G has the form:

$$
K_{G,3D} = \frac{N}{L_e}
\begin{bmatrix}
M1 & M2 \\
M2 & M3
\end{bmatrix},
\tag{4.28}
$$

where:

$$
M1 =
\begin{bmatrix}
0 & 0 & 0 & 0 & 0 & 0 \\
0 & \frac{6/5+2\phi_Y+\phi_Y^2}{(1+\phi_Y)^2} & 0 & 0 & 0 & \frac{L_e}{10/(1+\phi_Y)^2} \\
0 & 0 & \frac{6/5+2\phi_Z+\phi_Z^2}{(1+\phi_Z)^2} & 0 & \frac{-L_e}{10/(1+\phi_Z)^2} & 0 \\
0 & 0 & 0 & J/A & 0 & 0 \\
0 & 0 & \frac{-L_e}{10(1+\phi_Z)^2} & 0 & \frac{2L_e^2/15+L_e^2\phi_Z/6+L_e^2\phi_Z^2/12}{(1+\phi_Z)^2} & 0 \\
0 & \frac{L_e}{10(1+\phi_Y)^2} & 0 & 0 & 0 & \frac{2L_e^2/15+L_e^2\phi_Y/6+L_e^2\phi_Y^2/12}{1+\phi_Y}^2
\end{bmatrix},
\tag{4.29}
$$

$$
M2 =
\begin{bmatrix}
0 & 0 & 0 & 0 & 0 & 0 \\
0 & \frac{-6/5-2\phi_Y-\phi_Y^2}{(1+\phi_Y)^2} & 0 & 0 & 0 & \frac{L_e}{10(1+\phi_Y)^2} \\
0 & \frac{-6/5-2\phi_Z-\phi_Z^2}{(1+\phi_Z)^2} & 0 & 0 & \frac{-L_e}{10(1+\phi_Z)^2} & 0 \\
0 & 0 & 0 & -J/A & 0 & 0 \\
0 & 0 & \frac{L_e}{10(1+\phi_Z)^2} & 0 & \frac{-L_e^2/30-L_e^2\phi_Z/6-L_e^2\phi_Z^2/12}{(1+\phi_Z)^2} & 0 \\
0 & \frac{-L_e}{10(1+\phi_Y)^2} & 0 & 0 & 0 & \frac{-L_e^2/30-L_e^2\phi_Y/6-L_e^2\phi_Y^2/12}{(1+\phi_Y)^2}
\end{bmatrix},
\tag{4.30}
$$

$$
M3 =
\begin{bmatrix}
0 & 0 & 0 & 0 & 0 & 0 \\
0 & \frac{6/5+2\phi_Y+\phi_Y^2}{(1+\phi_Y)^2} & 0 & 0 & 0 & \frac{-L_e}{10(1+\phi_Y)^2} \\
0 & 0 & \frac{6/5+2\phi_Z+\phi_Z^2}{(1+\phi_Z)^2} & 0 & \frac{L_e}{10(1+\phi_Z)^2} & 0 \\
0 & 0 & 0 & J/A & 0 & 0 \\
0 & 0 & \frac{L_e}{10(1+\phi_Z)^2} & 0 & \frac{(2L_e^2/15+L_e^2\phi_Z/6+L_e^2\phi_Z^2/12}{(1+\phi_Z)^2} & 0 \\
0 & -\frac{L_e}{10(1+\phi_Y)^2} & 0 & 0 & 0 & \frac{2L_e^2/15+L_e^2\phi_Y/6+L_e^2\phi_Y^2/12}{(1+\phi_Y)^2}
\end{bmatrix},
\tag{4.31}
$$
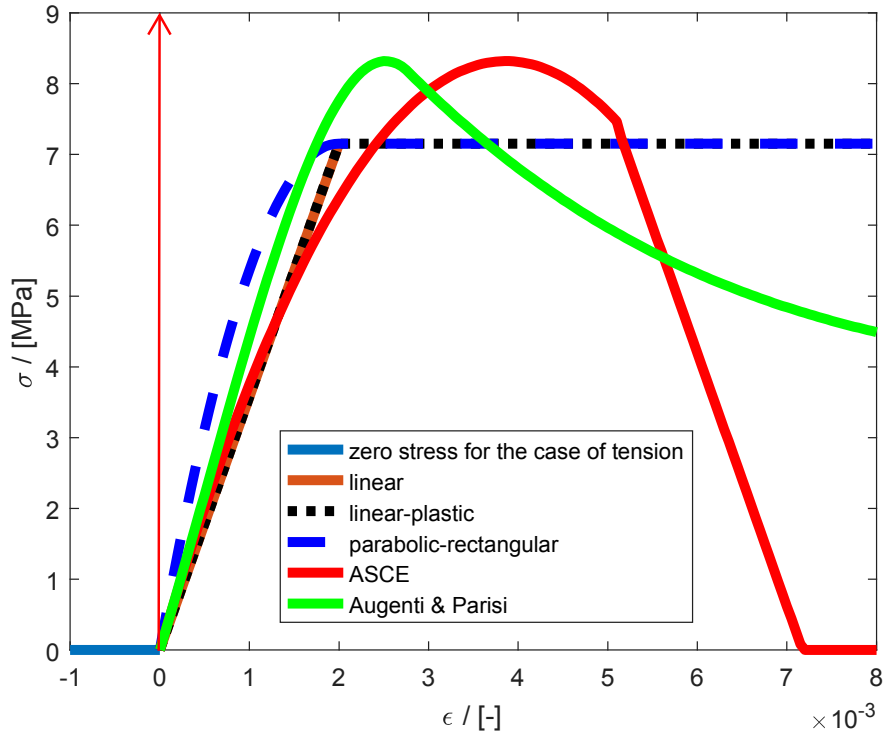
Figure 4.7: Various stress-strain diagrams.

$$\phi_Y = \frac{12EI_z}{GA_sL_e^2}, \tag{4.32}$$

$$\phi_Z = \frac{12EI_y}{GA_sL_e^2}, \tag{4.33}$$

$$J = BH^3/3, \tag{4.34}$$

where:

- A_s - shear area of cross section,
- L_e - length of an element,
- E - modulus of elasticity of masonry.

4.3.5 Material non-linearity

For the calculation of stresses, many stress-strain diagrams can be used. In the case study of the non-linear behaviour of masonry columns, six basic possibilities are used; see Figure 4.7, the rigid plastic see in Figure 4.8.

Linear-plastic, parabolic-plastic (parabolic-rectangular) and rigid-plastic diagrams are given in [PL07]. The ASCE diagram is shown in [KRJ07], Augenti and Parisi is shown in [AP10]. Finding the stress distribution in the cross section consists of two iterative
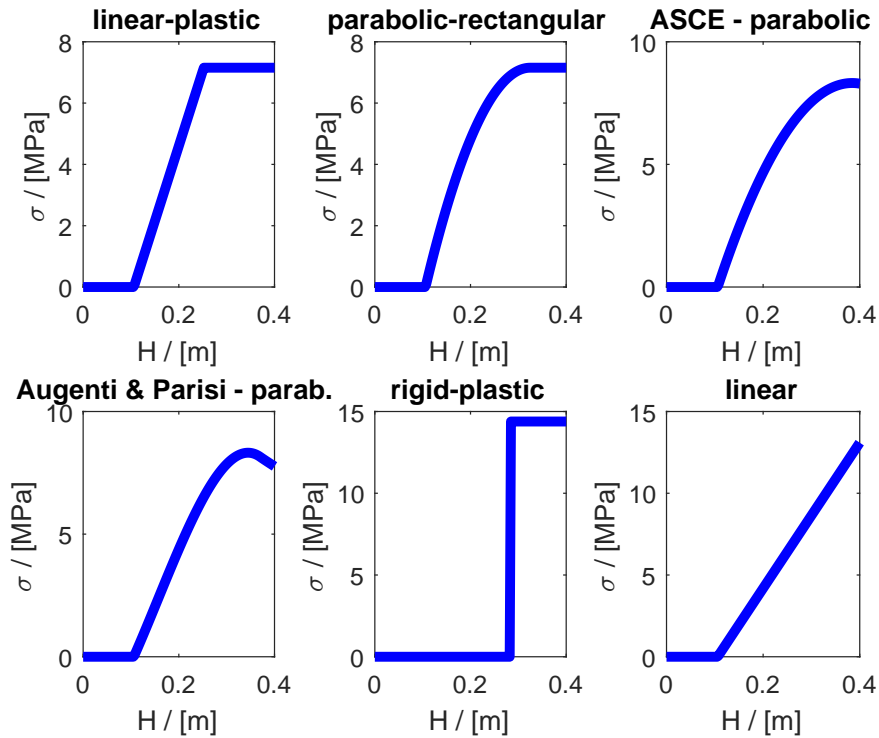
Figure 4.8: Resulting stress for various stress-strain diagrams, $B \times H = 0.4 \times 0.4$ m, $N =$670 kN, M=95 kNm.

calculations. The cross section is divided into a finite number of parts (for the final results, 300 parts were used). The stress arising from the strain is integrated numerically; internal forces are obtained. In the first iterative calculation, the E_{mu} – multiple of the modulus of elasticity is sought to fulfil the force equilibrium condition. If the bending moment acting in the cross section is not equal to the bending moment obtained by integrating the stresses, the neutral axis is moved, and the E_{mu} is sought again until both the moment and the force equilibrium conditions are fulfilled.

This calculation is provided for all elements. Then, the $(i + 1)$-th step (further step) of the calculation according to Section 4.3.4 is carried out. This step is repeated until the convergence criterion is fulfilled. In each step, the strain is controlled.

4.4 Results of modelling

The results can generally be divided into 3 cases:

1. Short columns – only two steps of calculation are enough to fulfil the criterion according to Equation 4.19. The failure occurs due to material crushing (overstress).

2. Long columns, for which the finite number of steps is enough to fulfil the convergence criterion and the stress does not exceed the tensile strength (which is considered zero).
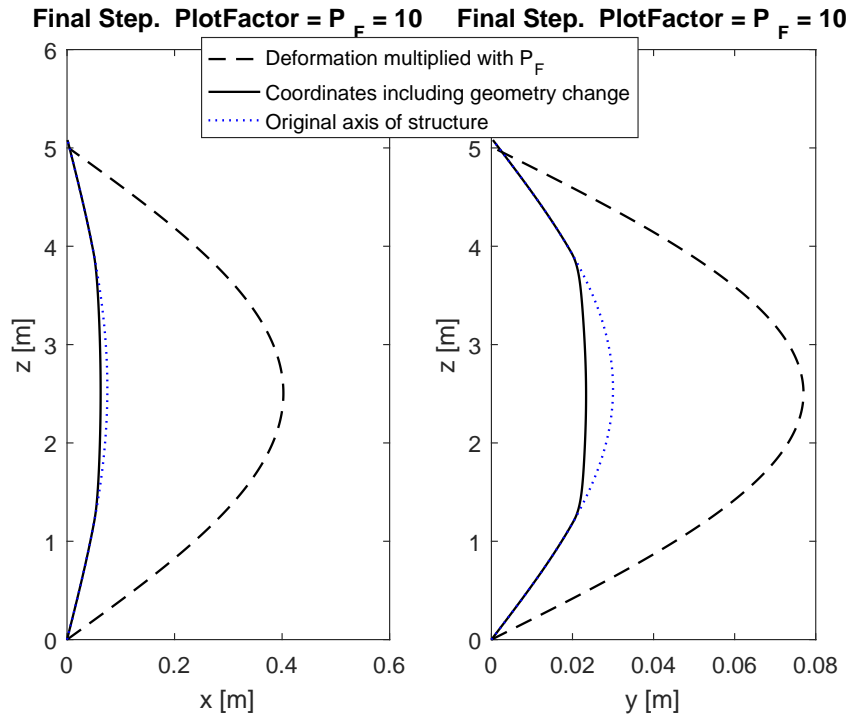
Figure 4.9: Final geometry in the global coordinate system x_g, y_g.

The failure occurs due to material crushing (the bending moments are increased by slenderness).

3. Slender columns, where the material non-linearity impacts the result, because the tensile strength is exceeded. The failure occurs because of buckling.

In this chapter, results of modelling of a single column are presented, and a case study of a relevant set of columns shows how the stability and resistance of the masonry column are impacted by the 3D effects, material non-linearity, and geometric non-linearity.

▪ 4.4.1 Example of single column

To demonstrate an example, a column of 5 m height is chosen. The dimensions of the column are $B \times H = 0.5 \times 0.3$ m. The eccentricity (initial imperfection) is chosen $e_y = 0.15B$, eccentricity $e_z = 0.025\,H$, $f_k = 6.42$ MPa, $E = 1000\,f_k$. See the results in Figure 4.9, 4.10, 4.11 and 4.12.

▪ 4.4.2 Case study of various columns

The approach of ACI [ms13] is compared to the result of the modelling used in this chapter (named "MVo code"). According to ACI, the stress at all points of the cross section must be negative (compression). Second-order moments should be included. In the case study,
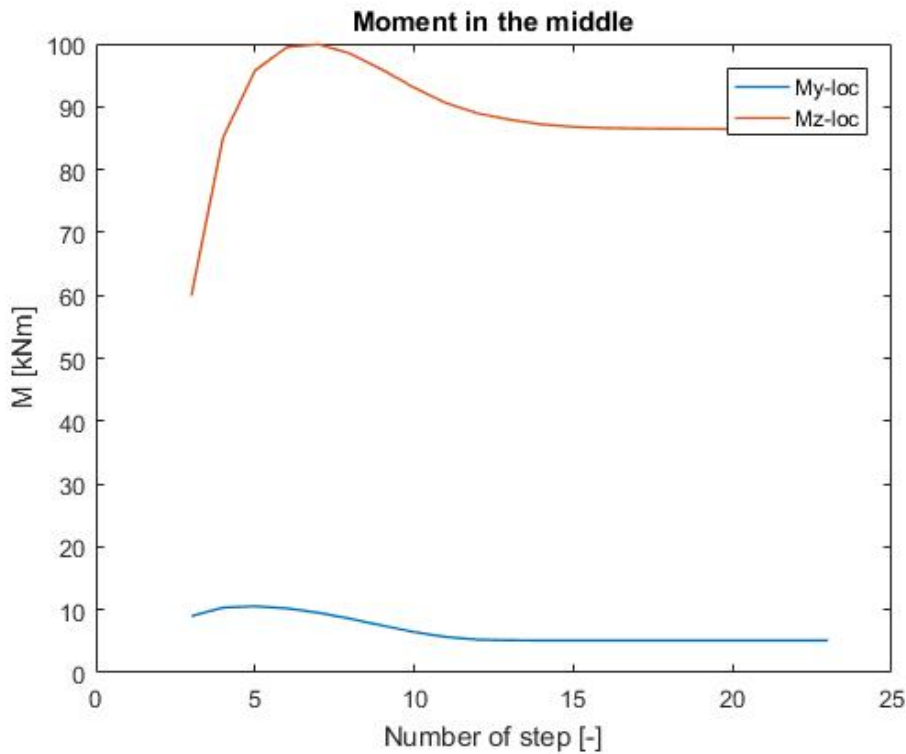
Figure 4.10: Bending moment convergence.

column thickness B was chosen as 0.4 m, and H was variable, as well as slenderness λ_s. The eccentricities were chosen the same, as in the example above. The result of modelling using the ACI criteria can be seen in Fig. 4.13; results of "MVo" code are shown in Fig. 4.14.

The following example is used to show the effect of using various stress-strain diagrams. The cross section with dimensions $B \times H = 0.4 \times 0.4$ m is loaded with the force $N_{Ed} = 670$ kN and various bending moments. After the convergence of an iteration of the bending moment is fulfilled, the different height of compressed area H_c was found for the various stress-strain diagrams, see Figure 4.15.

Due to a different resulting height of the compressed area, the final carrying capacity varies for the various stress-strain diagrams. Note that the carrying capacity is limited by the slenderness (and second-order effect) as well as the stress limitation according to the stress-strain diagram (see Figure 4.7 and 4.8). The limit stress, which should not be exceeded, is considered f_k for all the stress-strain diagrams for the reason of comparability, except for the ASCE and Augenti & Parisi diagrams, for which the maximal stress is equal to $f_k/0.86$.

It can be seen from Figure 4.16 that the resulting curve due to ACI requirements is quite similar to the curve representing the linear behaviour. This is because the eccentricities considered are the same for all the cases, and the decisive criterion was always the criterion of maximal stress, not the crack opening. For different eccentricities, the curves would vary.

49

Figure 4.11: Final internal forces - bending moment and shear force.

4.4.3 Comparison of all the methods

For the purpose of comparison, all of the methods are displayed in one plot - Figure 4.17. New curves are added:

1. $CSN731101$ is a standard valid before the Eurocodes (current standard), see [ifs80].

2. $EN1996$ is method according to Section 4.2.1.

3. $Masonry - VV$ is the calculation method of this article ("MVo code" implemented in MATLAB®), the boundary conditions were changed to column both-end-fixed (zero rotations).

4. $FcritEuler$ is the critical buckling force of the ideal beam with linear behaviour (Section 3.2.1). VV means both-end-fixed, KK means both-end-hinged.

4.5 Comparing the results from the experiment

The experiment, described in [Klo16a], was based on testing 5 columns of the height 2.75 m loaded by a force and an eccentricity in one horizontal direction (denoted "1e"), and 5 columns of a height 1.75 m loaded by a force and an eccentricity in two horizontal directions (denoted "2e"). The dimensions of the column are $B \times H = 0.44 \times 0.5$ m. Specimen 1 was

tested in a centric compression; the design stress f_{de} was taken from this specimen 1 and considered for the other specimens. The following expression was used:

$$f_{de} = \frac{N_{m,A2}}{BH},$$
(4.35)

where:

- f_{de} – the strength of specimen 1 which is used for other specimens,
- $N_{m,A2}$ – the normal force, at which the crushing of specimen 1 occurred.

The bricks tested are usually used in new masonry walls, and they have cavities due to the requirements of energy codes. As can be seen in Figure 4.18, the curves obtained by measuring the strain using strain gauges are linear until the end of the experiment. According to [Klo16a], "the way of deforming can be described as quasi-linear, mode of failure is brittle, and the crushing always occurred at the outer edge, closer to the applied force," which means that the collapse of one face of a brick means stopping further loading. The collapse is always caused by the combination of normal force, and bending moment; the collapsed shape was always by collapsing of one face of a brick.

experiment 1e					
specimen	1-0	1-1	1-2	1-3	1-4
Quantity name					
eccentricity e_z [m]	0	0.072	0.147	0.11	0.11
eccentricity e_y [m]	0	0	0	0	0
Max.force N_m [kN]	**1207**	**992.0**	**577.0**	**717.0**	**759.0**

EN1996 - rigid-plastic check (rec. shape)					
$A1_z$ [-]	1	0.673	0.332	0.5	0.5
$A2_y$ [-]	1	1	1	1	1
Ac [-]	0.22	0.148	0.073	0.11	0.11
u1 [-]	0.237	0.322	0.512	0.397	0.397
Φ1 [-]	0.972	0.950	0.877	0.924	0.924
Φ2 [-]	1.000	1.000	1.000	1.000	1.000
NRd [kN]	**1207**	**793**	**361.3**	**573.8**	**573.8**

Mason, lin. diagram -> rigid-plastic check (rec. shape)					
NRd [kN]	**1224**	**818.2**	**377.0**	**581.9**	**581.9**

Mason, rigid-plastic diagram and check (rec. shape)					
NRd [kN]	**1210**	**825.1**	**407**	**613.3**	**613.3**

Table 4.1: Uniaxial bending experiment "1e".

The results of the experiments can be seen in Fig. 4.19, Fig. 4.20 and Tab. 4.2. In the table 4.1, a new check is added for the comparison. In this check, "Mason – lin.

Diagram -> rigid plastic check", the normal force of resistance at the ULS – N_{Rd} is calculated in the following manner: internal forces and shape of the cross section were taken from the linear stress-strain diagram using the "MVo code" (see the example of stress-strain diagram in Figure 4.1). Then, the resulting effective cross section is loaded by force with eccentricities calculated from acting bending moments – the forces from the linear calculation are checked by the rigid-plastic check of the ULS.

experiment 2e					
specimen	2-0	2-1	2-2	2-3	2-4
Quantity name					
eccentricity e_z [m]	0	0.147	0.073	0.073	0.147
eccentricity e_y [m]	0	0.167	0.083	0.167	0.083
Max.force N_m [kN]	**955**	**225**	**691**	**420**	**488**

EN1996 - rigid-plastic check (rec. shape)					
$A1_z$ [-]	1	0.332	0.668	0.668	0.332
$A2_y$ [-]	1	0.332	0.668	0.332	0.668
Ac [-]	0.22	0.024	0.098	0.049	0.049
u1 [-]	0.12	0.258	0.163	0.163	0.258
u2 [-]	0.095	0.205	0.129	0.205	0.129
$\Phi1_z$ [-]	0.993	0.967	0.987	0.987	0.967
$\Phi2_y$ [-]	0.996	0.979	0.992	0.979	0.992
NRd [kN]	**955**	**100.8**	**422**	**207.1**	**205.4**

Cais, J. - rigid-plastic check (general shape)					
λ [-]	1.5	0.498	1.002	1.002	0.498
β [-]	1.5	0.498	1.002	0.498	1.002
λ . B [m]		0.219	0.441	0.441	0.219
β . H [m]		0.249	0.501	0.249	0.501
NRd [kN]	**959.3**	**115.8**	**478.8**	**236.1**	**233**

Mason, lin. diagram -> rigid-plastic check (rec. shape)					
NRd [kN]	**952.6**	**219.6**	**528.5**	**249.7**	**249.5**

Mason, rigid-plastic diagram and check (rec. shape)					
NRd [kN]	**941.6**	**106.4**	**431.3**	**214.3**	**214.2**

Table 4.2: Biaxial bending experiment "2e".

It can be seen that for all the cases, the results from the "MVo code" calculation are closer to the results obtained from the experiment than the resistance according to the current standard EN1996. It should be noted that more experiments should be carried out and columns in the experiments should be more slender.

Mathematical modelling was also part of the article [Klo16a]. The author used a 3D FEM model using 3D solid elements with non-linear behaviour – modified Drucker-Prager

model was chosen. The shortcut of this method is MN-S. It was stated that "computational models compared to the results of experiments reflect very well the behaviour of the tested masonry pillars and bodies as well as the way of their deformation and failure".

4.6 Results discussion

All the methods used in the mentioned literature review have at least one error. Mostly it is the assumption of rigid-plastic behaviour, which we consider incorrect (see below). Using a real stress-strain diagram leads to methods that cannot be used for a practical design. For example, article [Klo16a] deals especially with the preciseness of modelling of the boundary conditions – especially the supporting sheet metal of compression testing machine. In the case of a practical design, these conditions are unknown, so the 3D solid non-linear time-demanding and tough method seems to be impracticable. The calculation according to ACI gives results which are for small bending moments (small eccentricities, such as eccentricities chosen in the case study of this chapter) the same as by using the non-linear calculation, because the tension does not occur till the collapse of the column. On the other hand, the ACI approach is conservative because the larger bending moment, which causes tension, is not admitted.

The verification of a normal loading capacity provided in the current standard [PL07] by using the rigid-plastic stress-strain diagram is insufficient for a 3D case. Handling the 3D case by calculating the eccentricities from the equilibrium conditions and using the equation, which is also used to verify the shallow foundation of rectangular shape, we obtain:

$$N_{Ed} \leq N_{Rd} = (B - 2e_y)(H - 2e_z)f_d, \tag{4.36}$$

This formula also assumes the fully rigid-plastic behaviour. This can theoretically occur in the case of an infinite rotation of the cross section. This cannot be obviously considered for the slender columns; it would result in infinite deformation and in used second-order beam analysis also infinite acting bending moment and collapse of the structure. The results of calculating the compressed area using the Equation 4.36 without controlling the strain can be seen in Figure 4.16. The height of the compressed area is much lower than in the other stress-strain diagrams. For these reasons, we do not recommend the rigid-plastic stress-strain diagram for analysing the slender masonry columns.

From Figure 4.21 it can be seen that the function of the strain is more or less linear (even until the failure). Also, according to [Han03], the behaviour in experiments fits best with the linear behaviour of the material.

In addition, comparing the results of the experiments with various calculation methods showed a good agreement between the normal resistance force obtained by the linear calculation and the experiment.

Based on the previous paragraphs, we recommend verifying the slender column's loading capacity in terms of the ULS and the SLS by using a linear stress-strain diagram for the practical design. The difference between the ULS and the SLS should only be in the value of the coefficients γ_M, γ_F used (see the explanation in EN 1990 - [ÚN05b] and [PL07]). The method for calculating the internal forces should include the material and

geometric non-linearity. The cross section area, which remains after the reduction due to the material non-linearity and after fulfilling the convergence criterion, was minimally 50 % in this case study. This tally well enough with standard [HD08]. This standard recommends limiting eccentricity to $e \leq H/3$ in the SLS (see also Equations 2.4 and 4.37); the author of this thesis recommends using this limit also for the ULS, i.e., using the relation:

$$H_{compressed} \geq H/2 \rightarrow e \leq H/3, \tag{4.37}$$

for the uniaxial bending and

$$A_{compressed} \geq A/2 \tag{4.38}$$

for biaxial bending (A – the total area of a cross section). This recommendation is suitable for slender columns, $\lambda_s > 10$. For short masonry elements, loaded by force with large eccentricity, which reduces effective area significantly, the author of this thesis recommends analysing the column as a new column with a reduced – effective area, i.e., to use for the calculation of u and λ the effective dimensions of the column, not the original ones.

The article [HD17] recommends modifying the Equation 4.37 in dependence on a category of the masonry (categories are defined in [PL07]), namely to limit the maximal eccentricities in ULS to $0.45H$ for category 1 and $0.4H$ for category 2.

The shear criterion of the resistance according to [PL07] or Equation 2.2 should be for the columns loaded in two planes replaced with the formula:

$$V_{Ed,3D} \leq V_{Rd}, \tag{4.39}$$

where:

$$V_{Ed,3D} = \sqrt{V_{Ed,y}^2 + V_{Ed,z}^2}, \tag{4.40}$$

where $V_{Ed,y}, V_{Ed,z}$ are applied shear forces in the direction of axis y, z respectively. V_{Rd} see in Equation 2.2.

The results of the experiment showed that the non-linear model used in this chapter is closer to the result of the experiment than the approach of the standard. The number of specimens tested in the experiment is not enough to establish the new detailed criteria for calculating the load capacity of slender columns. The slenderness ratio λ_s for the experiment "1e" is 21.65, for the experiment "2e" it is 13.78. Both ratios are lower than 27, which shows that the investigated columns are not very slender. Further experiments should test a larger number of columns of various slenderness.

4.7 Conclusions

A mathematical method of verifying the slender masonry column was proposed. The method was implemented in MATLAB®, and a case study of the resistance of various columns was carried out. Then, the results of the mathematical modelling were compared with the results

of the experiments. The methods used in the literature were also compared. According to the combination of these methods, it was stated that the method of the currently valid standard – Eurocodes – is not suitable for the slender masonry column check. The results of the loading capacity of columns obtained by the calculation according to the standards are conservative. The behaviour of slender masonry columns with various stress-strain diagrams is quite similar, except for the rigid-plastic model, which was stated as unsuitable. Based on the previous sections, new recommendations for the design of columns were made. Second-order analysis should be used; the linear stress-strain diagram can be used for compression (tensile strength neglected). The compressed area should be at least one-half of the total area of the cross section.

Figure 4.12: Final shape of the column (excluding tensioned parts) in the global coordinate system.
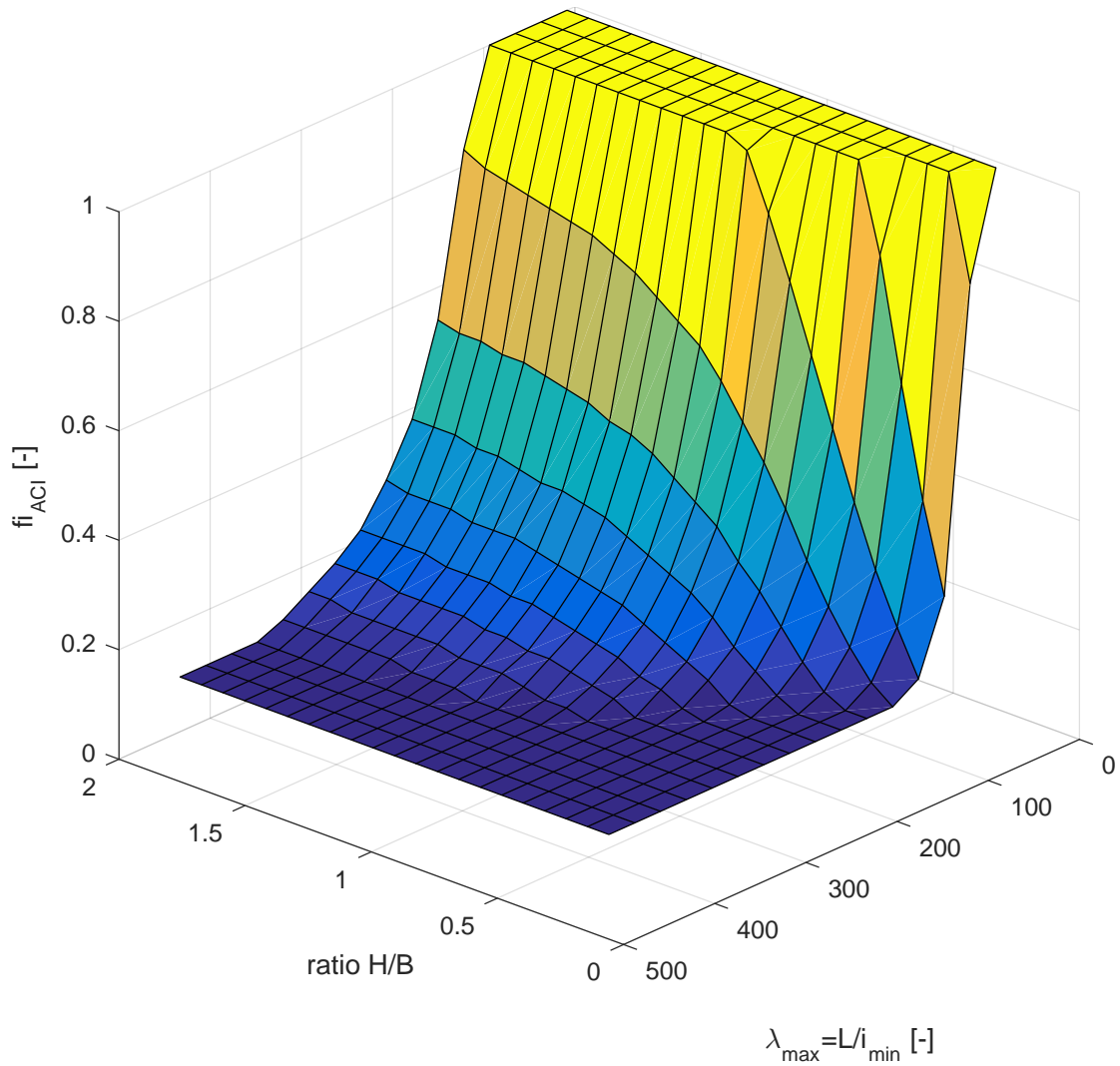
Figure 4.13: The slenderness reduction factor $fi = \Phi$ from the algorithm, using the ACI approach.

Figure 4.14: The slenderness reduction factor $fi = \Phi$ from the algorithm, using the "MVo code" approach.
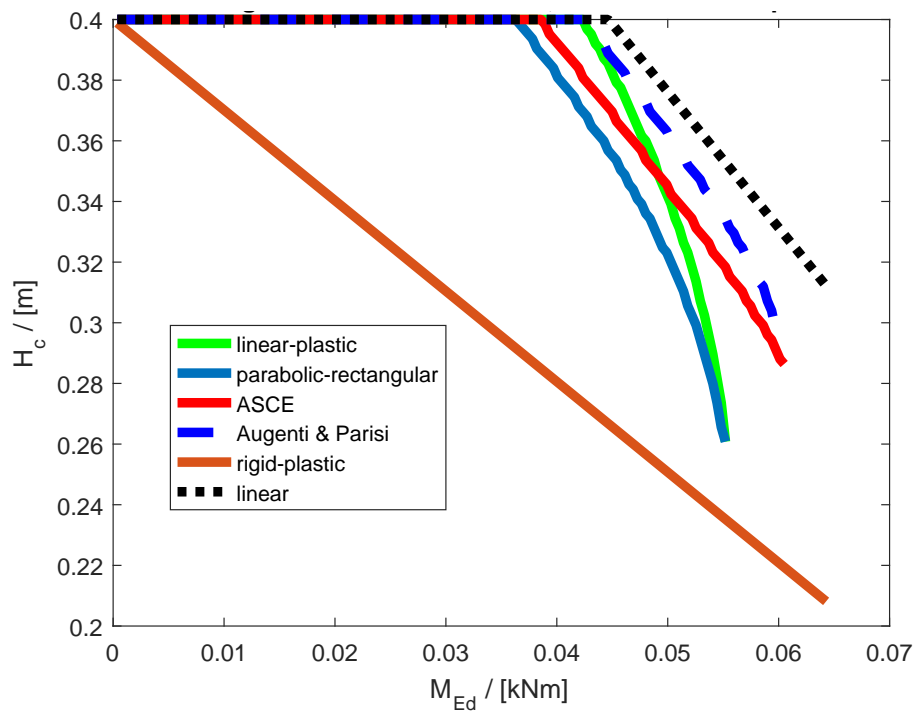
Figure 4.15: Comparing the resulting heights of the cross section from various stress-strain diagrams.

Figure 4.16: Comparing the final slenderness reduction factor from various stress-strain diagrams.
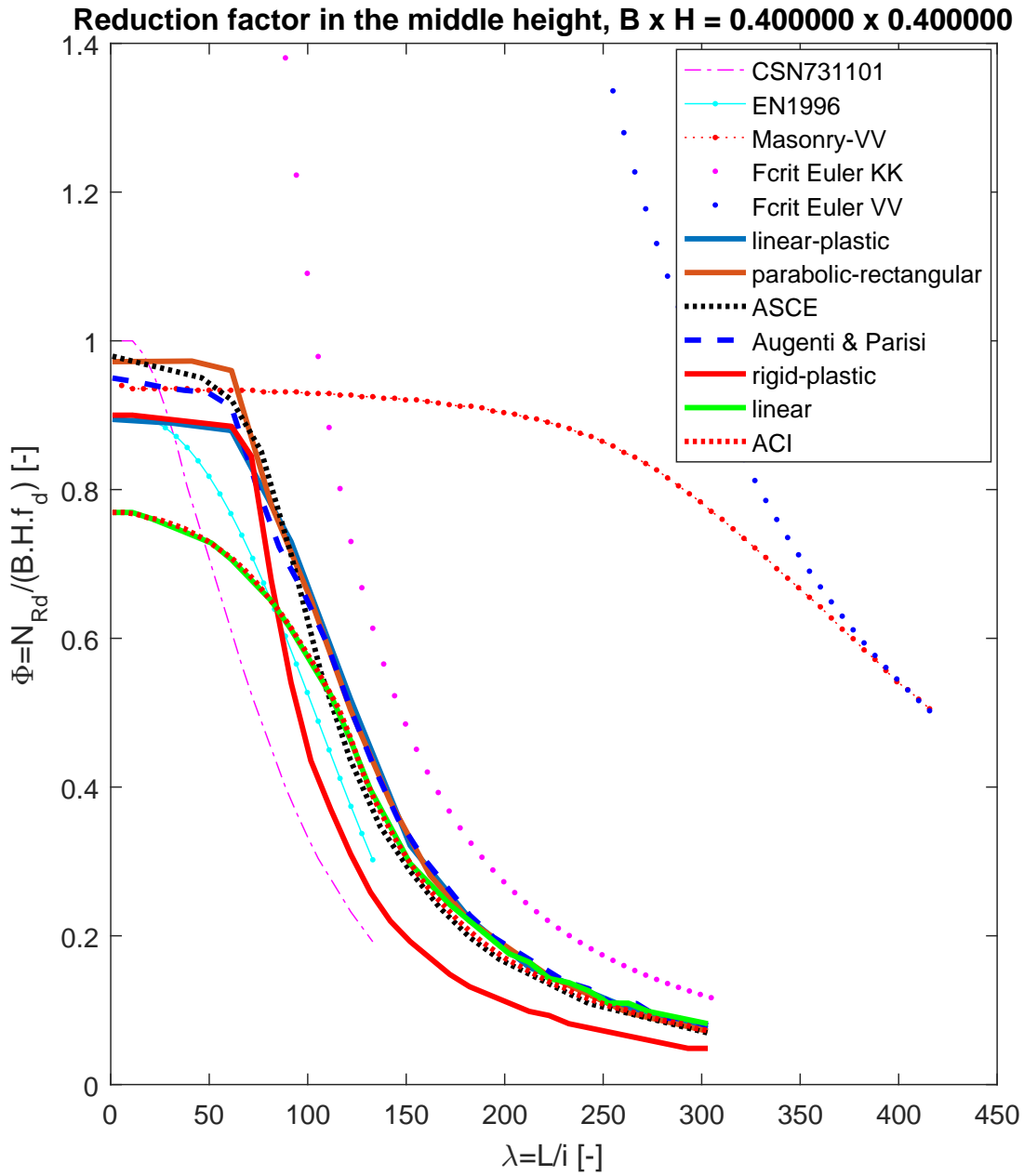
Figure 4.17: Comparison of all examined methods for calculating the slenderness reduction factor Φ.

Figure 4.18: The detail of failure of specimen loaded by force with eccentricities in two directions.

Figure 4.19: The graphical expression of the maximal forces of "1e".

62
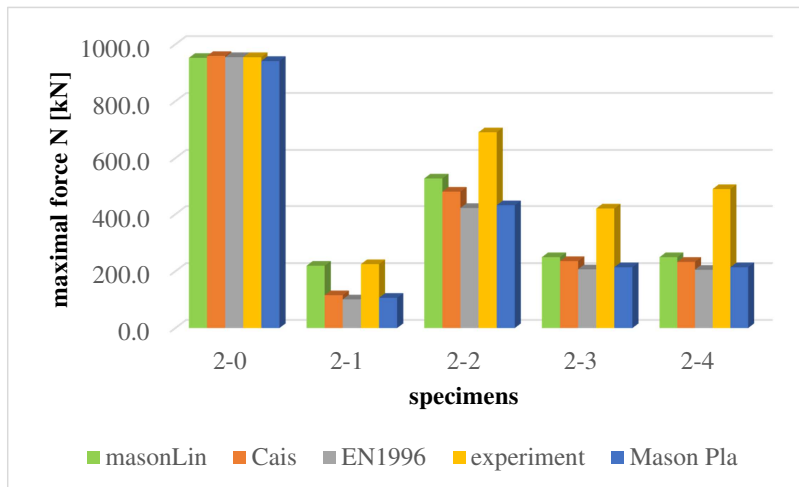
Figure 4.20: The graphical expression of maximal forces of "2e".
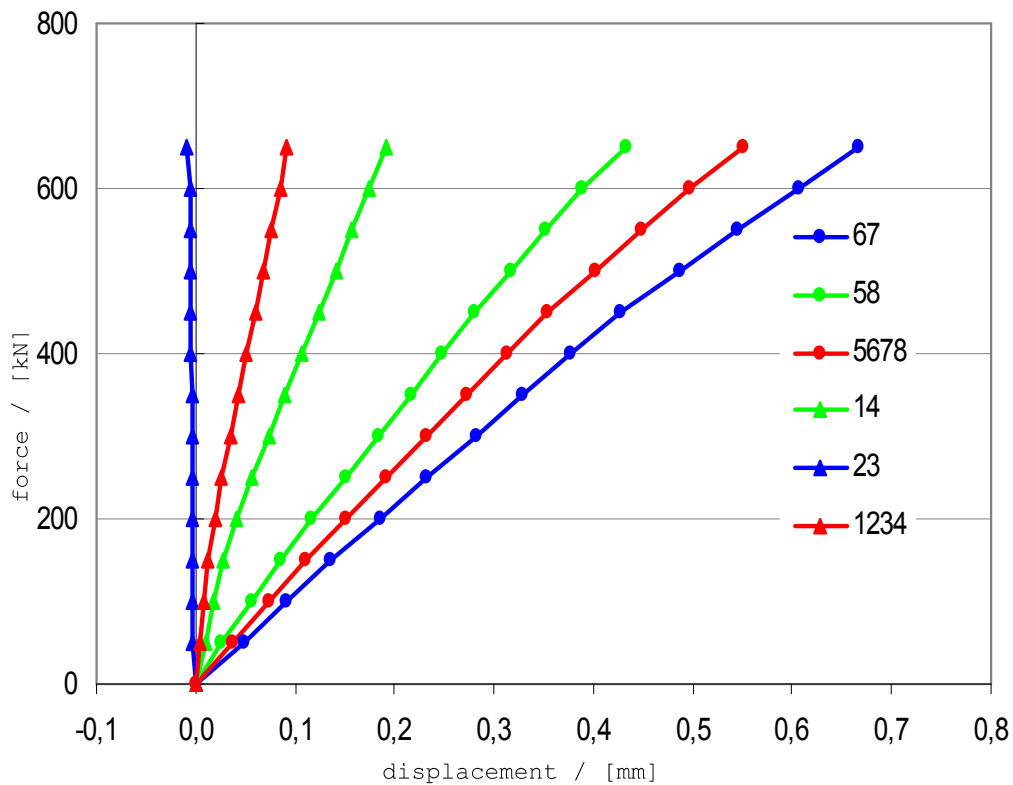
Figure 4.21: Typical strain on the perimeter of the pier.

Part IV

Masonry vaults

Chapter 5

Introduction

Masonry arch bridges are some of the oldest types of bridges. Within the last century, these structures stopped being constructed. Therefore, the arch bridges, which are now still used as railway or road bridges, are between fifty and one hundred and fifty years old. For this reason, the tensile strength of the mortar should be considered to be at the level of zero.

It is modelled by an appropriate stress-strain diagram – zero for the tension (the mortar, which forms the joints, cannot transfer tension). Most of the arch bridge calculation methods consider the tensile strength zero, such as [BdFG01]. "Arch material is compression capable with a negligibly small tensile resistance" according to [Web99]. Due to [Lou02], "Masonry possesses very limited tensile strength and it is usually not possible to make provisions to cover all zones where tensile stresses may appear". According to [Hey98], "the necessary assumptions for the application of plastic theory to masonry is that masonry has no tensile strength". The tensile strength of the material is small, but for example, in the article [RLP16], the tensile strength is used, and the increase of bearing capacity is shown.

The opening of cracks, which might occur due to zero tensile strength, impacts the geometry of a thrust line of an arch. The linear calculation cannot handle the crack opening, which causes significant changes in the final thrust line. The linear calculation and other methods are compared in this chapter.

In the Czech Republic, masonry vault bridges represent 35 % of railway bridges. A similar portion of masonry bridges can be found throughout Europe. According to [Ste12], 80 % of Czech masonry vault railway bridges are older than 100 years. Furthermore, 85 % of Czech masonry vault railway bridges are in a "good" structural state, 14 % are in a "bad" structural state, and 1 % are in a serious, unsatisfactory structural state.

This poor structural state is due to the lack of bridge maintenance and the uncertainty of the inspectors in the assessment. The consequence of such a structural state is the low load carrying capacity (hereinafter referred to as "LCC"), given by the bridge inspection by multiplying the original LCC by α_s, which is ≤ 1. See the general information on the bridge inspections in Section 11.2.2. Consequently, the bridge manager chooses to replace the vault with another bridge. However, the real load capacity determined by the calculation is often significantly higher. The various methods of calculating the LCC and the influence of individual input calculation parameters on the resulting load capacity are discussed in this chapter.

When assessing existing bridges, the requirement for sufficient mechanical resistance and stability is usually given by the LCC – the maximal load that the structure can carry safely, i.e., the maximal weight of the vehicle that can pass the bridge under the specified conditions. The determination of the LCC of the existing bridge is governed by the same principles as the design of the new structures (see applicable technical standards and regulations EN, DIN, and MVL). However, some material and load factors have different values.

Because of the zero tensile strength, the procedures for the determination of the LCC are non-linear and must involve many parameters with significant variability. Therefore, setting up a simple analytical model is very difficult and special programs developed directly for vault structures are usually used.

Chapter 6

The state of the art

Many methods were used throughout history. Methods are described for example in [Knu17] and [SSF16]. Our structuring of methods was taken from [PG09] and enhanced:

- Graphical method - is explained in Section 10.6.1 and [Knu17]. According to [Hey95]: "If the structure is not collapsing, but is in a stable state under the given external loading, there is, in general, a wide choice of possible positions of the thrust line". The solution method according to [Lip98], therefore, consists of choosing the position of a thrust line at the top of the arch and graphically adding the force of the neighbour element. When this is completed for all the elements, and the thrust line lies in the chosen part of the cross section, the vault satisfies the verification.

- Empirical rules.

  - Historical rules: Many empirical relations for the design of masonry arch bridges were suggested. For example, in [PG09], there are twelve relations for the minimal crown joint thickness of the arch.
  - Modern rules:
    - MEXE Method – is explained in [MW10]. "The MEXE method is approximate" – [oR17] and a very simple method for the user. "It is generally accepted that the MEXE method of assessment is derived from Pippard's elastic method (with a point load at the crown)" - [WHM13].
    - Pauser's Method – "Is a simple analysis tool" [Orb07]. The program was created that was based on the linear-elastic failure concept. The method handles just the ULS.

- Beam models.

  - Single beam models – the simplest arch model for the case of consideration of linear behaviour of the material. See the method of using beam elements with non-linearities in Section 8.1.2.
  - Compound beam models – the way of modelling was proposed by [Goc78]. An example of such a model can be seen in Section 11.3.1, where the 2D model was enhanced to 3D to consider spatial behaviour.

- Finite element method: FEM is nowadays the most common method. 2D or 3D models can be done using the beam, planar, or solid elements; assumption of linear or non-linear behaviour is possible. In general, the more is the assumption about material behaviour complicated, the more is complicated the way of observing the input parameters. The example of the use of 2D planar elements can be seen in a comparison of two approaches in [BDS08]. The approach of fill modelling by planar elements with Mohr–Coulomb failure criterion is compared to the approach, where the fill is modelled by a set of non-linear springs in a horizontal direction to represent active or passive earth pressure. Both approaches showed good agreement with the experimental collapse load. Another use of 2D planar elements was shown in [PeD07], where the mortar, stones, backfill, and asphalt-concrete are modelled (micro-modelling). In the article [FAT03], the 8-node quadrilateral elements are used. The tensile strength is limited; in the diagram used, it drops to zero when the limit strain is reached. In the article [ML12], FE discretization of the structure by means of rigid infinitely resistant eight-noded parallelepiped elements and non-linear interfaces is used. The tensile strength is considered for both masonry and backfill. The skew arches can be analysed by this approach; the real 3D geometry and stiffening of the arch by spandrel walls are included.

- Discrete element method (DEM) – is explained in [TOB09], [FSB17], and [SFL19]. The method is useful for large deformations and for a large opening of cracks, which is problematic in FEM, especially from the point of view of convergence.

- Equilibrium method for rigid blocks – see [GM94] and [Gil07].

  - LimitState:RING – see [Gil01] and Section 11.3.3.

- Specialized elasto-plastic software for masonry arch bridges.

  - Archie-M - the program uses basic bridge geometry and material properties to establish the locations of three hinges, followed by calculation of reactions and vector algebra to position the resultant line of thrust - [Cob18]. It is based on plastic theorems. According to [HS95], the Archie software gives results comparable to much more complicated models.

  - A new method was proposed according to [AFSP08]. The results from Limit-State:RING, Archie-M and this new method were compared in [AB10].

The way of material modelling (interaction of masonry units and mortar) is discussed in Section 1.

Chapter 7

Sensitivity analysis of input parameters for the load carrying capacity of masonry arch bridges - ULS

Content of this section was taken mainly from the article [VD20].

In this chapter, nine circular-shaped masonry vault railway bridges and a special case of the Legion Bridge were analysed using the program LimitState:RING [Lim20].

The spans were chosen 6, 12, and 20 m, ratios of v/L (sagitta/intrados span length) were chosen 0.1, 0.3, and 0.5. In the plot legend, "06_0.6" means span 6 m, sagitta 0.6 m, which means ratio 0.1. The ratio p/L (depth of backfill at the top of the arch/intrados span length) is 0.08333. Therefore, the total depth of the backfill is 0.5 m for the 6 m span, 1 m for the 12 m span, and 1.666 m for the 20 m span. The default value of the specific weight of masonry is $25\,\text{kN/m}^3$, of backfill is $18\,\text{kN/m}^3$, design compressive strength is 5 MPa, the friction coefficient 0.6, the angle of internal friction of the soil 30 °, and the cohesion of the soil is considered zero. The thickness of the vault is considered 0.4 m for the 6 m span, 0.5 m for the 12 m span, and 0.6 m for the 20 m span. For further details of the input parameters of the Legion Bridge, see Section 10.

Average input parameters were used for the nine vault bridges, and then, one parameter was considered variable and its impact on the final LCC was examined. The resulting LCC in dependence on this parameter was plotted in a separate graph. This chapter aims to determine which parameters impact the resulting LCC the most.

7.1 Methodology and methods

The methods used to assess masonry arch bridges are described in [PG09]; for the purpose of this chapter, the methods can be divided into:

- Historical simple methods, such as a graphical method.

- Methods used for a real-time praxis, which tend to be as precise as possible.

- Scientific methods, which might be used mainly for academic purposes.

An example of a scientific method is a fracture model used by the software ATENA, which is described, for example, in [Som11]. The parameter "Specific fracture energy" G_f is

an important input parameter ("higher values of fracture energy considerably increases both the limit displacement and the load-bearing capacity"). Despite this fact, the parameter G_f is practically impossible to obtain. Therefore, this chapter uses real-time methods and describes how to use them in praxis by showing examples. The sensitivity analysis shows the importance of obtaining the values of the input parameters.

7.1.1 Methodology of analysing LCC

LCC is described by moving load, which can the bridge safely carry. Conditions, which must be fulfilled, are specified by current codes – Eurocodes, namely by [PL07]. Eurocodes define the Serviceability limit state – SLS (which provides the usability and durability of the structure) and the ultimate limit state – ULS (state of collapse of the structure, but also ensures the durability of the structure in general). The LCC of the railway bridges is based on the load model 71 [ÚN05a], which is also used for the design of new railway bridges. (It consists of forces 4x250 kN and a uniform continuous distributed load of 80 kN/m. See the model view in Figure 9.1). The LCC (in plots named Z_{LM71} according to [SŽ15]) is equal to the multiple of load model 71, which can pass the bridge while fulfilling the conditions of ULS and SLS. The LCC of the new bridges must be at least 1.

7.1.2 Assumptions of analysis, used methods

In this chapter, the program which uses the equilibrium method for rigid blocks (also called Rigid block analysis) and which was created especially for modelling of masonry arch bridges was used:

LimitState:RING

This program is designed for collapse analysis – the ultimate limit state. Cracks can open up, parts of the cross section can crush. See the details of the crushing below in this section and Section 7.2.1.

The method was proposed in [GM94] and was further described in [Gil07] and [Gil01].

In the program LimitState:RING, the masonry vault is modelled as a system of rigid blocks. The method is based on computational limit analysis methods (also known as "plastic" or "mechanism" methods). If the thrust lines lie entirely within the masonry cross section and the hinges form at the locations, where the lines of thrust touch maximally the exterior faces of the blocks, the structure does not collapse. A hinge is created if the thrust lines lie outside the cross section. The formation of a sufficient number of hinges (and/or planes of sliding) leads to a collapse.

The calculation is carried out in following steps: calculation of internal forces on linear beam model; finding the points of a vault, where the collapse of masonry block occurs; finding the collapse mechanism; build up the equation (equilibrium of blocks) with the unknown of the safety factor – multiple of traffic loads, which cause collapse. These equations are built upon the theory of rigid bodies, where the vault is divided by the collapsed block.

The number of such a collapsed block has to be as big as to create a moveable mechanism. See the collapse modes also in [Och02].

The minimal multiple of all load positions shall be selected. This minimal value is called the "Safety factor". If the Safety factor is greater than or equal to 1, the structure can carry the specified load. There are two possibilities of modelling: considering masonry blocks as rigid slabs or considering crushing of masonry blocks at a certain value of stress. Considering the crushing always decreases the LCC, see Figure 7.4. In this chapter, the value of design masonry strength f_d was considered. See also Section 7.2.1.

The resulting collapse mechanisms can be divided into the following cases:

- Mode I - collapse by the crushing of masonry - see Figure 7.1.

- Mode II - see Figure 7.2; the line of thrust touches the exterior faces of the masonry blocks and forms the four-hinge mechanism.

- Mode III - collapse by the shearing between the blocks - see Figure 7.3.
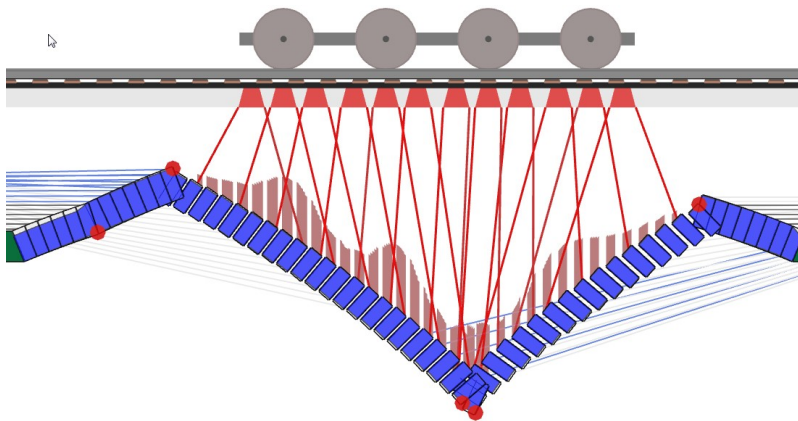
Figure 7.1: Collapse by crush of masonry (mode I).
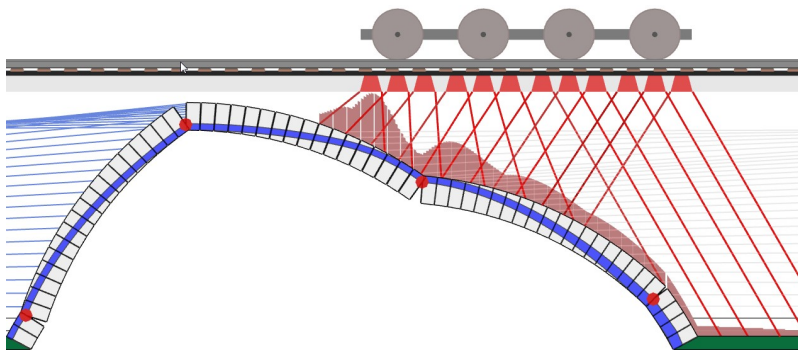
Figure 7.2: Collapse by opening of cracks and forming the four-hinge mechanism (mode II).
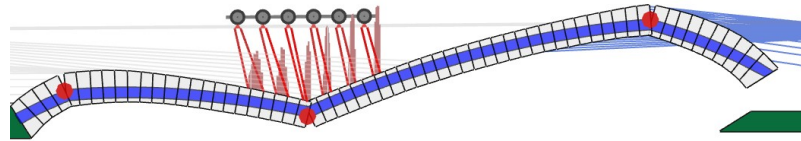
Figure 7.3: Collapse by shear between the blocks (mode III).

The temperature loads cannot be handled in this program. This comes from the idea that the temperature effect is minimal if the structure is at a state of collapse due to the crack opening (or other collapse mechanisms).

The program LimitState:RING gives two options for analysis. The joints transfer the compressive force in the vault:

(i) Through an infinitely thin strip of stone at the edge of the vault (external when collapsing towards the inside of the arch, internal when deflecting outside the arch), if infinite strength of the masonry is assumed.

(ii) Through a rectangular strip representing the stress at which the masonry is crushed.

It is possible to plot a graph of the M-N diagram (the combinations of the acceptable moment and axial capacities of a structural member at the ULS) for both options:
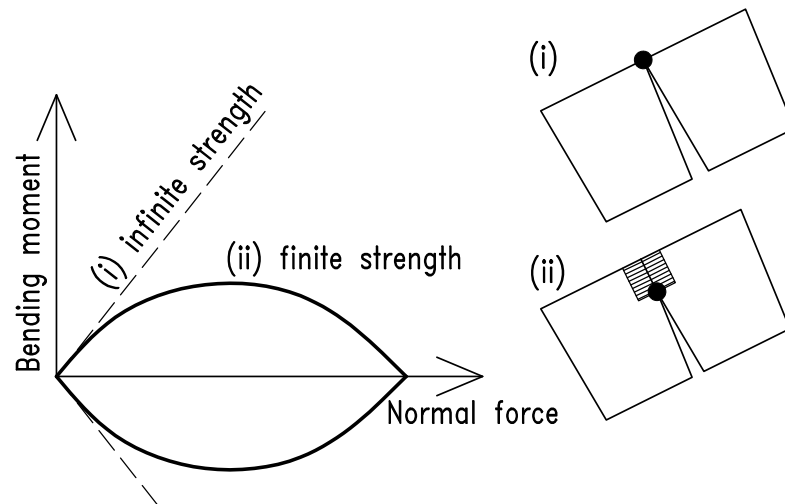
Figure 7.4: The M-N diagram, compressed area.

For the case of infinitely stiff blocks, the curve of the M-N diagram is linear. The black dot is the point of rotation of the blocks when creating a moveable mechanism.

In the case of infinite strength (i), the task is linear; in the case of finite strength (ii) - considering crushing - the task is non-linear. The program solves the non-linear crushing problem as an iterative linear problem with defined boundary conditions under which sufficient calculation precision is fulfilled. In this chapter, the crushing of masonry is considered.

The live load dispersion (distribution) is done after Boussinesq, see the [Lim20]. The example of distribution in the longitudinal direction see in Figure 10.8. The distribution in the transverse direction see in Section 7.2.9 and 11.3.3. The load is distributed at angle ϕ_{Ball} in the ballast and ϕ_{Back} in the backfill.

7.1.3 Investigated parameters

1. Masonry strength.

2. Coefficient of friction in joints of masonry.

3. Backfill depth.

4. Backfill slope.

5. Specific weight of masonry.

6. Specific weight of backfill.

7. Backfill angle of internal friction.

8. Backfill cohesion.

9. Effective vault width.

10. Poisson number.

11. Shape of vault.

12. Vault thickness.

7.2 Results of the modelling

7.2.1 Masonry strength

See the equations for calculation of masonry strength in Section 1. The determination of the characteristic masonry strength according to Equation 1.2 is very sensitive to both the strengths of the masonry units and strength of the mortar. One can see directly that the power of 0.7 is higher than that of 0.3, and therefore, the parameter of masonry units is more sensitive. On the other hand, the values of strength of mortar usually have a much larger variance.

For the example of Legion Bridge (see Section 10), mortar strength varies from $3.5 - 20$ MPa in 59 tests, coefficient of variation equals 54 %, masonry unit strength varies from $100 - 164$ MPa in 20 tests, coefficient of variation equals 16 %.

See the details of the assessment of masonry unit strength in [Klo16b]. The design strength of the masonry is calculated according to Equation 1.3.

See the results obtained from modelling in the program LimitState:RING in Figure 7.5.

.
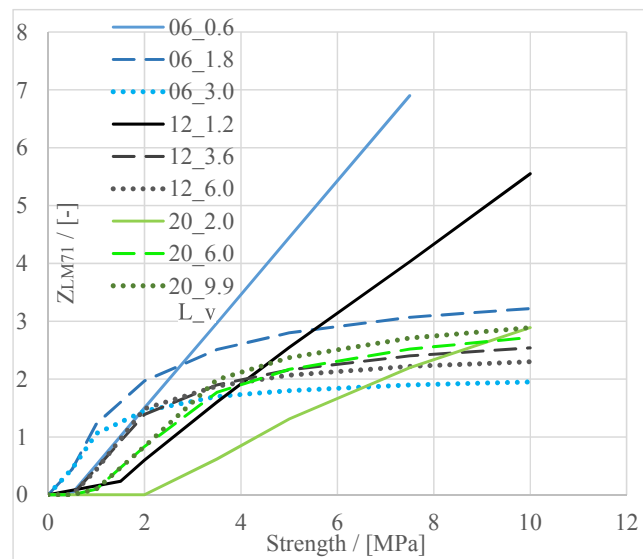
Figure 7.5: Load carrying capacity in dependence on the design strength of masonry. For the legend, see Section 7.1.2

▪ **7.2.2 Coefficient of friction in joints of masonry**

The collapse mode III (the shear mode) might occur if the shear resistance is not satisfactory. The shear is checked at the ultimate limit state only. The shear resistance is determined according to Equation 2.2.

The most significant influence on the shear resistance has normal stress multiplied by the coefficient of friction μ. The normal force arises from the shape of the vault and the load applied. Figure 7.6 shows the LCC of nine circular bridges depending on the coefficient of friction. The LCC according to the shear is quite high:
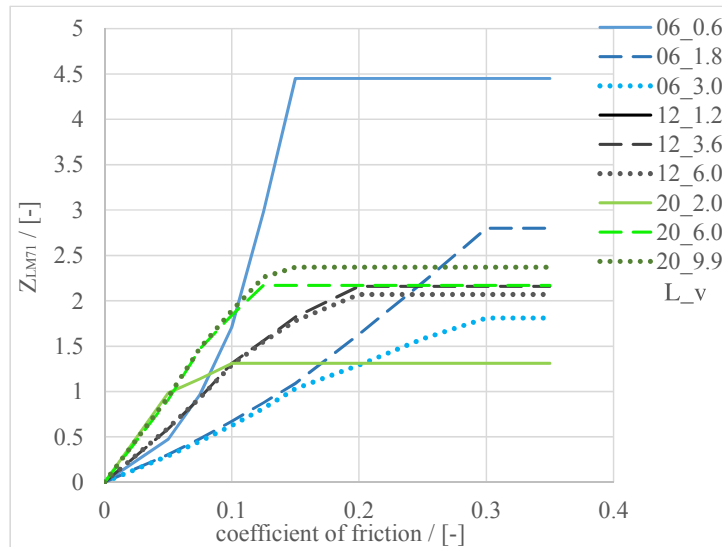
Figure 7.6: Load carrying capacity in dependence on the coefficient of friction.

Figure 7.7 displays the LCC of the Legion Bridge (see Section 10), which is significantly lower. Differences are due to the shape of an arch. For circular arch shape, the collapse occurs if the value of μ is zero, for the Legion Bridge the collapse occurs if the value of μ is 0.3 for the span 4 and 0.03 for the span 5. For the purpose of comparing Figure 7.7 and 7.6, the Z_{LM71} was calculated for the road bridge.
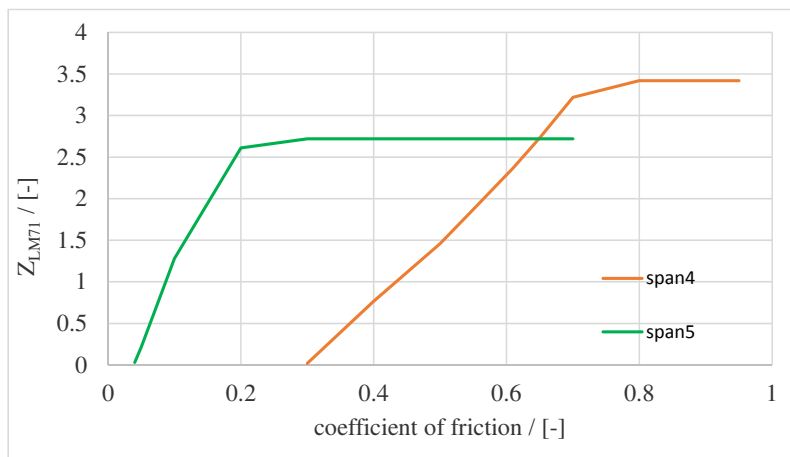
Figure 7.7: Load carrying capacity in dependence on the coefficient of friction – Legion Bridge, spans 4 and 5.

LCC for shear depends strongly on the shape of the arch; LCC of part-of-ellipse is much lower because of the shear. In general, this is a common problem of ellipse vault bridges. Therefore, it is necessary to consider the combination of shear forces from transport load with shear forces from a temperature change (increasing the temperature of structure is decreasing the LCC). For the sensitivity analysis of vaults of different shapes, see Section 7.2.11. It can also be seen from Figure 7.7 that for each vault there exists a value

of a coefficient of friction, which increasing does not cause an increase of LCC because collapse mode III does not occur any more.

According to [OET16], the coefficient of friction has the value from 0.597 to 0.705. According to the LimitState:RING manual, the coefficient value is 0.6. According to the current standards –[PL07], the coefficient of friction μ is 0.4 and should be divided by a coefficient γ_M, which is usually equal to 2. Therefore, the coefficient of friction is equal to 0.2 for new structures. For Legion Bridge, the LCC is around zero according to Figure 7.7. However, this is not true; the real coefficient of friction is much higher. Current standards do not specify the value of the coefficient of friction for existing bridges.

■ 7.2.3 Depth of backfill

Figure 7.8 was taken from [oR17]. The depth of backfill impacts the final LCC several ways:
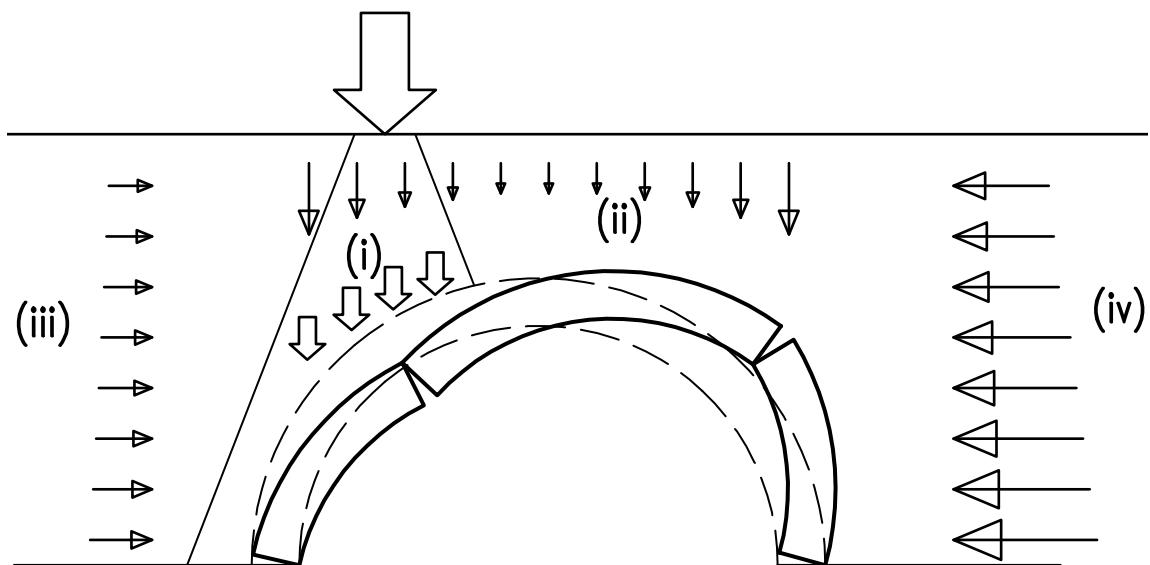
Figure 7.8: Impacts of backfill on the vault (i – disperse of live load, ii – self-weight of the soil, iii – active earth pressure, iv – passive earth pressure.

For the vaults of low sagitta (rise of the arch), the LCC decreases when the depth of backfill is increasing because the compression, which is decisive, is growing. For other vaults, the LCC is growing because the vault is stabilized; see Figure 7.9.
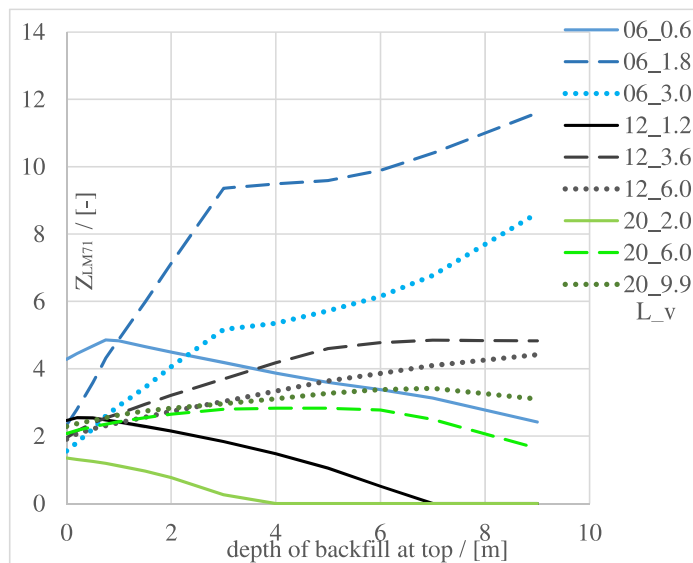
Figure 7.9: Load carrying capacity in dependence on the depth of backfill.

Since the backfill influences the final LCC in many ways, further investigation of some parameters of backfill are provided:

7.2.4 Backfill slope

The longitudinal slope of the railway or road causes an asymmetric load of the vault. For ease of construction and considering the fact that the longitudinal slope of the bridge can be changed during reconstruction, the vault shape has usually not been changed (is symmetrical). Therefore, the longitudinal slope is a factor that always reduces the final LCC of the bridge, see Figure 7.10.
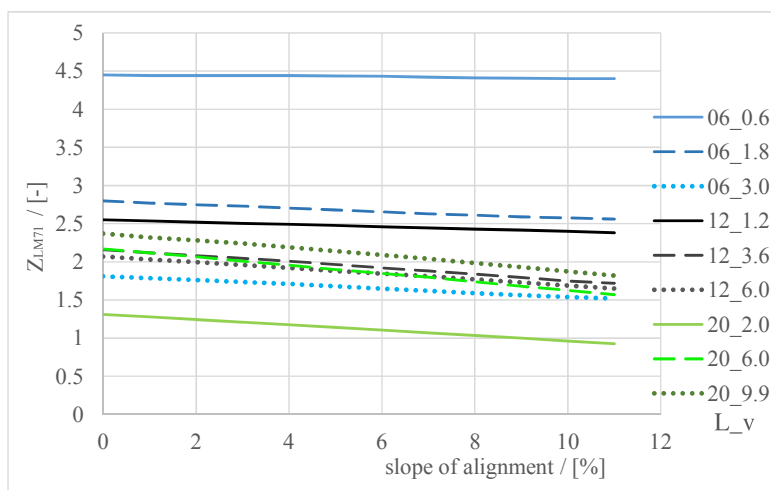
Figure 7.10: Load carrying capacity in dependence on longitudinal slope.

79

7.2.5 Specific weight of masonry

Increasing the symmetric load is positive for the overall stability of the vault, as the effect of unsymmetric loads (e.g., traffic load) is reduced. Therefore, it usually increases the final LCC. The calculation assumed a finite compressive strength; a value of 5 MPa was considered. For the arch, with low sagitta (solid line in the plot), the increase of specific weight causes that stresses exceed the compressive strength, and crushing failure mode occurs, which decreases the final LCC, see Figure 7.11.
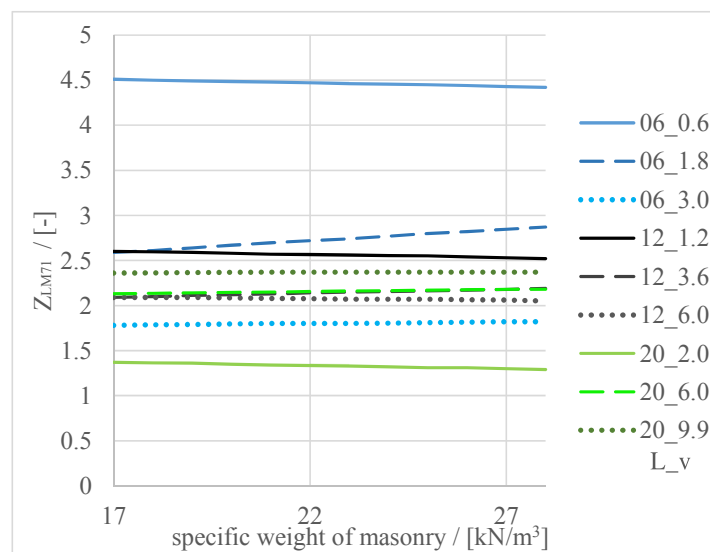
Figure 7.11: Load carrying capacity in dependence on the specific weight of masonry.

7.2.6 Bulk density of backfill

The effect of the bulk density of the backfill is similar to the effect of the specific weight of the masonry. Within the range of relevant specific weight, which can occur, we can say that the masonry specific weight parameter is less sensitive than the parameter of bulk density of the backfill, see Figure 7.12.

80
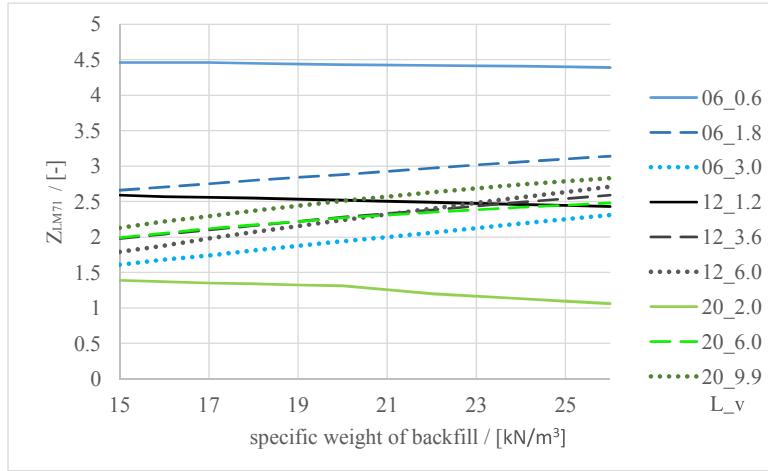
Figure 7.12: Load carrying capacity in dependence on the specific weight of the backfill.

7.2.7 Angle of internal friction of soil

Horizontal stress, which acts on the extrados (if the direction of deformation is towards the soil – see the blue lines in Figure 7.2) is calculated according to [Lim20] as:

$$\sigma_h = m_p.K_p.\sigma_v + m_{pc}.K_{pc}.c, \tag{7.1}$$

where:

$$K_p = \frac{1 + sin\,\varphi}{1 - sin\,\varphi} = tan^2\left(45° + \varphi/2\right), \tag{7.2}$$

$$K_{pc} = 2\sqrt{K_p}, \tag{7.3}$$

where:

- $m_p = 0.33$ – coefficient obtained experimentally,
- σ_V is vertical earth pressure due to dead loads,
- $m_{pc} = 0.05$ – coefficient obtained experimentally,
- c is cohesion of the soil,
- φ is angle of internal friction of the soil.

Values of m_p and m_{pc} (see [Lim20]) have been shown to give a reasonable prediction of collapse load in physical model tests on single-span bridges. By default settings of the program and according to [Lim20], which arises from experiments, the value of $m_p.K_p$ is greater than or equal to 1, which means, that $\varphi \geq 30$. From these assumptions, we obtain the following plot - Figure 7.13.

81
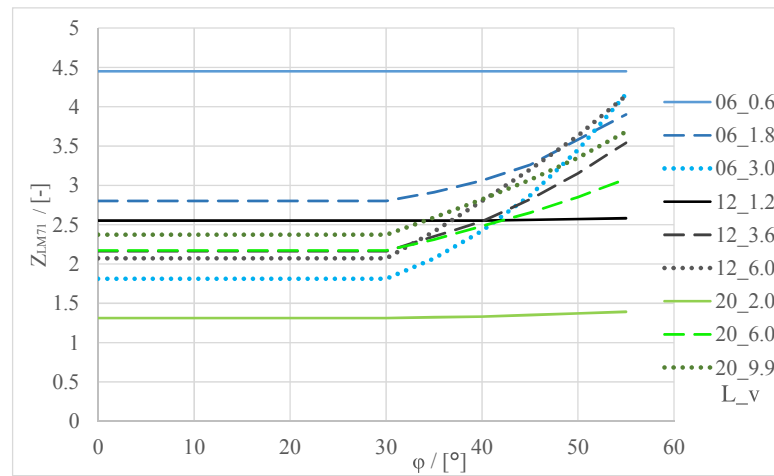
Figure 7.13: Load carrying capacity in dependence on angle of internal friction of soil.

If we consider, that $m_p.K_p$ can be lower than 1, we obtain following plot - Figure 7.14:
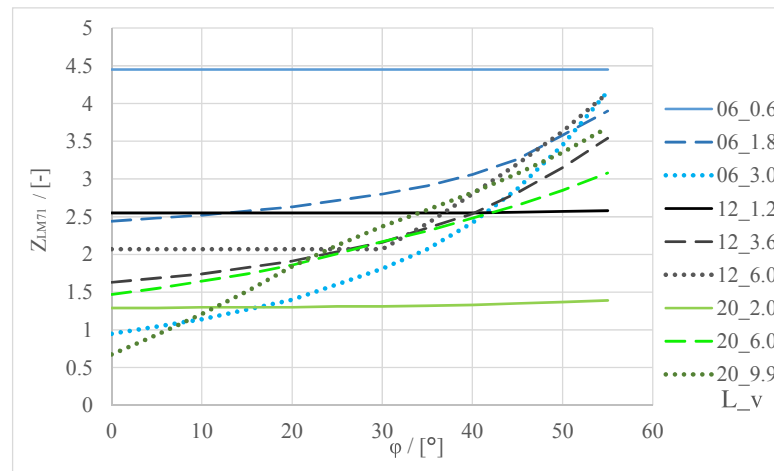
Figure 7.14: Load carrying capacity in dependence on angle of internal friction of soil.

As can be seen in Figure 7.14, the increase of the angle of internal friction increases the final LCC significantly. It is caused by a passive earth pressure, which stabilizes the vault in the horizontal direction in ULS very well. Note that for arches with low sagitta, the increase of LCC is minimal because the mode of failure is governed by the crushing of the masonry, according to Fig. 7.1.

▣ 7.2.8 Cohesion of soil

As can be seen in Figure 7.15, the increase of soil cohesion slightly increases the final LCC. Cohesion helps to increase the passive earth pressure (see Equation 7.1) and stabilizes the vault. Due to the value of m_{pc}, which is equal to 0.05, the increase of LCC is very low.
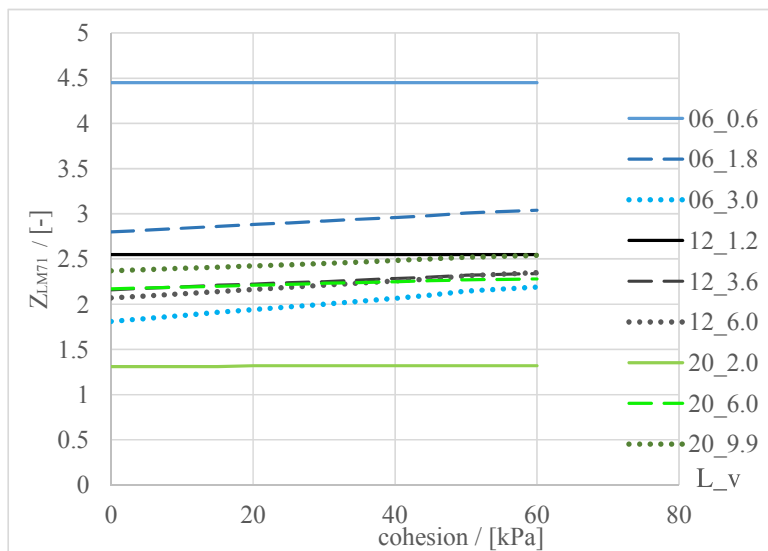
Figure 7.15: Load carrying capacity in dependence on cohesion of the soil.

▣ 7.2.9 Effective width

For analysis in 2D and specific cases of 3D analysis, program LimitState:RING uses effective width concept. This method is used because the shear and tensile strength between the masonry blocks in the transverse direction are unknown and probably very small, so detailed modelling is usually not possible. The method of graphical assessment of effective width can be seen in Fig. 7.16. See more ways of assessing the effective width in Section 11.3.3. In LimitState:RING, the "classical model" is used.
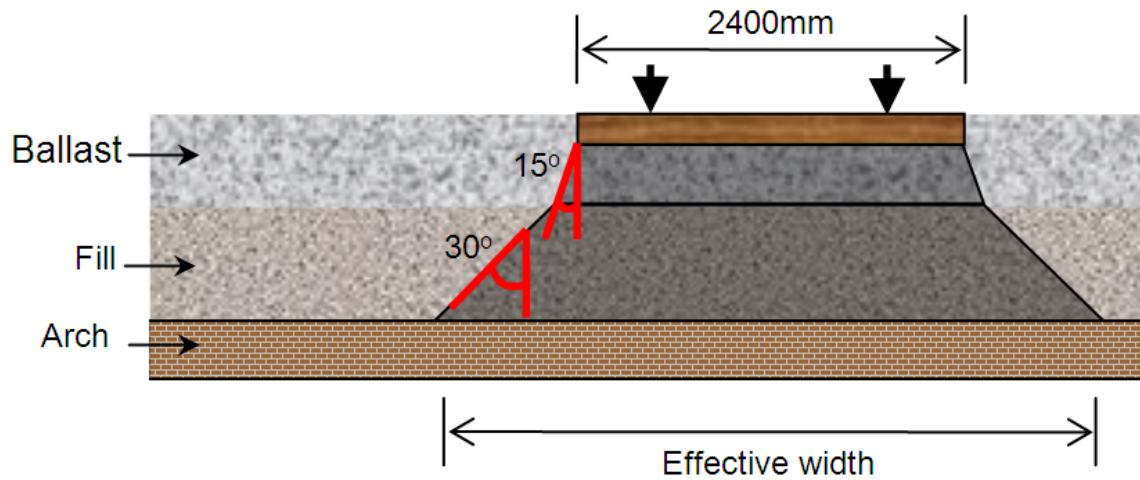
Figure 7.16: Assessment of the effective width used in the LimitState:RING program.

The effective vault width used in the calculation depends on the load distribution angle and the depth over which the load can spread. The dependence of LCC on effective width is linear.

7.2.10   Poisson ratio

The poisson ratio does not impact the normal and shear stresses in the longitudinal direction of the vault, which are verified. The transverse direction of the vault is not verified. The standard [PL07] does not demand it.

7.2.11   Shape of the vault

All common or uniquely occurring shapes (according to [Lip98]) of the vault were analysed; see the shapes in Figure 7.17.
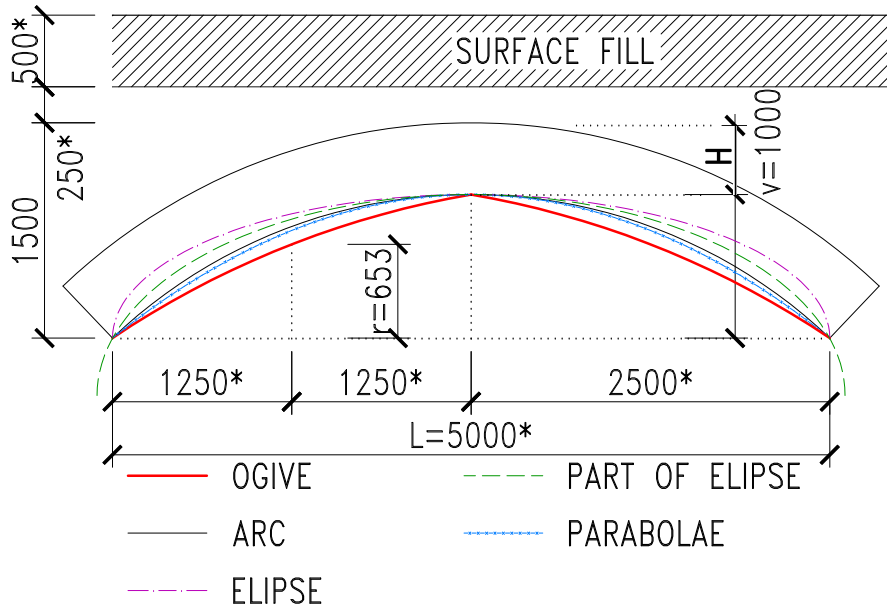
Figure 7.17: Considered shapes of vaults.

Parameters marked with * are considered fixed in this study. A vault with intrados span length L of 5 m and depth of the backfill at the top of 0.25 m and ballast of 0.5 m was considered. Four different vault heights in the middle of the span (= sagitta) of 2.5, 1.75, 1, and 0.5 m were compared. In building structures, there are special vaults, which are not considered in this chapter, e.g., arches composed of several circles and ellipses, rising arch (one support is higher than the second one), or arch of Islamic architecture. Figure 7.17 shows the assessed shapes of intrados of the vault. The extrados is shown only for the circular arch for clarity.

The resulting safety factors for different shapes of vaults can be seen in Figure 7.18:
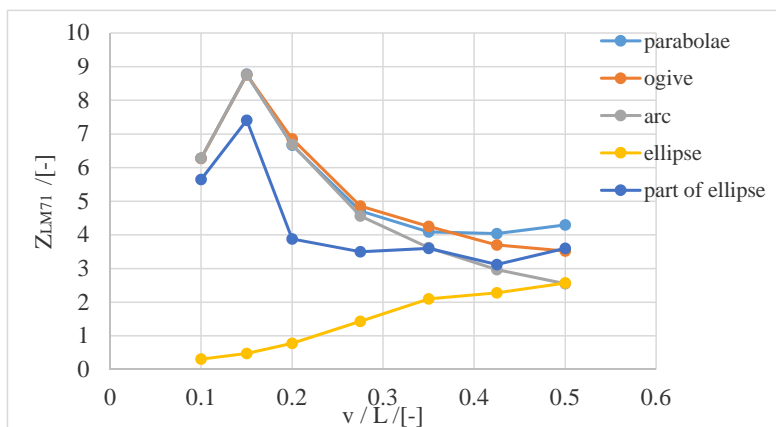
Figure 7.18: Load carrying capacity in dependence on ratio v/L.

The results are influenced by the fact that all possible failure modes can occur, which

85

means that the LCC is significantly decreased by shear force, especially for the ellipse. Depending on the chosen part of the ellipse, the resulting LCC of the ellipsoid bridge is between the two curves in the plot. The curve "ellipse" represents one-half of the ellipse. For the ogive (Gothic) shape, only the maximal LCC is plotted. See detailed results of the ogive-shaped vault in Figure 7.19 (name of set "0.5" means vault $v/L = 0.5$). The variable parameter of the ogive shape is r, see Figure 7.17.
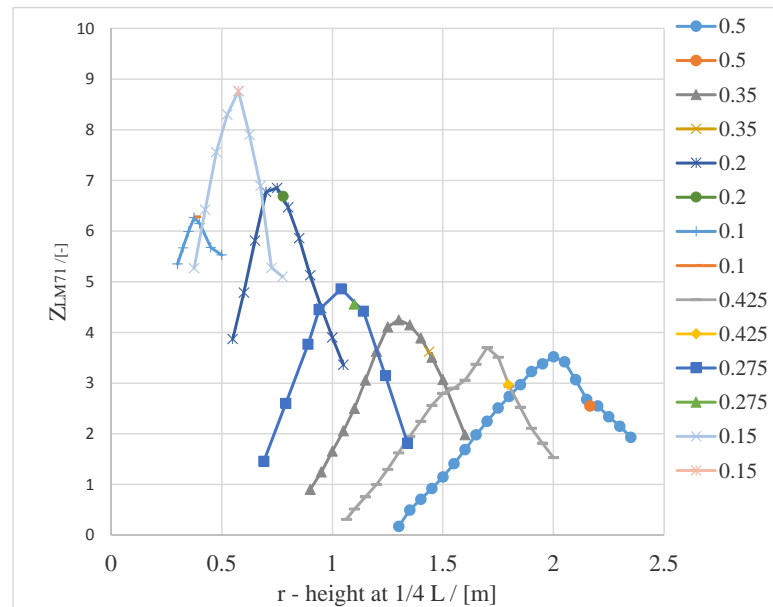
Figure 7.19: Dependence of LCC on r (see Figure 7.17).

The highlighted value (always the second set from the two sets with the same name) represents the value of r such that the shape of an arch is circular. For the low ratio v/L, the circular shape has the highest LCC; for the high ratio v/L, the Gothic shape has a higher LCC than the circular shape.

■ 7.2.12 Thickness of the vault

The thickness of the masonry blocks of a vault is a very sensitive parameter. Increasing thickness leads to an increase in the area where the thrust line can develop. It also increases the compressed area; the stresses from the load decrease rapidly. See the results of the modelling in Figure 7.20.

■ 7.3 Conclusions

See the conclusions of the sensitivity analysis in Section 8.4.
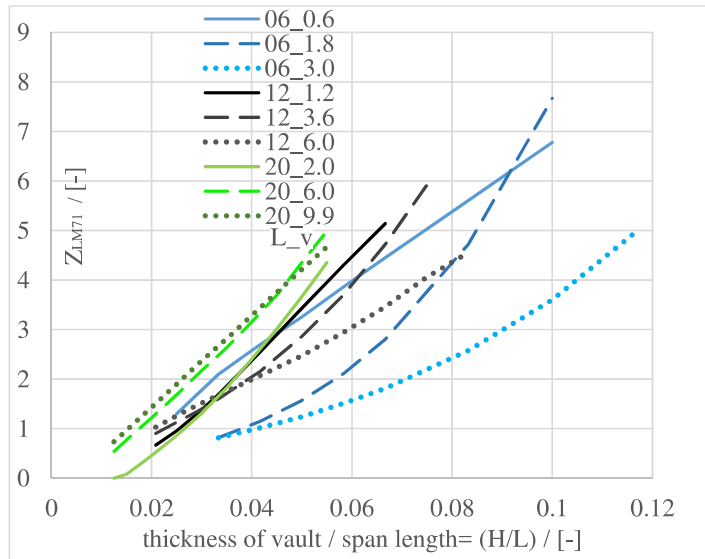
Figure 7.20: Dependence of LCC on the ratio H/L.

Chapter 8

Sensitivity analysis of input parameters for the load carrying capacity of masonry arch bridges - SLS

The content of this chapter is taken mainly from the article [VD22a]. The motivation and introduction are given in Section 5.

In this chapter, nine circular-shaped masonry vault railway bridges were analysed. The parameters of nine vaults were chosen according to the previous chapter, Section 7. The spans were chosen 6, 12 and 20 m, ratios of v/L (rise/intrados span length) were chosen 0.1, 0.3 and 0.5. In the legend of the plot, "06_0.6" means span 6 m, rise 0.6 m, which means ratio 0.1. The ratio p/L (depth of backfill at the top of the arch/intrados span length) is 0.08333. Therefore, the total depth of the backfill is 0.5 m for the 6 m span, 1 m for the 12 m span, and 1.666 m for the 20 m span. The default value of the specific weight of the masonry, the specific weight of the backfill, the friction coefficient, the angle of internal friction of the soil, and cohesion of the soil are the same as in Section 7.1.2 above. The characteristic compressive strength is 5 MPa. The thickness of the vault is considered to be 0.4 m for the 6 m span, 0.5 m for the 12 m span, and 0.6 m for the 20 m span.

Then, LCC was analysed for the road bridge – span 4 of the Legion Bridge in Prague (see Section 10), which has an elliptic shape, and span 5, which has circular shape. This bridge was loaded by the railway load model 71 to compare the result with other bridges studied in this chapter. The finite element program Midas [MID19] was used for modelling, which allowed us also to mode the temperature load. As a source for this calculation, the real diagnostic survey is available – see [IPI19]. This survey is very detailed and was quite expensive. This chapter was created to help save some money for the diagnostic surveys and to focus only on the most critical parameters.

8.1 Methodology and methods

8.1.1 The method of verification

The equations for the verification at the SLS see in Section 2.2, at the ULS see in Section 2.1. The first main indicator of how the cross section of the height H is loaded is the position of the thrust line. The thrust line is a locus of points through which the resultant force

89

STATE OF STRUCTURE IN DEPENDENCE ON POSITION OF THE RESULTING THRUST LINE
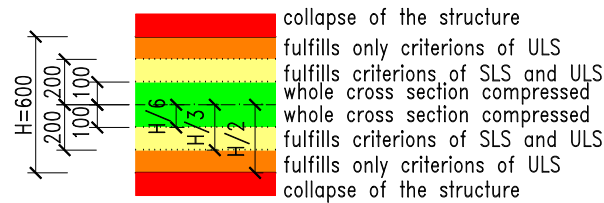
Figure 8.1: Verification of the position of the thrust line. The state of structure is represented by the colour.

goes. For each point of the vault, it can be (for the case of beam model) calculated as $e_{Th} = M/N$, where M is the bending moment, and N is the normal force applied on the cross section – from the load in given combination. The higher the bending moment is applied on the cross section, the higher is e_{Th}, and the more reduced is the compressed area. To fulfil the criteria of the SLS, e_{Th} must be less than $H/3$ according to [HD08], to fulfil the criteria of the ULS, e_{Th} must be less than $H/2$. Eccentricity larger than $H/2$ means that the thrust line lies outside the cross section, leading to the collapse of the structure (if the tensile strength is neglected); this is illustrated by Figure 8.1.

The method of obtaining the e_{Th} depends on the chosen model. For the case of 2D planar elements, the verification can be done by checking that the height of the compressed area is at maximum $0.5\,H$. For the case of the linear beam model, e_{Th} can be obtained in a single step. For the case of the non-linear beam model, the e_{Th} varies for each step of calculation, and only the steps which fulfil the criterion of convergence (and equilibrium conditions as well as limit strain conditions) can be taken as a final value of e_{Th}.

The second main indicator of the state of the vault is normal stress acting on the cross section due to the given load. In the SLS, the stress should be less then or equal to $0.45 fk$. This criterion ensures that no point of the structures will crush during the usual loading conditions. On the other hand, the crushing is permitted in the case of the ULS, a state of collapse of the structure.

■ 8.1.2   The used method - MVo

The algorithm which was created using MATLAB® software, can deal with circular arch bridges or arch bridges given by the set of points representing arch axis and input of the desired degree of a polynomial, which will be used to find a smooth geometry of the arch axis by the least square method. It is assumed that such a set of points can be obtained, for example, by geodetic measurements. In this chapter, the results of circular arch bridges will be presented. See the example of the Legion Bridge in the literature [VD19] (or Section 10.6.3), for which the geometry was fitted by the least square method of the polynomial of 8th degree. The main property of the model is that it uses beam elements. From 128 to 256 elements are used. The axis of the original arch is considered for the first step of the calculation. Then, due to crack opening, the geometry changes. The cross section properties (area and moment of inertia) are changed correspondingly according to
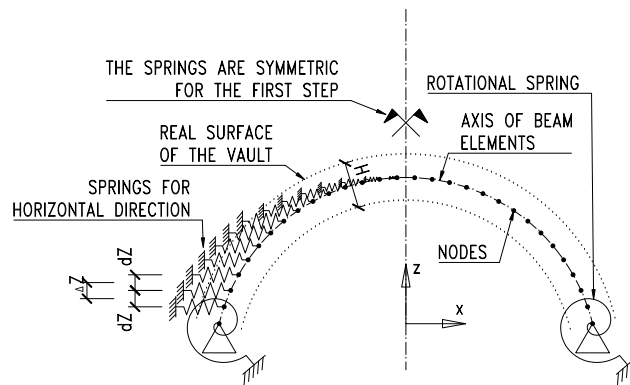
Figure 8.2: The model used in the first step of the calculation.
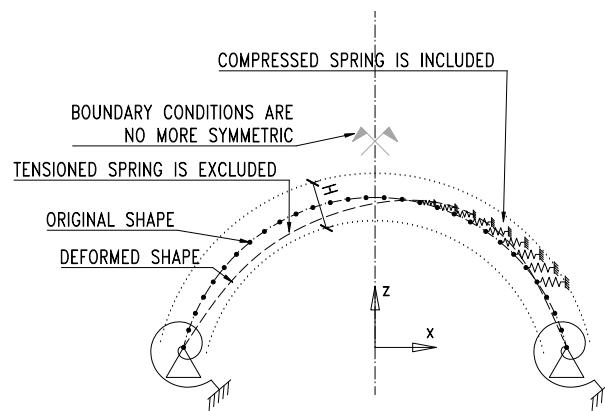
Figure 8.3: The model used in the second and every other step of the calculation.

these geometry changes. The new geometry of every node in every step is "guessed" as the geometry of a thrust line of the previous step.

The masonry can be modelled in several ways. The simplest method is to use a homogenized model, which merges the mortar and units in one single material. This approach is also used in the MVo code. See the details of masonry homogenization in Section 1. The geometric non-linearity is solved only in the created algorithm – MVo code; other used methods do not consider it. The effect of geometric non-linearity cannot be neglected just for the case of arches of a large span and low ratio sagitta over span of the arch. In this chapter, a sensitivity analysis of key input parameters is done using the MVo code.

The initial boundary conditions and model view can be seen in Fig. 8.2. The springings are supported by hinges (fix both x and z displacements) and rotational springs (partially fix rotations). The springs representing the backfill behaviour act linearly for compression in the soil, and the stiffness in the tension is considered to be zero. The fact that the stress in the soil is either tension or compression is assessed by the deformation from the live load. The spring acts only in a horizontal direction. The boundary conditions for the next steps see in Fig. 8.3. The stiffness of the spring is calculated from E_{def}:

$$K_{spring} = E_{def}.\Delta Z.B/\Delta L, \tag{8.1}$$

91

where:

- K_{spring} is the stiffness of the spring in the given node,
- E_{def} is the deformation modulus of the soil,
- B is the width of the vault. In most cases, the effective width b_{eff} is used. See also Section 11.3.3.
- ΔL is the length of the substituted soil (different for each node), see Figure 9.1.
- ΔZ is one-half of the horizontal projection of the distance between two adjacent nodes to the given node.

Assumptions of the calculation

- the supports at the arch springing are considered infinitely stiff, no deformation is allowed, i.e., no uneven settlements of supports are considered.

- The Bernoulli-Navier hypothesis (also called the Euler–Bernoulli beam theory) for beam elements is considered.

- Only one soil is considered for all points of the backfill.

- There is no inflection point in the geometry of the arch in the case of polynomial shape.

- The new position of the nodes must lie on a normal line of the curve of the original axis geometry.

- In the study of the sensitivity of input parameters, the arch is symmetric; the longitudinal slope of alignment of a railway is considered zero. The thickness of the arch is constant.

See the loading conditions in following Figures 8.4, 8.5 and 8.7. The structure is loaded by self weight, weight of the backfill, ballast, earth pressure, and live loads.

The live load dispersion (distribution) is done in the same way as in LimitState:RING, see example from the LimitState:RING manual in Figure 10.8. Example of output of MVo code see in Figure 8.6 and 8.7. The Boussinesq distribution is used, see the [Lim20]. The load is distributed at angle ϕ_{Ball} in the ballast and ϕ_{Back} in the backfill. This distribution is displayed in Figures 8.6 and 8.7 and it is denoted as "left and right dispersion lines". The figures are examples of a moveable load position. The "length of model" means the length of load model 71. In the MVo code, the length is calculated as 4.8+0.8*2=6.4 m because the concentrated axle forces are considered as distributed in the uniform load. The nodes, which are between left and right dispersion lines, are loaded by the load model, the other ones are not loaded by the live load at the examined load position. The length of the blue vertical lines represents the value of force acting in the node.

The algorithm developed can be used to calculate LCC at the SLS or the ULS. In this section, only SLS is handled. The collapse load can be calculated in other software, such as LimitState:RING, see [Lim20] and [VD20]. RING was also used in other sections, such as 7.1.2.
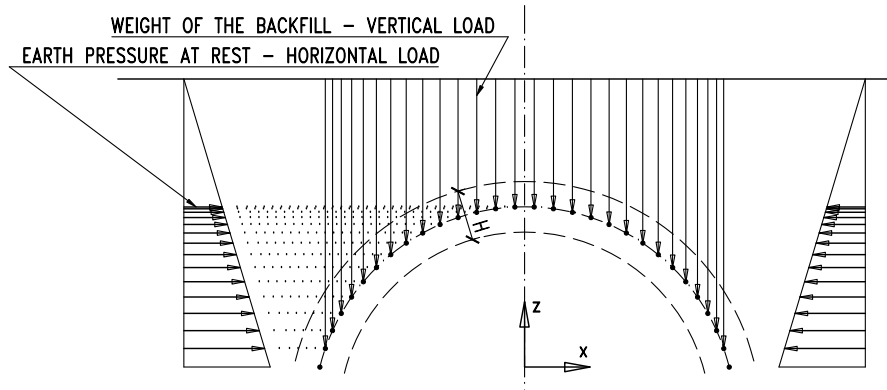
Figure 8.4: The load of the model by earth pressure.
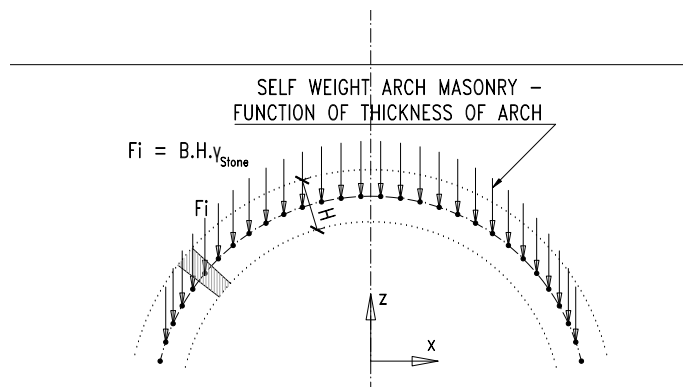
Figure 8.5: The load of the model by self-weight of the masonry arch.

The geometric non-linearity is solved by the second-order analysis; the material non-linearity is modelled by the crack opening and changes of cross section, which are sought iteratively. The equations used are described in [VD21], [VD18] and Section 2 and 4.3.3.

The smooth geometry is needed for all steps of a non-linear calculation. This is a typical property of the beam model. Even a small aberration from the smooth geometry causes the unreal values of internal forces, especially the bending moment and the shear force. In the algorithm, the small aberration always occurred during tens of steps, which led to unreal results. There are two ways to deal with this problem. The first is to use many (at least thousands) elements; the second way of handling this is to smooth all the new coordinates of nodes. The first way is very time-consuming. Therefore, smoothing was used. On the grounds of that, in circular arch bridges, the functions of bending moments are functions of sine and cosine functions; Fourier curve fitting was used. This curve fitting for the geometry of the new calculation step leads to the fastest calculation convergence.

During the first few steps, the fitted data have some errors. They can be seen in Figure 8.8. When the calculation converges, the error is equal to chosen precision ε. $eTh4Fit$ means e_{Th} before fitting, $fitted$ means after the curve fitting. In Figure 8.8, the fitting is performed for an example of the third step of the vault bridge calculation. In the next steps, the error

93
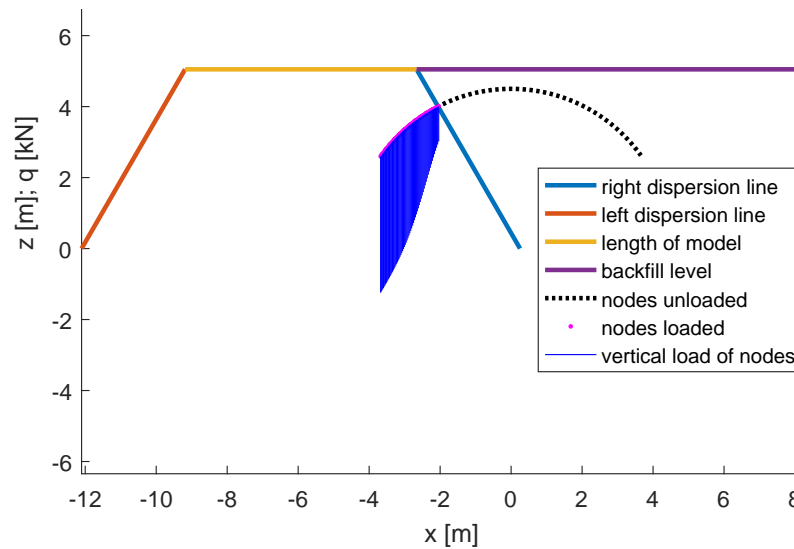
Figure 8.6: Example of live load dispersion and values of nodal forces. q is a nodal load from the live load, x and z are coordinates of the global coordinate system.

is usually close to ε, and the curves look identical.

■ Midas

Midas is typical FEM software. Its basic assumption is "small" deformation; see the definition in [Sad05] and [MR75]. For masonry structures, a small deformation assumption is fulfilled. It is therefore used to verify structure in an elastic state – at the Serviceability limit state. For modelling of the Legion Bridge, elastic plate elements were used, see Fig. 10.7. Material non-linearity is modelled in the joints between masonry blocks only. The model was used, for example, in [Dra13], see the details about this model in [VD18] and Section 11.3.2. There are around 20 elastic links in every joint that represent the mortar, which can only resist shear and compressive forces (tension prevented). The calculation is carried out iteratively. The load is increased until the capacity of at least one of the cross sections according to Equation 2.3 or (and) 2.4 is exhausted.

The parameters of this model according to [IPI19]: the modulus of elasticity of masonry is 27.085 GPa, span 4 is 42.5 m, the thickness of the arch is ranging from 1.45 m to 2.1 m, span 5 is 27.9 m, the thickness of the arch is changing from 1.0 m to 1.5 m. The specific weight of the masonry is considered 26.44 kN/m^3 (granite stone blocks), specific weight of soil 19.5 kN/m^3, coefficient of thermal expansion 4.5e-06 °C^{-1}, see Figure 8.12 in Section 8.2.1.

■ 8.1.3 Investigated parameters

The investigated parameters are:

1. Using Midas software:

94
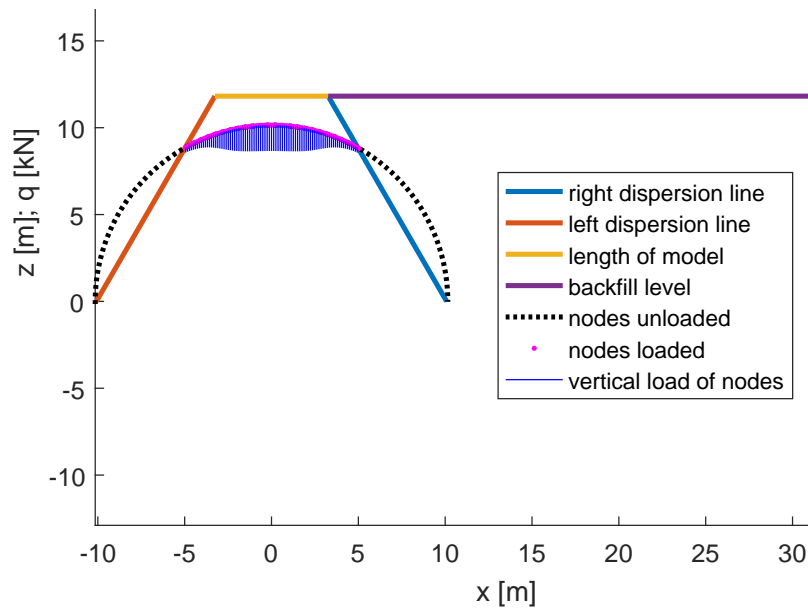
Figure 8.7: Example of live load dispersion and values of nodal forces.

    a. Uniform change of temperature.

    b. Coefficient of thermal expansion.

    c. Modulus of elasticity.

2. Using MVo code:

    a. Deformation modulus of the soil E_{def}.

    b. Coefficient of friction μ.

    c. Ratio H/L – arch thickness over span length (intrados).

    d. Characteristic masonry strength f_k.

8.2 Results of the modelling – sensitivity analysis of input parameters

Figures 8.9 to 8.13 have resulted from modelling using the Midas non-linear analysis.

Figures 8.14 to 8.17 have resulted from modelling using the MVo non-linear analysis. This is related to the article [VD20]. In the cited article and Section 7, the sensitivity of parameters is calculated at the ULS. In this chapter, the results depicted in the plots are calculated at the SLS.
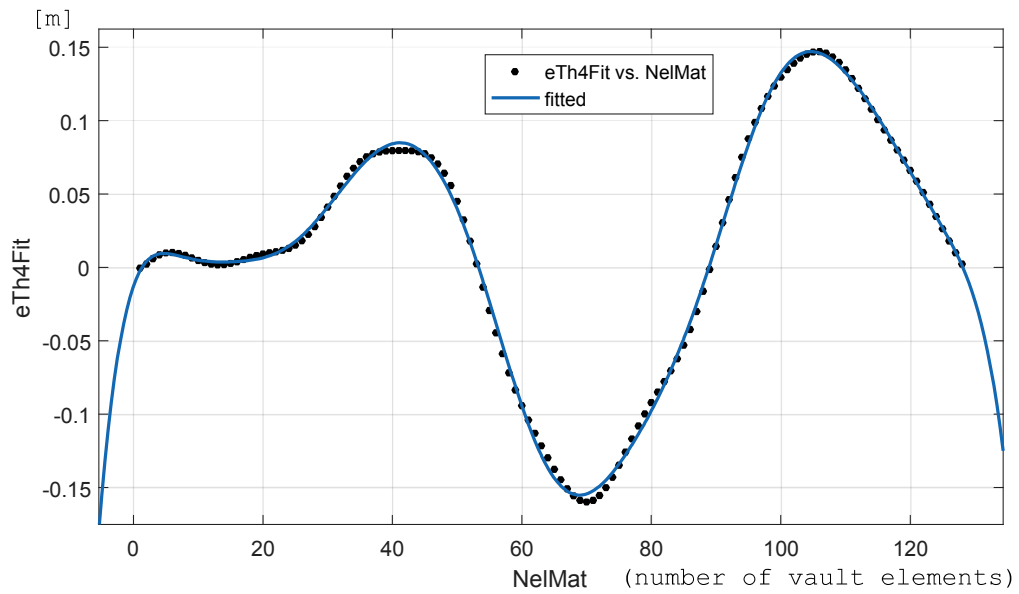
Figure 8.8: Curve fitting of geometry for the next step of the calculation.

8.2.1 Temperature changes, coefficient of thermal expansion, modulus of elasticity

This section presents the results of modelling of the Legion Bridge in the program Midas. The final plot of LCC is based on the input parameters from the diagnostic survey.

The bending moments due to the uniform temperature changes – increasing (+) and decreasing (-) of superstructure temperature can be seen in Figure 8.9:
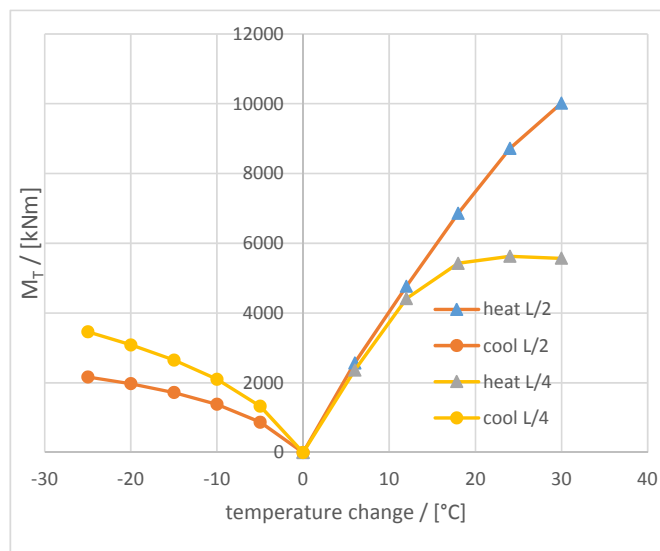
Figure 8.9: Bending moment of span 4 due to the uniform change of temperature (absolute values).

The bending moments were obtained by integrating of normal stresses over the cross section at the points of the structure with the highest value of the bending moments – $L/2$ and $L/4$, where L is the length of the span (intrados). The resulting bending moment was obtained by subtracting the moment caused by a dead load from a combination of dead load and a change of temperature. An example of the stress distribution in the cross section is shown in Figure 8.10:
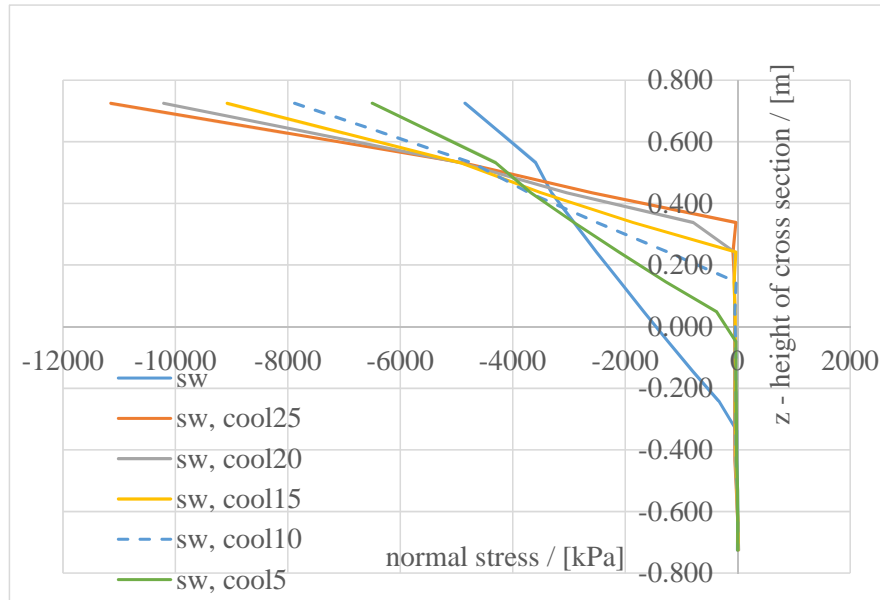
Figure 8.10: Normal stresses in the middle of span 4. "Cool5" means cooling of the structure by 5 °C.

An analogy to both-end-fixed beam subjected to uniform temperature gradient is used:

$$\sigma = E.\alpha_t.\Delta t, \tag{8.2}$$

where:

- E – modulus of elasticity of masonry,
- α_t – coefficient of thermal expansion,
- Δt – change of temperature.

As ε and σ depends on E, α_t and Δt, because $\varepsilon = \alpha_t.\Delta t$ and $\sigma = E.\varepsilon$, more detailed analysis is provided for investigation of the effect of temperature change.

The resulting stress arises from the multiplication of three parameters. Afterward, we will focus on them together. All the three parameters can be considered as parameters of linear function – if the modulus of elasticity of masonry considered in the calculation decreases twice, resulting stress also decreases twice. The fact that this rule can be applied to masonry arch bridges is proven in Figure 8.12. In the Midas model, the coefficient α_t was changed while the Δt and E are considered constant (which is known from the diagnostic

97

survey). As a result, the linear function of the deformation in dependence on the coefficient of thermal expansion was obtained.

In the case of the Legion Bridge, the geodetic survey was performed several times, w was measured, and the temperature of the structure was known. The measured vertical displacement at the top of the arches of span 3 and 4 of the Legion Bridge in the dependence on temperature can be seen in Figure 8.11. The fitting of curves by the least square method showed the best accordance with a linear function.
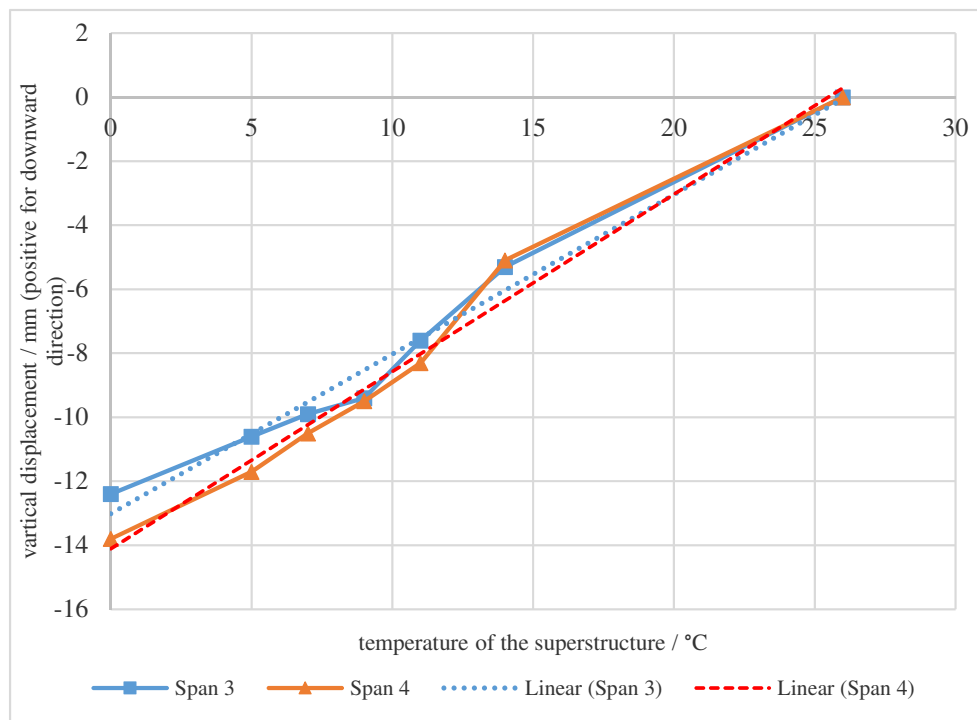
Figure 8.11: Finding the α_t from a geodetic survey.
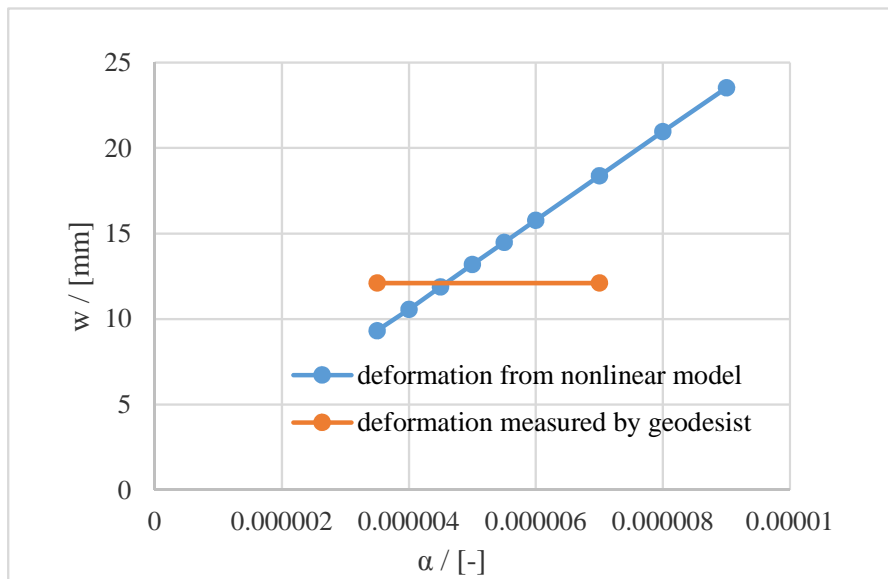
Figure 8.12: Finding the α_t from a geodetic survey.

In Figure 8.12, w is vertical deformation in the middle of span 4.

The value of the coefficient of thermal expansion could be obtained from the intersection point of a linear function, and constant w, which was obtained from the measured spans; the average value of the coefficient was used (the resulting α_t equals 4.5e-06 °C^{-1}).

The resulting LCC can be seen in Figure 8.13.
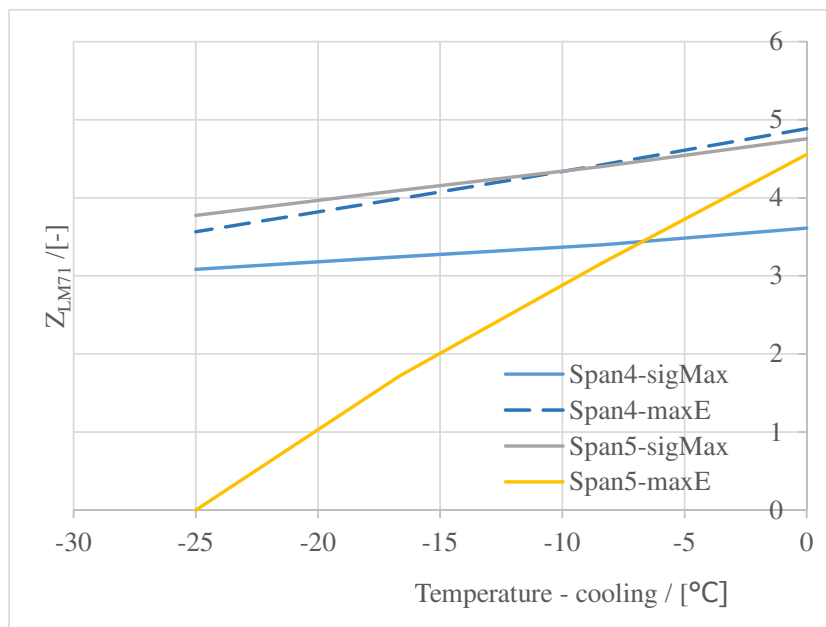
Figure 8.13: Load carrying capacity in dependence on temperature.

A positive temperature change of the structure is not considered because it does not
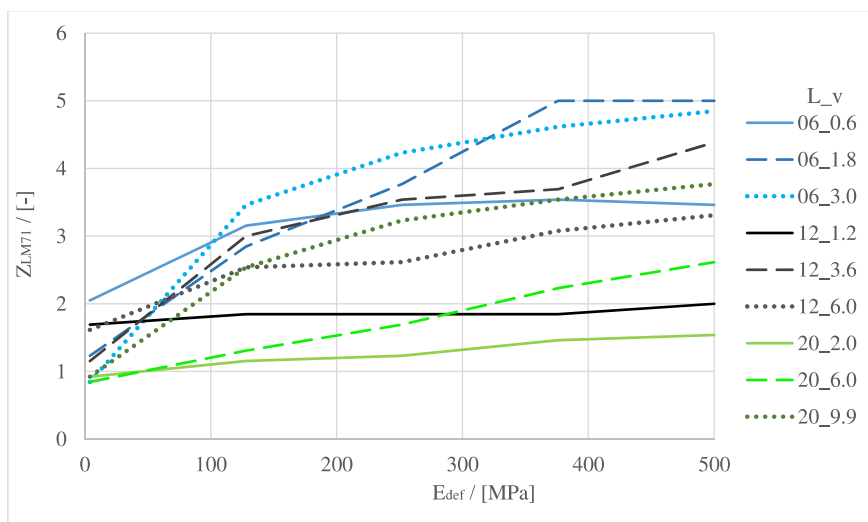
Figure 8.14: Load carrying capacity in dependence on E_{def}. For the legend, see Section 8.2.

have an adverse effect on the load carrying capacity at the SLS.

In the legend of Figure 8.13, $sigMax$ and $maxE$ denote two conditions to be fulfilled at the SLS according to [SŽ15]:

1. Maximal stress (sigMax) according to Equation 2.3.

2. Maximal eccentricity (maxE) according to Equation 2.4.

It can be seen from Figure 8.13 that the circular shape of the vault is more sensitive to cooling.

▉ 8.2.2 Deformation modulus of the soil E_{def}

The chosen scope of E_{def} corresponds to the variation from the clay-sand to compacted gravel of ideal grain size. It can be seen that the parameter is the most sensitive for the case of arch bridges with a high ratio v/L. The lower is the ratio v/L, the lower is the sensitivity to E_{def}.

▉ 8.2.3 Coefficient of friction μ

The sensitivity analysis of the coefficient of friction between the blocks of masonry elements is done just for circular bridges. As was shown in the article [VD20], the shear resistance depends mainly on the shape of the vault. The circular bridges usually have enough shear resistance. This fact is also proven in Figure 8.15, which shows the results of the calculation at the SLS. The ratio V/N – shear force over normal force – which should be less than or equal to 0.4 due to [PL07], and which should be less or equal to 0.6 due to experimental data according to [Lim20], is for all the investigated arch bridges not higher than 0.225. Hence
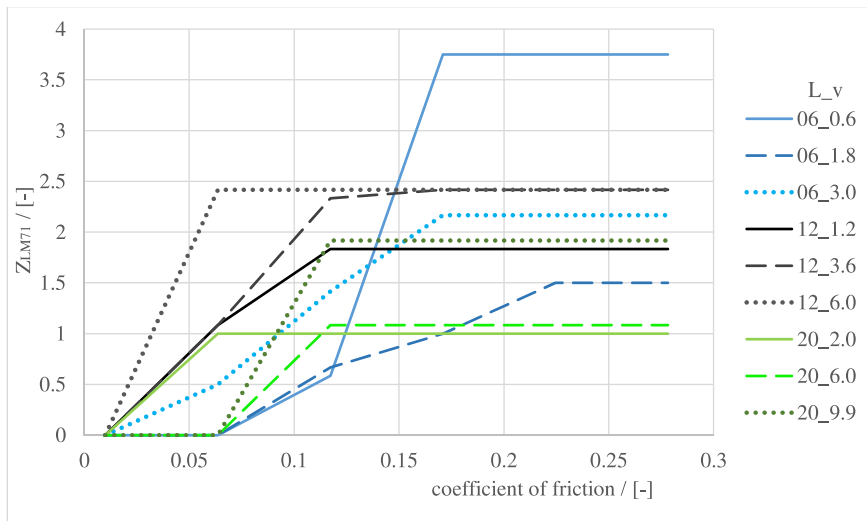
Figure 8.15: Load carrying capacity in dependence on coefficient of friction. For the legend, see section 8.2.

the LCC is not affected by shear strength. However, for the lower values of the coefficient of friction, the sensitivity to change of this parameter is high.

8.2.4 The thickness of arch

The thickness of the arch is the most sensitive parameter. That is why there should be an effort to obtain this parameter during the diagnostic survey. The thickness of the arch is sensitive both due to maximal stress and eccentricity of the load. The higher is the thickness, the higher is the range where the thrust line can occur. In the non-linear calculation, the crack opening is allowed, and therefore, the possibility of finding the ideal geometry increases with increased thickness. The result of the modelling can be seen in Fig. 8.16.

8.2.5 Characteristic strength of masonry

The characteristic strength of masonry is a parameter with similar sensitivity to the change to E_{def}. At the SLS, there is always some limit for which increasing the strength does not increase the LCC because the maximal eccentricity is a decisive criterion. This can be seen in Figure 8.17, but mainly from the study and comparison of the three mentioned methods for handling SLS criteria in Section 9.3.

8.3 Discussion

The comparison of the investigated parameters is carried out in two ways:

- In Figure 8.18, the total differences of Z_{LM71} within the investigated scope of parameters are compared.

101
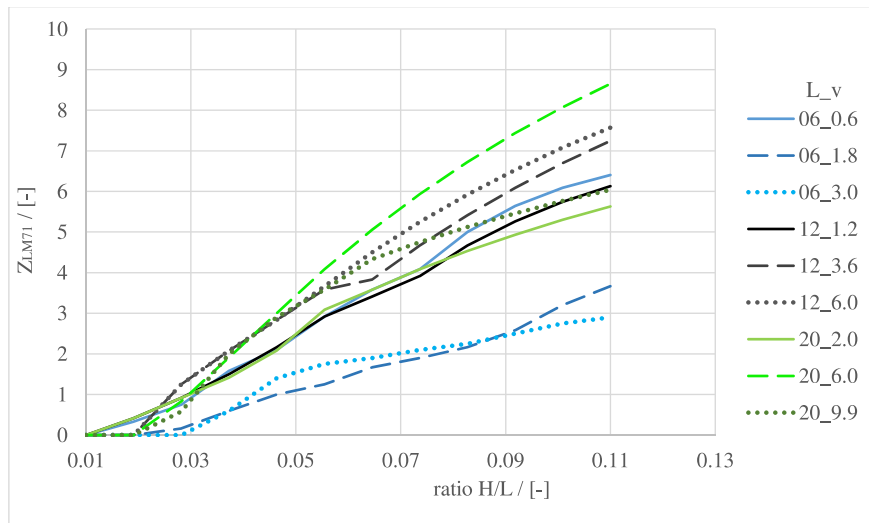
Figure 8.16: Load carrying capacity in dependence on ratio H/L, the thickness of the arch. For the legend, see section 8.2.

▪ In Figure 8.19, the average "normalized" derivatives of resulting functions are compared. The "Normalized" derivative is used because of differences between the scopes of investigated parameters. For example, the angle of internal friction varies from 0-55 °, and the ratio H/L varies from 0.008 to 0.1166. Derivatives are incomparable due to this fact. The "normalized" derivative means that for all functions, the scope of the investigated parameter is set to 1.

For both cases, the average of all investigated bridges is displayed.
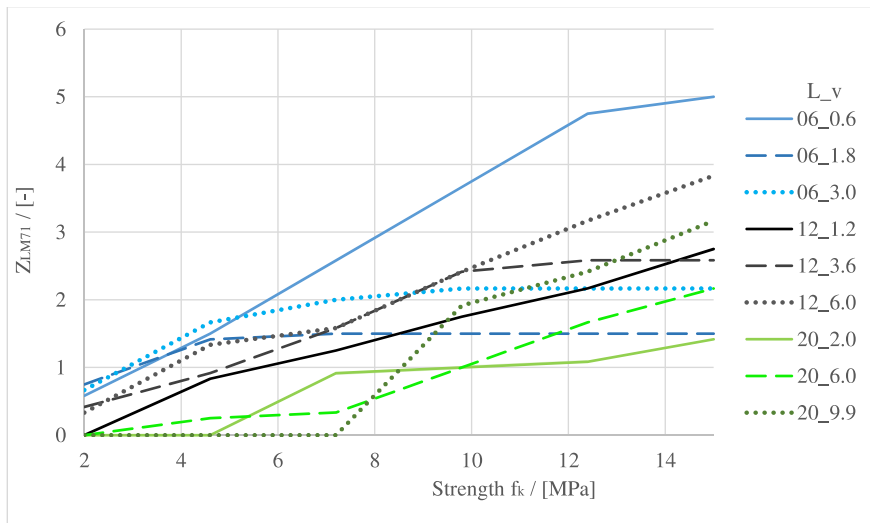
Figure 8.17: Load carrying capacity in dependence on characteristic strength of masonry. For the legend see section 8.2.

.
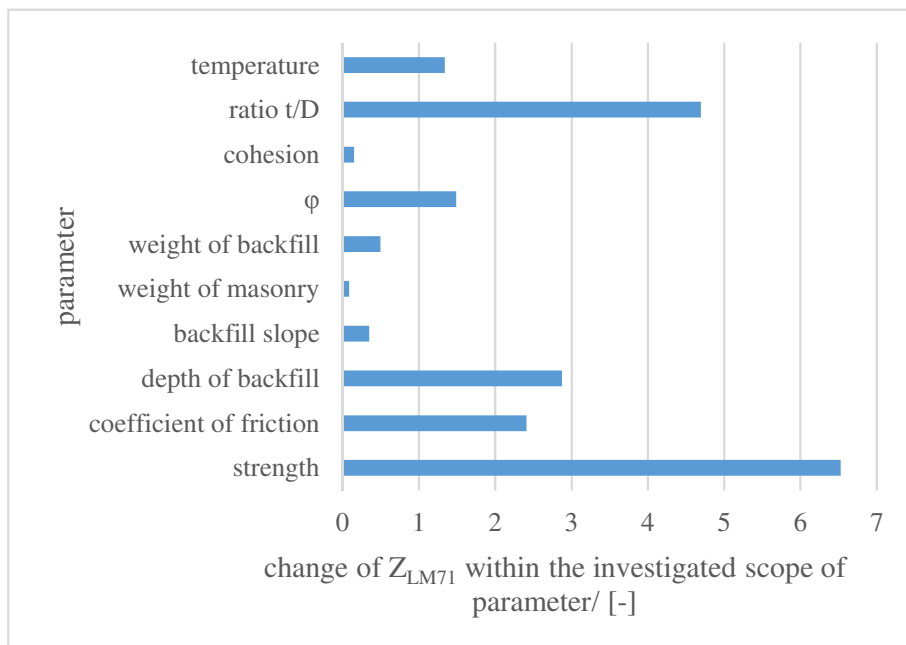
Figure 8.18: Comparison of investigated parameters - total differences between final Z_{LM71}

.
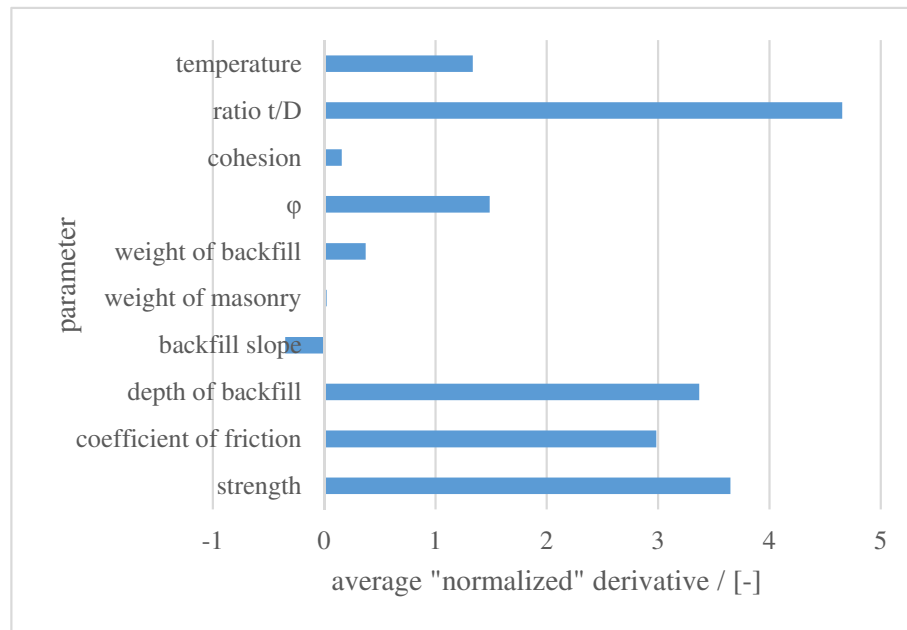
Figure 8.19: Comparison of investigated parameters - "normalized" derivatives

8.4 Conclusions

The sensitive parameters identified by this study are the ones, which should be investigated precisely by the diagnostic survey. The medium-sensitive parameters are good to know, but few tests are usually enough.

The most sensitive parameters are the masonry strength and thickness of the vault. Masonry strength is essential, especially for vaults of low sagitta, for which the masonry crushing of is usually the decisive failure mode.

The coefficient of friction between blocks is not important for circular vaults, but other shapes, especially ellipse and ogive, are very sensitive to the coefficient of friction. The Eurocode significantly underestimates the value of the coefficient of friction, especially the LCC of elliptic shape vaults would be very low according to Eurocode.

The modulus of elasticity, the considered change of temperature, and the coefficient of thermal expansion are three parameters, which work together on the final stresses in the structure. The final resulting stresses caused by the temperature load might be so high as to cause a collapse of the vault due to crushing of the masonry for the low strength of the masonry or the maximal eccentricity of the load. Therefore, the parameters for the calculation are also very sensitive.

The depth of the backfill, soil angle of internal friction, the effective width of a vault, and the shape of a vault are medium-sensitive parameters. The longitudinal slope of a railway, the specific weight of the masonry, the specific weight of the backfill, the Poisson number, and the cohesion of the backfill are parameters, that have a low impact on final LCC.

Comparison of the sensitivity of input parameters due to the SLS (MVo) and the ULS (RING – see in Section 7 and [VD18]) gives very similar results when comparing the sensitivity to change of E_{def} in the SLS and the sensitivity to change of angle of internal friction in ULS. The same applies to the coefficient of friction between the masonry blocks, the ratio H/L, and the strength of the masonry. Individual curves behave slightly differently, but, in general, the agreement of the compared plots was very good. There is no obvious breakpoint between the growing and constant segment in the RING result plots, which can be seen in SLS methods. The reason is that in the RING analysis, the criteria are different: low strength arches collapse by the crushing of the whole cross section. The middle range of strengths is affected by the crushing and, with increasing strength, the crushed area decreases. When the strength is higher than the usual masonry elements can have or is close to infinite, the criterion of the maximal eccentricity of the load is decisive, and the constant segment of the plot occurs.

Chapter 9

Load carrying capacity of masonry arch railway bridges - case study

The content of this chapter is taken mainly from the article [VD22a].

The results of four calculation methods are compared:

- MVo code – modelling using beam elements (according to previous Section 8.1.2),

    - Linear (SLS analysis),
    - Non-linear (SLS analysis),

- Scia – planar elements were used (SLS analysis),

- RING (ULS analysis).

9.1 Input parameters

The parameters used in the case study using the MVo code: $E_{def} = 40$ MPa; $E_{masonry} = 1000 * f_k$; $\varepsilon = $ 10e-8 m; γ_{Fill}=18 kN/m^3 – weight of the backfill; $\varphi = 30$ ° – angle of internal friction – cohesionless soil is considered, earth pressure at rest is calculated as: $K_0 = 1 - sin(\varphi)$; $\mu = 0.4$ – friction coefficient; γ_{Stone}=25 kN/m^3; $h_{Ballast}$=0.3 m – height of the rail ballast (under the sleeper); γ_{Bal} =18 kN/m^3 – weight of ballast; $L_{Sleeper}$=2.4 m – length of sleeper in the transverse direction; $\varphi_{Ball} = 15°$ – disperse angle of live load through the ballast; $\varphi_{Back} = 30°$ – disperse angle of live load through the backfill.

9.2 The used methods

9.2.1 The MVo method

The algorithm developed (referred to as the "MVo" - described in Section 8.1.2) has two modes. In the first mode, just one linear calculation is completed, and the forces are verified directly after the first step. In the second one, the arch verification is done after
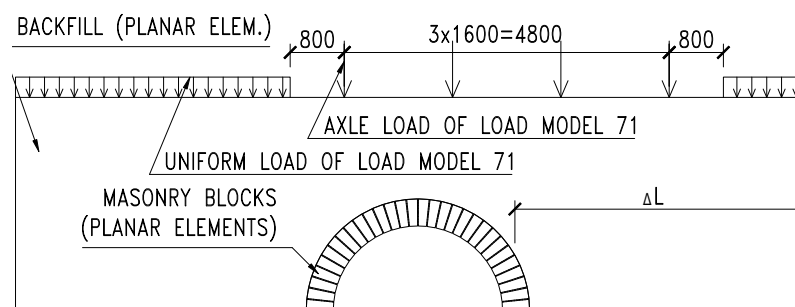
Figure 9.1: View of whole model using Scia software.

the convergence of the steps of the non-linear analysis. The algorithm developed uses a beam model; it has two advantages: the algorithm is simplified and there is less computation time. The non-linear calculation means that the LCC is calculated iteratively for all load steps of the moveable load, which is time consuming even when using the beam model (for this chapter, around a hundred arch bridges were analysed using a usual computer, and the total computation time was around four hundred hours). The disadvantage is that the model parameters, such as the geometry of nodes and cross section properties, must be completely renewed in every step of a calculation; therefore, creating the algorithm of such a calculation was time-consuming for the programmer.

9.2.2 The LimitState:RING method

The method is described in Section 7.1.2 and 11.3.3. The collapse shapes of the vaults are described in [Och02].

9.2.3 The control method taken from article [VD18] - Scia

The models use 2D planar elements. The model properties are the same as the properties of model described in Chapter 8.1.2. See the view of the whole model in Figure 9.1 and the detail of a joint in Figure 9.2. Planar elements with a linear behaviour represent the masonry blocks. The joints between the blocks are modelled by a set of beam elements that are "compression-only". The soil is modelled by elements with a modulus of elasticity equal to E_{def}, which allows us to model also live load dispersion and all other effects of backfill, except for passive earth pressure. For the calculation of the SLS, these deformations are small and the passive earth pressure is not activated. As mentioned above, this analysis was done using the Scia commercial software [Nem20].

For the details of this model, see [VD19], [VD18] and Section 10.4.3. Scia parameters used in this chapter: E_{def}, $E_{masonry}$ are chosen the same as in the MVo code, $\nu_{Mason} = 0.2$, $\nu_{backfill} = 0.333$; ν – Poisson's ratio.

Figure 9.2: Blocks of masonry and beam elements representing the joints between the blocks.

9.3 The results of the case study of the set of arch bridges - a comparison of the four forementioned methods

The LCC of the bridge spans $L = 2.5$, 5 and 7.5 m was calculated, the characteristic strength of the masonry was (1 for special cases) 2, 4, 6, 8, and 10 MPa, sagitta v was for all cases considered to be $L/2$ and $L/4$. The depth of backfill p was for all cases considered to be 0.5, 1, 1.5 m. Owing to the fact that Scia results were considered for a control reason, the LCC of the medial thickness (of total 3) was not calculated.

The difference between the MVo code and the Scia model is that in Scia, the behaviour of the backfill is linear – in the horizontal and the vertical directions. In the case of arches, where the height of the backfill is similar to or even larger than the span of the arch, the results are significantly impacted by the soil behaviour. The problem becomes more influenced by the impact of soil and its modelling rather than the behaviour of the masonry arch. See the result of RING modelling (check of ULS) in Figure 9.3, the MVo non-linear code (check of SLS) in Figure9.4, the results of the MVo linear code (check of SLS) in Figure9.6, the results of control Scia calculation (check of SLS) in Figure 9.5 and comparison of RING method with the MVo code in Figure 9.7.

9.4 Result discussion

It was confirmed that the results of the two models, which should have similar results, give similar results. The most significant difference is for the smallest arch of the 2.5 m span. For this geometry, the calculations are significantly impacted by the behaviour of the backfill. The linear backfill behaviour helps the arch in both vertical and horizontal directions. For the arch with a high effect of backfill, special modelling should be done using special geotechnical software.

It should be noted that the results of the control model – the Scia model – are imprecise due to the reading of the graphical results. Especially the verification of the maximal eccentricity is sensitive to interpreting the compressed area. Seeking the LCC iteratively is time-consuming when using the Scia software. On the other hand, the MVo code is
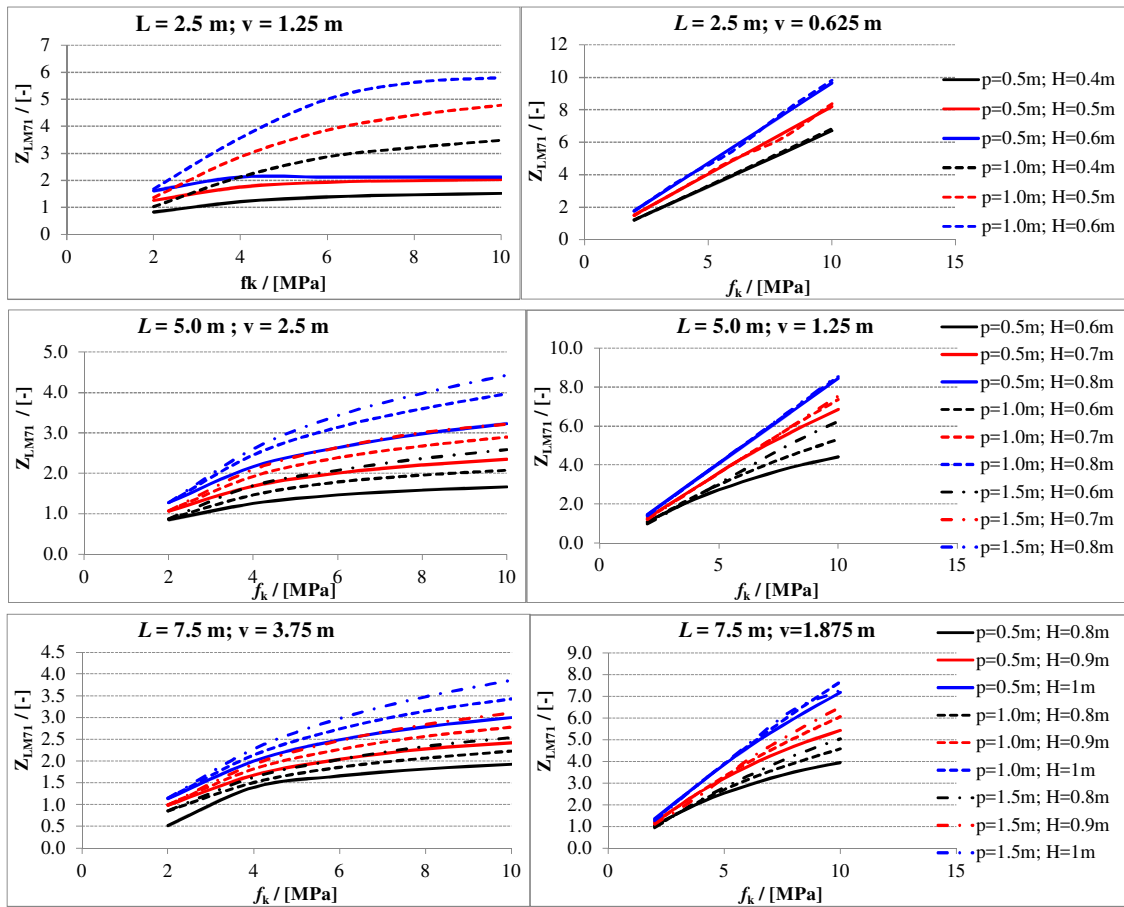
Figure 9.3: Results from the modelling using the RING software.

created to calculate the LCC, and the results are obtained simply and straightforwardly; the verification is done with precise numbers.

The linear calculation must obviously give a lower LCC. In the non-linear analysis, the arch axis is "optimized", the geometry is updated to decrease the bending moments in the next step. The limits of changing the geometry are given by the arch extrados, intrados, and SLS criteria. The resulting bending moments depend mainly on the crack opening. If the height of the cross section decreases and is close to the limit - one-half of the cross section height, then the moment of inertia decreases eight times. As a result, the bending moment in the next step decreases up to eight times. The geometry optimization is done for every load step, every position of the live load, so the non-linear calculation is much more time demanding.

The authors tried to find the dependence of LCC using RING on LCC using the MVo code. Such an evident dependence was not found. The curves of the LCC ratio Z_{RING}/Z_{MVo} are similar in shape, but the tendency to grow or decrease with increasing strength differs for every analysed arch. For most cases, the ratio is the lowest for the highest depths of the backfill. For the majority of the cases, the LCC is higher at the ULS, usually up to two times higher.
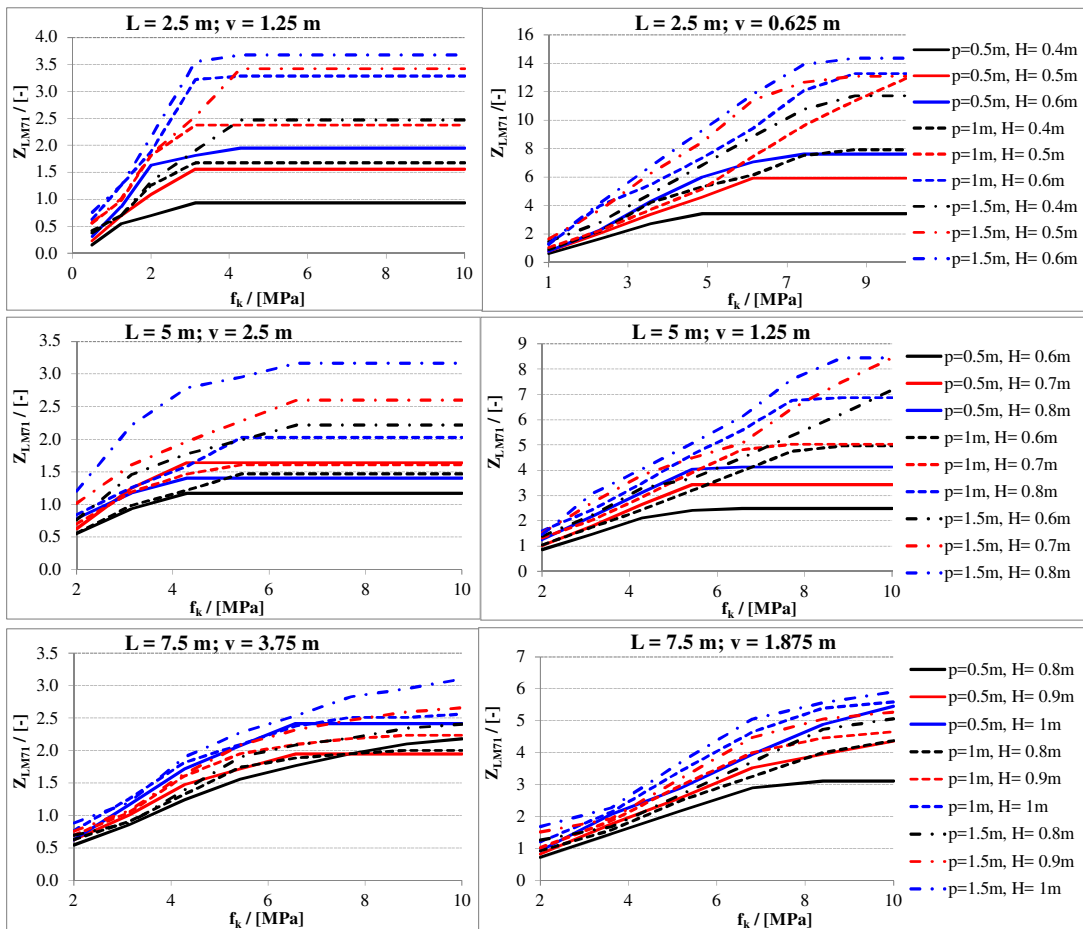
Figure 9.4: Results from the modelling using the MVo software – non-linear analysis.

▉ 9.5 Conclusions

Comparison of the sensitivity to change of input parameter due to the SLS and the ULS gives very similar results. This comparison was made for key parameters, which were proven to be the most sensitive in the article [VD20]. The comparison of analysis using Scia software with 2D planar elements to the MVo results showed good agreement, except for small arch spans, where the behaviour of the backfill significantly affects the final LCC. For this reason, a further study of backfill behaviour with advanced methods explicitly designed for soil behaviour should be conducted.

The comparison of the analysis using the MVo non-linear method with the RING results showed no particular dependence. The LCC from the RING method is mostly higher than the LCC from the MVo method. The RING results are up to two times higher.

The linear calculation gives very conservative results; LCC is usually from two to three times lower than from the non-linear model. This is because the non-linear model can change its geometry to minimize the bending moments, and the only boundary conditions

111
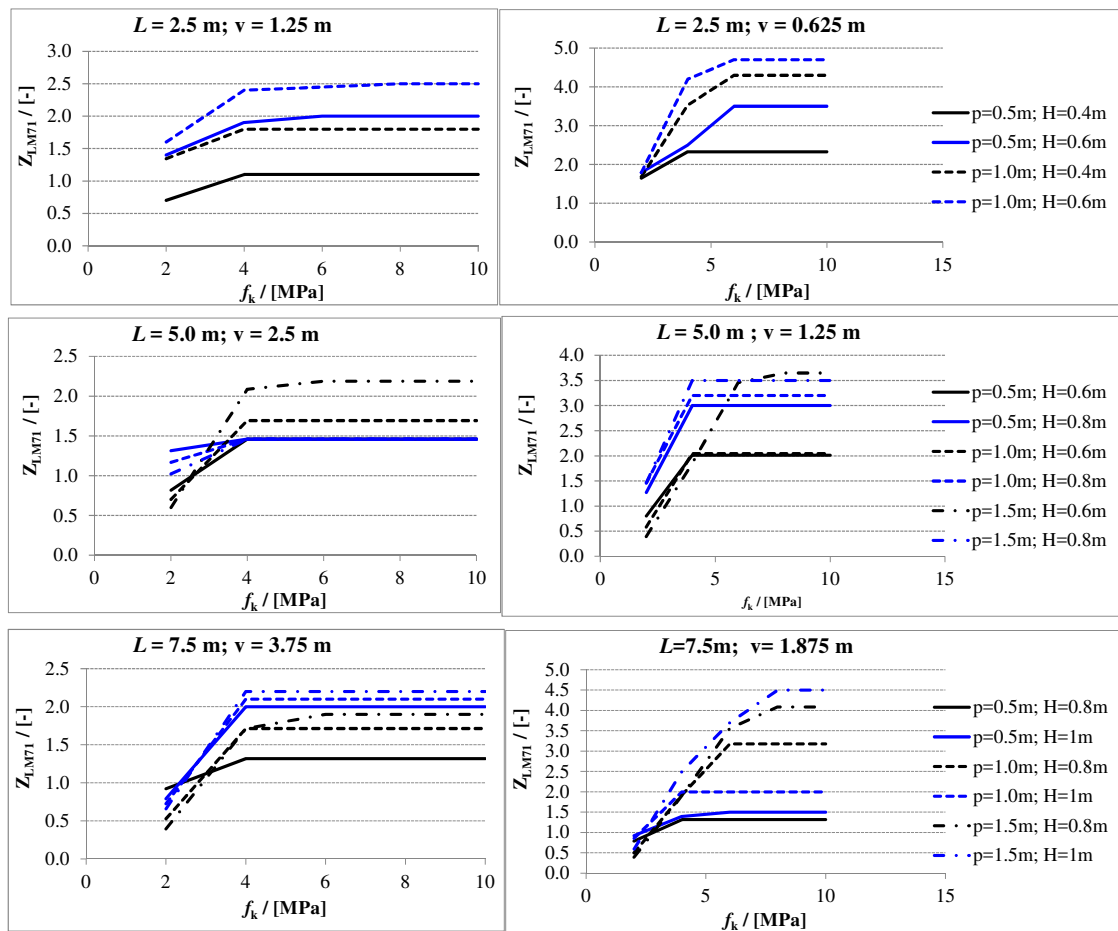
Figure 9.5: Results from the modelling using the Scia software – non-linear analysis.

for the geometry of the arch are the extrados and intrados of the assessed arch. The effect of crack opening, which reduces the bending moment for the critical points of the arch, also increases the final LCC.
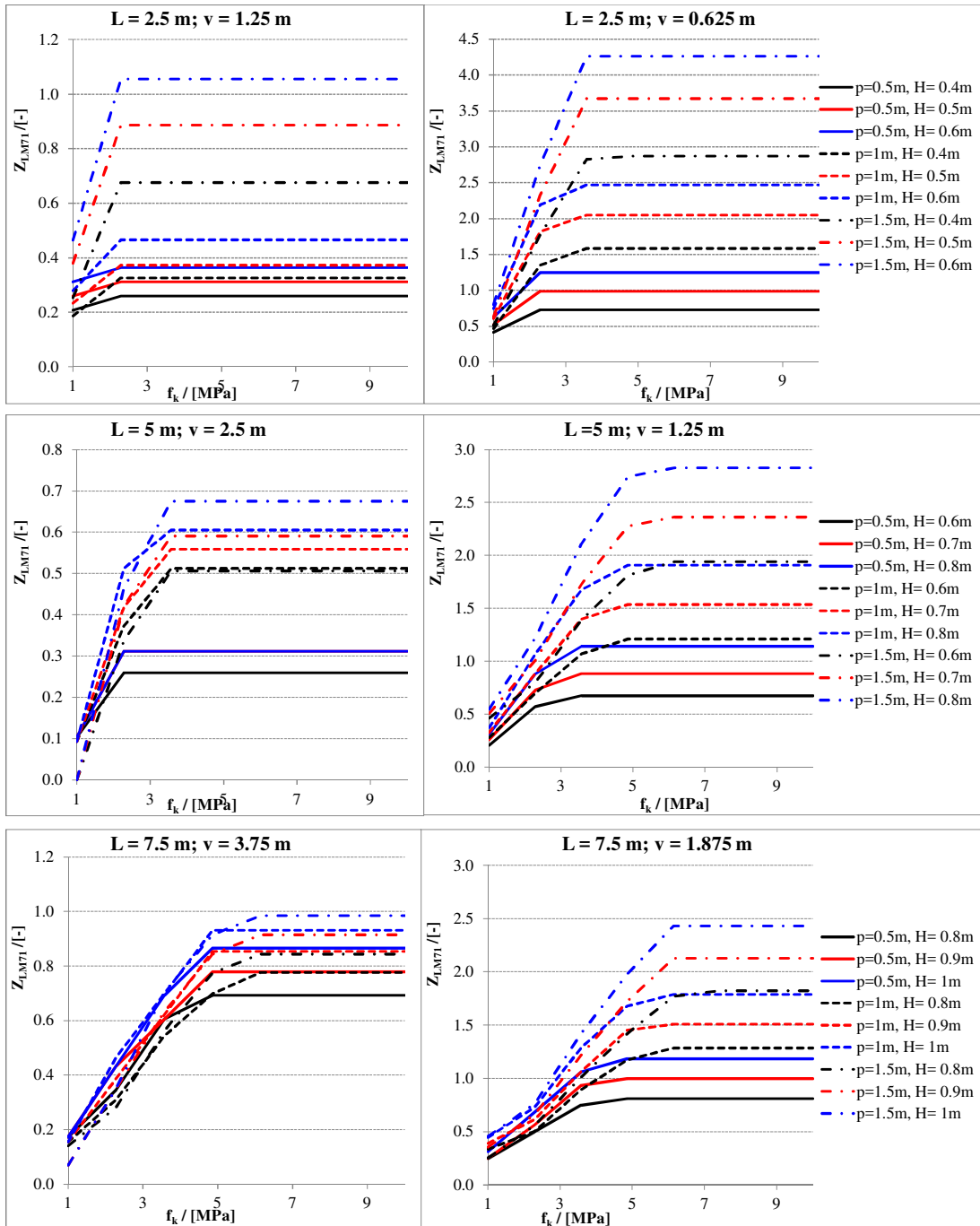
Figure 9.6: Results from the modelling using the MVo software – linear analysis

113
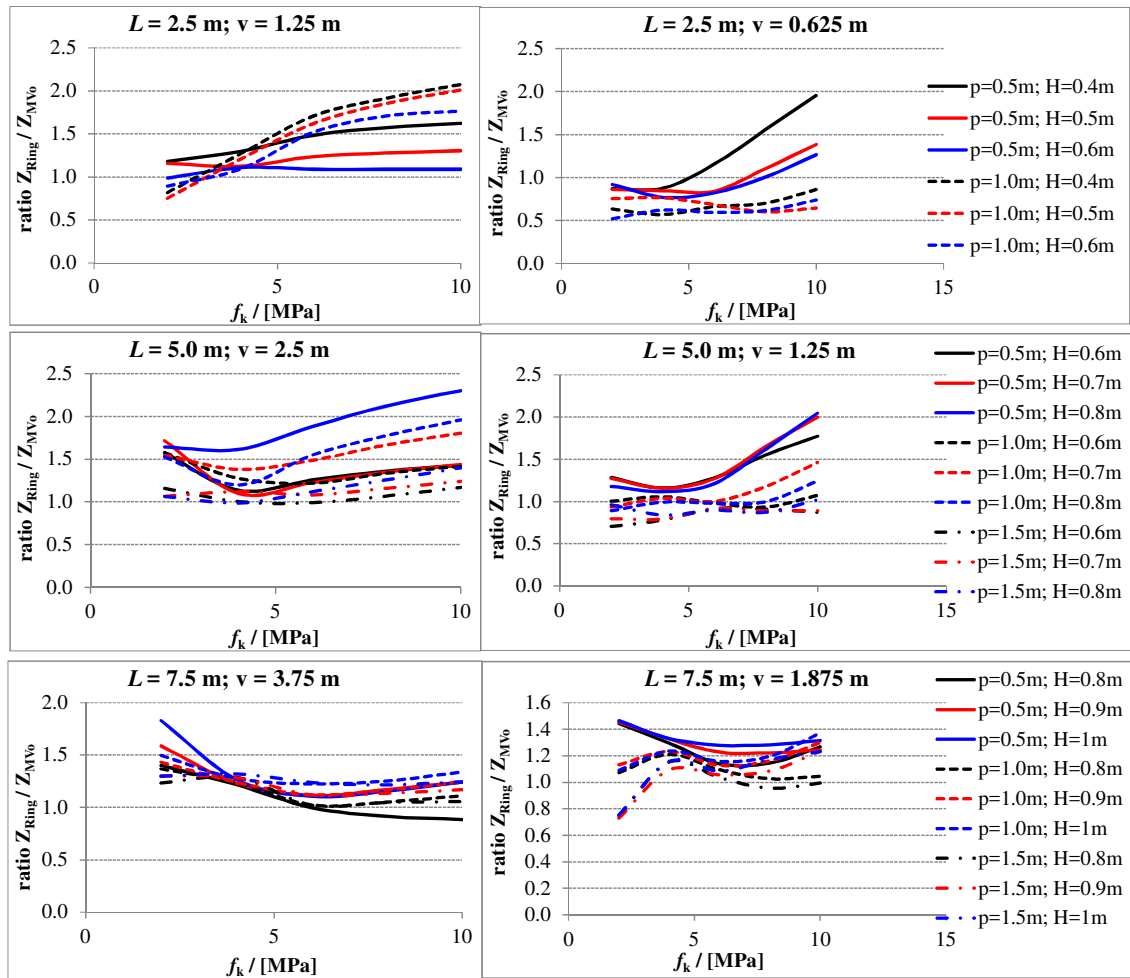
Figure 9.7: The ratio of $Z_{LM71,RING}/Z_{LM71,MVo}$ is simplified as Z_{RING}/Z_{MVo}.

Chapter 10

Load carrying capacity of stone arches of Legion Bridge

The content of this chapter is taken mainly from the article [VD19].

10.1   Introduction

In the case of road bridges in Czech Republic, three kinds of load carrying capacity (referred to as "LCC") are to be calculated (according to [ÚN13b]):

- Vn - normal LCC of the bridge – represents the maximum weight of one typical lorry, which may pass the bridge without any restrictions (position limited by safety barriers or curbs only).

- Vr - exclusive LCC – represents the maximum weight of one vehicle, which can pass the bridge as a single vehicle in any position or lane, respectively (no other traffic load except pedestrians is permitted).

- Ve - exceptional LCC - which represents the maximum weight of a special heavy vehicle, which can pass the bridge under special conditions (specified velocity, specified path, and eccentricity to the axis of the bridge).

If the LCC Vn is lower than 26 t or Vr is lower than 48 t, the traffic sign must be placed on the bridge to signal the LCC, and drivers of heavier trucks must avoid the bridge. For the bridge reconstruction, the minimal LCC is Vn=32 t, Vr=80 t and Ve=180 t (lower values show the need for strengthening or a demolition and replacing it with another object).

The determination of each LCC presents a separate calculation in both of the limit states (SLS and ULS), considering all other relevant loads (temperature, wind, flood, etc.).

10.2   Brief history and description of bridge

The Legion Bridge connects the Old Town with the Lesser Town of Prague through the Střelecký Island. The foregoer bridge of Legion Bridge was the Bridge of Emperor
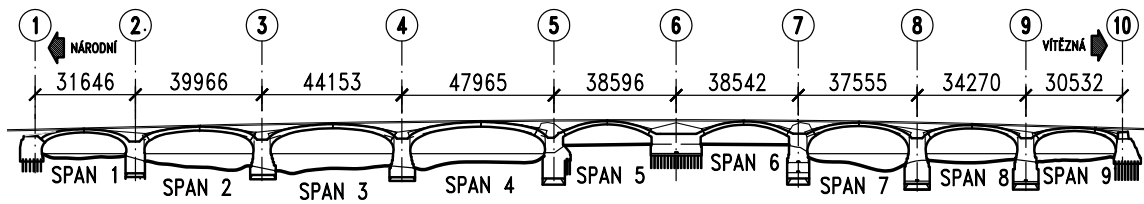
Figure 10.1: Longitudinal section of the whole bridge.

František, and it was the second bridge in Prague finished in 1841. The Legion Bridge was constructed at the position of the Bridge of Emperor František. The construction of a new bridge ran from 1898 to 1901.

In contrast to the original bridge, the superstructure is a massive stone vault structure. The construction of the bridge consists of nine flat (with a low rise) vaults of different spans: 26.6 + 34.3 + 38.5 + 42.0 + 27.8 + 27.8 + 31.9 + 28.7 + 25.6 m. Two vaults above the Střelecký Island are vaults of circular segments, and the other vaults are elliptical. According to [IPI19], the vaults of the bridge are made of granite blocks with a gap of 12 - 15 mm filled with cement mortar. The stone facade of front walls of light sandstone and red granite symbolizes national colors. The bridge has wide pathways and motorway lanes. Electric tracks were also built on the bridge; trams run along an existing bridge from June 17, 1901.

The Legion Bridge is listed as an immovable cultural heritage and is therefore protected according to the law on State Monument Care, as amended. Furthermore, because it is a building located in the territory of the Prague Historical Reserve (PPR), it is protected by the provisions of the Government Decree On the Historical Heritage in the Capital City of Prague. The historic monument in Prague, representing the historical center of Prague, was included in the UNESCO World Heritage List in 1992.

See the cross section view in the midspan of span 4 in Fig. 10.11 and the longitudinal section in Fig 10.1.

■ 10.3   Diagnostics of the bridge

In order to find the geometric and material properties of the bridge, the following procedures were carried out. For detailed results see [IPI19]:

1. detailed mapping of all visible damages,

2. topographic survey,

3. geotechnical investigation,

4. core boreholes to the superstructure (to obtain E, f_b, f_m),

5. georadar survey of thickness of arches,

6. continuous measurement of temperatures,
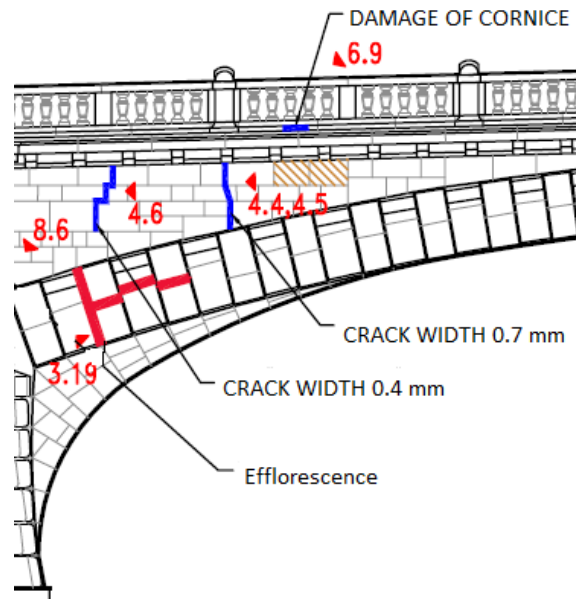
Figure 10.2: Mapping of visible damage in the spandrel wall near pier No. 2.

7. diving survey of substructure,

8. static and dynamic load test – see Section 10.6.5.

10.3.1 Detailed mapping

As an example of detailed mapping of visible damages, which was done together with the acoustic test of degradation of stones of arches, Figure 10.2 is shown.

Because of the cracks in the spandrel walls, the wall is considered just as a load in the models, not as a carrying element.

10.3.2 Geotechnical boreholes

Piers number 2, 3, 4, 6, and 8 were drilled from the bridge deck to the foundations. From this we obtain information about the thickness and material properties of asphalt layers, the backfill, the masonry of piers, and the foundation ground. It was found that the masonry of a pier has much lower strength than the superstructure, see section 10.3.3.

10.3.3 Core boreholes

The compressive strength was tested on 34 granite samples of the superstructure. The measured mean strength was $f_b = 132$ MPa. The superstructure mortar has an average strength $f_m = 25.8$ MPa, tested on 114 specimens.

117
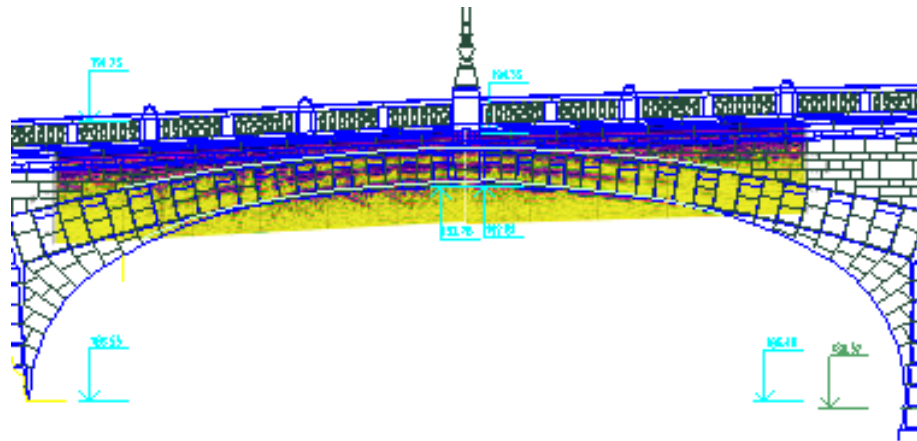
Figure 10.3: Georadar method in span No. 9.

The compressive strength was tested on 131 granite and sedimentary rock samples of the substructure. The measured average strength was $f_b = 86$ MPa. The substructure mortar has an average strength $f_m =$ 25.2 MPa, tested on 169 specimens.

The input parameters for assessing the f_k of the superstructure are: $\alpha_m = 0.7$ for the usual mortar, $\beta = 0.3$ for the usual mortar, $K_z = 0.45$ for blocks of natural stone.

The characteristic compressive strength of the masonry was calculated according to Equation 1.2, its value is 28.9 MPa for the superstructure and 22.8 MPa for the substructure (which are very high values),

The granite modulus of elasticity of superstructure was found 41.3 GPa on 17 specimens, and the granite modulus of elasticity of substructure was found 31.1 GPa on 29 specimens.

■ **10.3.4 Georadar survey of the thickness of arches**

The Georadar method (GPR) is based on the principle of transmitting high-frequency electromagnetic waves into the examined environment and then registering the wave image of the reflected waves. The wave image is affected by local inhomogeneities, especially with different conductivity and other electromagnetic properties. Inhomogeneities can have both planar character (discontinuity surfaces, structural interfaces) and local character (e.g., cavities, etc.). Inhomogeneities are manifested by amplification of the registered reflected signal amplitude. In Figure 10.3, the blue lines represent the arch shape taken from the topographic survey. The yellow area and the white lines are taken from the Georadar method.

The measurements in the longitudinal direction of the bridge were in good agreement with the archive documentation. On the vault of span 7, a 0.15-0.2 m concrete layer was found, which was not expected. The measurement in the transverse direction showed constant thickness, which was expected.

∎ 10.4 Methods of calculation - arch

In all the methods, the masonry is homogenized; see the details of homogenization in Section 1. Methods used in this chapter:

1. Graphical method (checking of all the requirements)

2. Linear calculation using FEM (controls all the requirements)

    a. Beams – 2D or 3D (checking of all the requirements)
    b. 3D solid elements (controls all the requirements)

3. Non-linear calculation

    a. 2D – plane elements (checking of SLS requirements)
    b. 2D – beam elements - MVo code (controls all the requirements)

4. Equilibrium method — LimitState:RING (checking of collapse of the structure only)

The requirements of codes see in Section 2.

∎ 10.4.1 Graphical methods

Various graphical methods had been used until computer-aided design came to engineering practice. It provides a simple and quick design approach independent of arch bridge shape. Graphical methods are based on the thrust line determination. The thrust line of the cross section can be found as the centroid of the axial stress diagram. When the thrust line is known, the stress at the cross section can be calculated as well. The method of finding the thrust line runs in the following order (symmetric arch according to [Lip98]):

1. Divide the arch into 2 symmetric parts, find the weight of one-half, and from the arch geometry, we find the force H_f (horizontal force at the top of the arch).

2. Divide one-half of the arch into several partitions (vertical lines can be used to divide).

3. Draw a graphical representation of all parts – F_i - the size of vector in chosen scale, acts in its centroid.

4. Force H_f we locate, for example, in the upper bound of cross section core and reaction in the lower bound of cross section.

5. To obtain the resulting force $R1$ in the first partition, we graphically add the force F_i to H_f; to obtain the following resulting forces in each partition, we graphically add the forces F_i to the previous resulting force.

The basic principle of the calculation is shown in Fig. 10.4 and [Vok18].
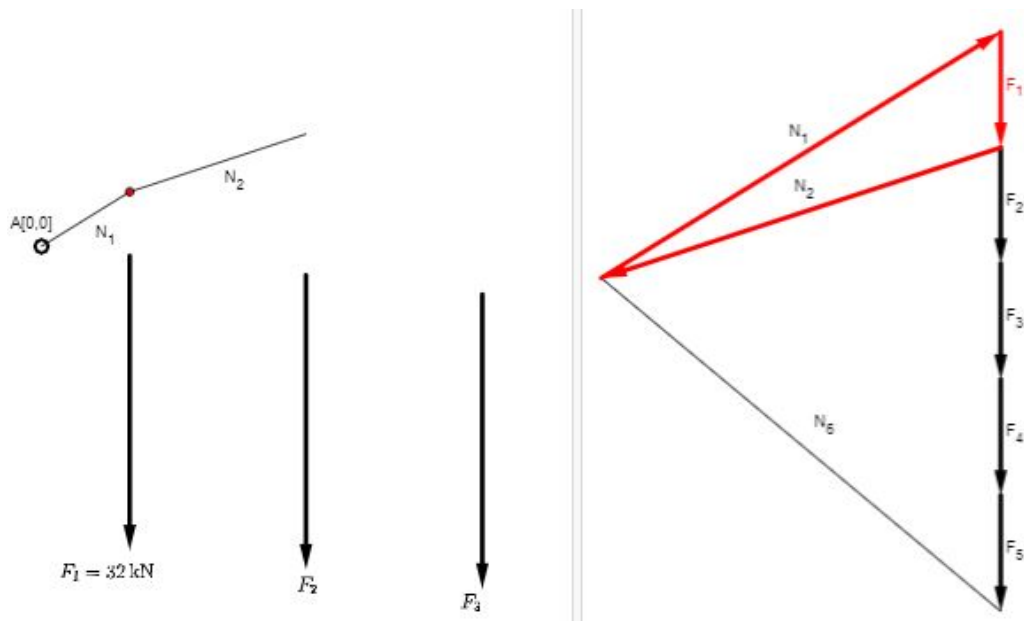
Figure 10.4: Basic principle of the graphical method.
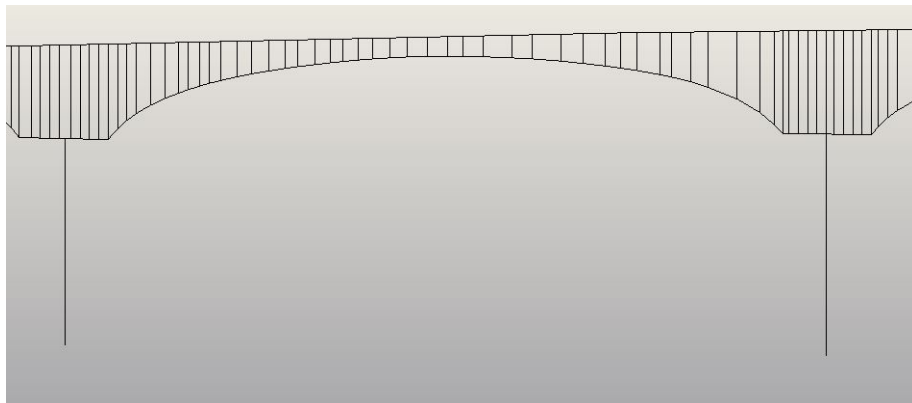
Figure 10.5: Linear 2D beam model.

◼ 10.4.2 Linear calculation

Structural analysis using the linear calculation method was done in two different options. In the first one, the arch was represented by a sequence of beams in its center-line. Vertical beams placed at the appropriate longitudinal distance represent the backfill; see Figure 10.5. While modelling using linear calculation, one should not forget that this calculation method does not take into account material non-linearity (and geometry changes due to excluding the tensioned part of cross section).

For the second option, the arch and backfill were modelled by the 3D solid elements with various mechanical properties – see Figure 10.10.
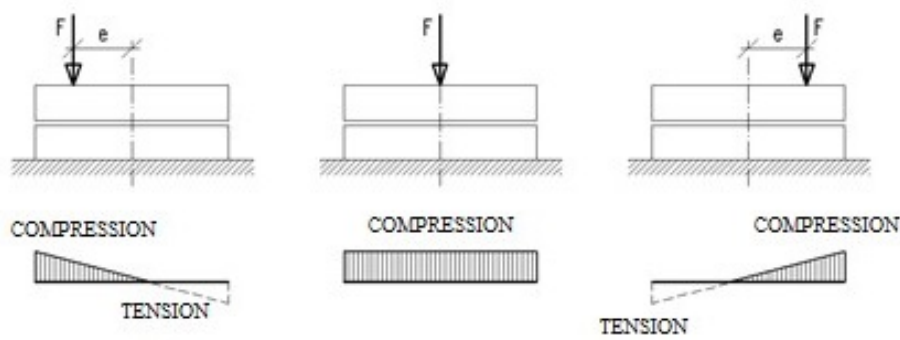
Figure 10.6: Non-linear behaviour of masonry.
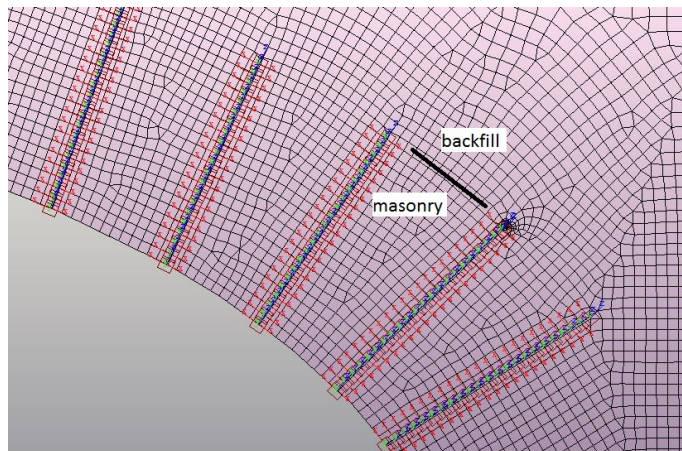
Figure 10.7: Elastic links between nodes in joints of masonry.

10.4.3 Non-linear calculation

For performing a non-linear analysis and assessment of the structure, the material – mortar and masonry elements - is homogenized to preserve its properties concerning the real behaviour of the structure or its part. It is assumed that the dimensions (thickness) of the masonry elements and the joints between them do not significantly affect the distribution of stress in the masonry element. See the details of homogenization in Section 1. The real stress-strain diagram of the masonry shows non-linear behaviour (see [Vok17]), particularly due to negligible tensile strength. In this chapter, it is considered that the material acts only in compression, and when the tensile stress occurs, the cracks open up, see Figure 10.6). If subsequently (e.g., in another load combination), the tensile stresses in the cross section disappear, the cracks close, and the cross section acts again as full.

Non-linear calculation using Midas

The structural model in the program Midas was prepared using plane-stress elements. The joints between the granite blocks were modelled as a set of elastic links with the property "Compression only", see Figure 10.7. For another example of such a model see in Section 11.3.2.
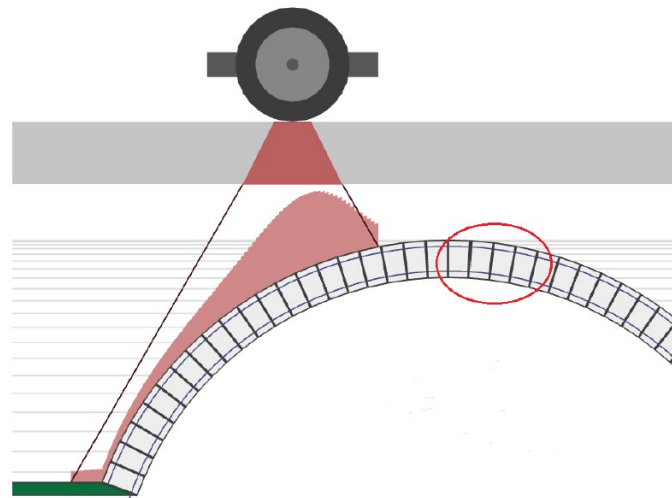
Figure 10.8: Vertical traffic load distribution (dispersion) to the vault considered for arch modelling in LimitState:RING software.

Non-linear calculation using MVo code

For the details of the model see Section 8.1.2. The geometry of the model and the results can be seen in Figure 10.17. A beam model with geometric and material non-linearity was used.

10.4.4 Equilibrium method on rigid blocks

LimitState:RING is a special analysis software for checking the LCC of the vault in the plane of the longitudinal section of the bridge structure, including the load distribution by the backfill. The load distribution is considered according to Bousinesq, see the example in Figure 10.8. For more details, see Section 7.1.2 and [Dra14].

10.5 Methods of calculation - transverse direction

10.5.1 Linear calculation

Beam elements

Modelling using this method is done by representing the arch by beams in its middle line and dividing the backfill in a chosen interval to represent it by beams as well, see Figure 10.5. If the model shown in Figure 10.5 is copied several times in the transverse direction, the analysis model representing the arch as a 3D body can be arranged. The stiffness of the transverse beams, which connect the beams in the longitudinal direction, is chosen as the stiffness of the arch; the beams have both bending and shear stiffness. Such a 3D linear model can be used to study the effect of the eccentricity of a live load on the load distribution in the transverse direction – see Figure 10.9.
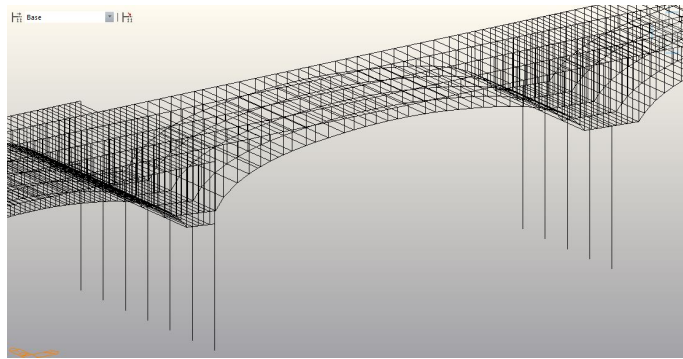
Figure 10.9: Linear 3D beam model.
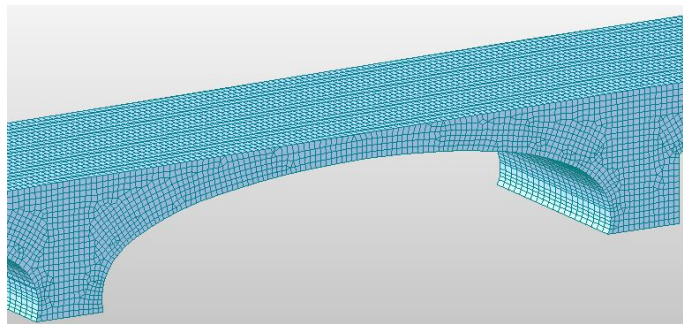
Figure 10.10: 3D solid model.

■ Solid elements

Another option for linear analysis is to model the body of the structure using 3D solid elements – see Figure 10.10. This way can model both longitudinal and transverse directions. In this model, we assume that the backfill is connected to the masonry arch; there are just different material properties. The precise way of modelling includes the frictional connection between these two materials, but the real friction between the masonry arch and the fill is unknown; this way was, therefore, not used.

■ 10.5.2 Effective width

The principles of "modelling" of the bridge span 4 in the transverse direction using effective width can be seen from Figure 10.11. This way of modelling is used in most codes. According to [Har06], the "classical" model was used. Other possibilities of considering the effective width can be seen in Figure 11.8. The classical model considers the conservative idea that the non-loaded part of the arch does not carry any load. So the shear and bending stiffness between loaded and non-loaded elements are considered to be equal to zero. This approach is applied to 2D modelling methods; the effective width is used for the third dimension.
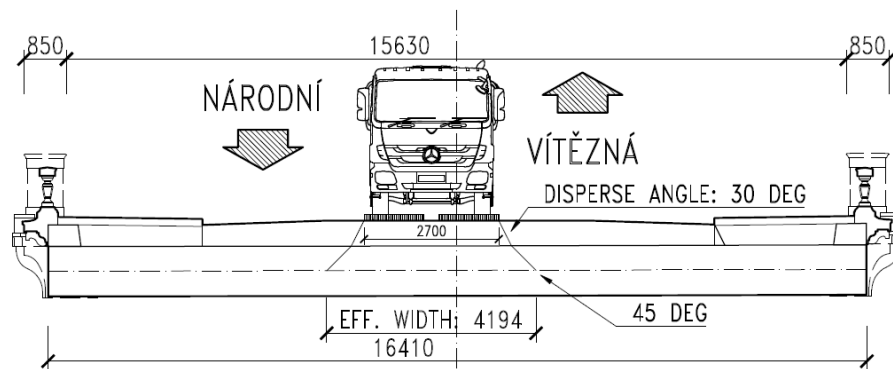
Figure 10.11: Graphical calculation of effective width is carried out on the view of cross section in the bridge midspan.
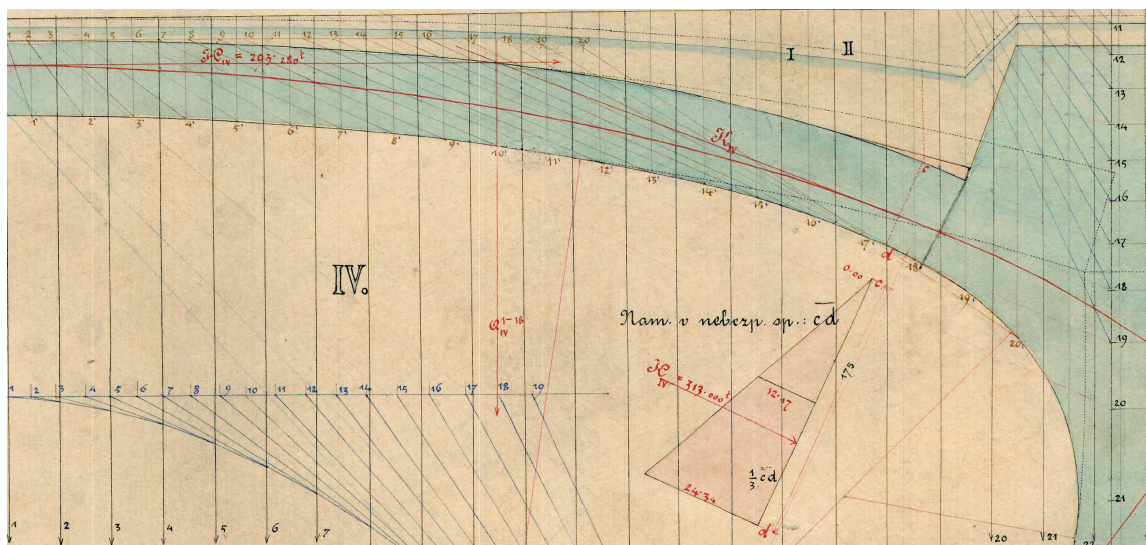
Figure 10.12: Graphical solution of the span 4 from the archive documentation.

10.6 Results

10.6.1 Graphical method

The result of the graphical method for span 4 is shown in Figure 10.12. The red line represents the thrust line, see its values also in Figure 10.22. In Figure 10.12, the stress distribution is displayed at the point d (the arch springing) by the red triangle. The structure is loaded just by self-weight.

10.6.2 Linear calculation

The bending moments on the beams representing the vault are shown in Figure 10.13.

The stress of the linear model of solid elements can be seen in Figure 10.14. The positive sign means tension; the results are taken from the lower edge of midspan 4.
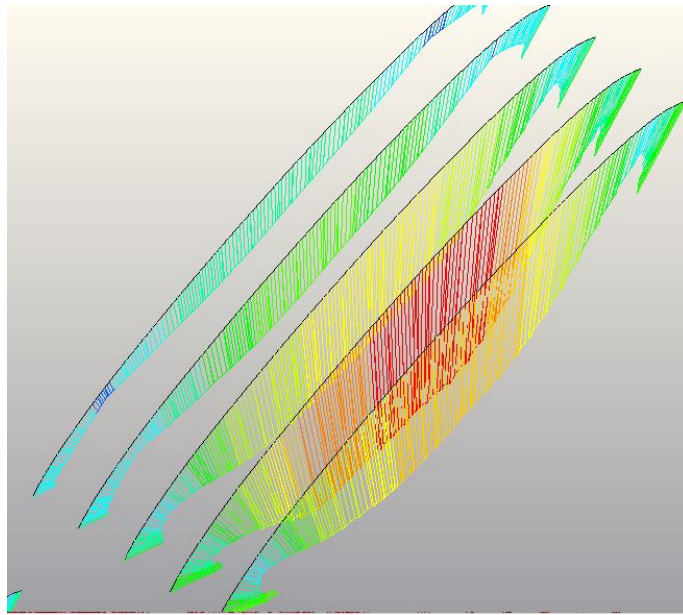
Figure 10.13: Bending moment Mmax on the beams representing arch in longitudinal direction. (The load model Vr is on the right side of the bridge).

The linear model of solid elements, which included the spandrel walls, showed that stress in the spandrel walls from the decrease of temperature by 10 °C reached 3.2 MPa. This explains the vertical cracks in almost all of the spandrel walls.

10.6.3 Non-linear calculation

Non-linear calculation using Midas

Principal stress in the arch of span 4 can be seen in Figure 10.15.

The legend of curves in Figure 10.16 is the following:

- *sw* means self-weight,
- $N\hat{}$ means non-linear combination,
- *ohr* means heat-up,
- *och* means cooling,
- $4VnT!$ means load by live load,
- number 1 or 2 means the position of live load.

Non-linear calculation using MVo code

The shape of the arch with the excluded tensioned areas can be seen in Figure 10.17.
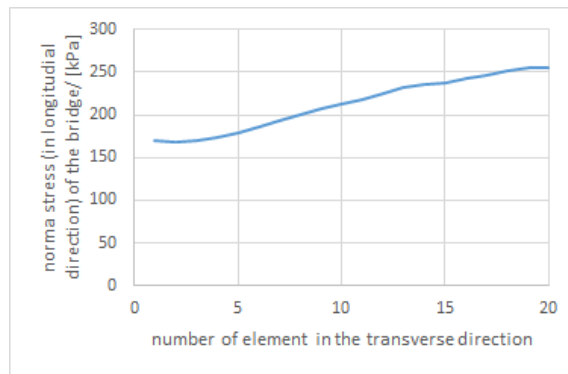
Figure 10.14: Resulting normal stress from the 3D solid model loaded by the exclusive load model Vr on the right side of the bridge.
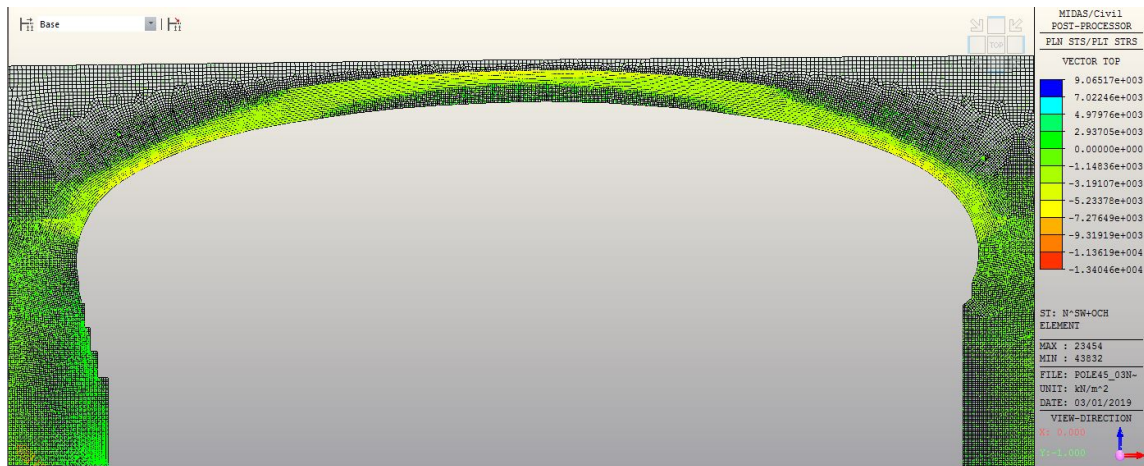
Figure 10.15: The principal stress from the non-linear model.

10.6.4 Shear between the blocks

As a demonstration of failure mode, the picture of span 4 from program LimitState:RING is attached (see Figure 10.18).

The resulting shear force acting on the cross section depends on the geometry of the arch. In the beam model, it depends on the geometry chosen of the axis of the beams. In the solid model, it depends on the choice of material model – linear or non-linear. Figure 10.19 shows examples of moving the center-line of a beam near the bottom of the arch. $e = M/N$ is the eccentricity of the load. The higher is the eccentricity, the lower is the resulting shear force. In Fig. 10.20 it can be seen that changes in the geometry of a beam model according to material non-linearity affect the resulting shear force highly.

The Legion Bridge was also assessed in other sections of this thesis. The sensitivity to change of coefficient of friction on the resulting LCC was carried out in Section 7.2.2 and 8.2.3.
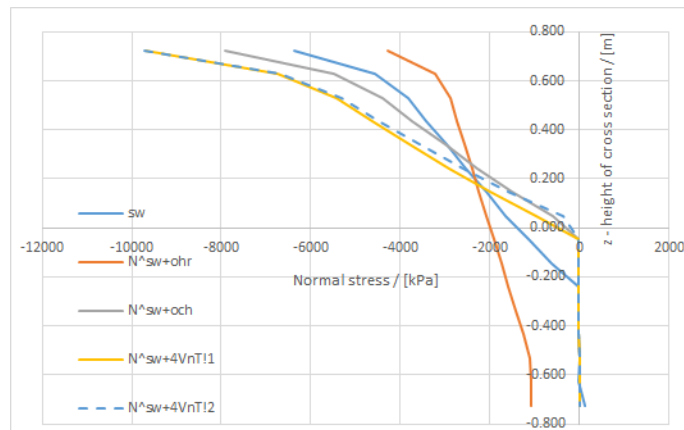
Figure 10.16: Normal stress distribution in the middle of span 4 versus the cross section height.
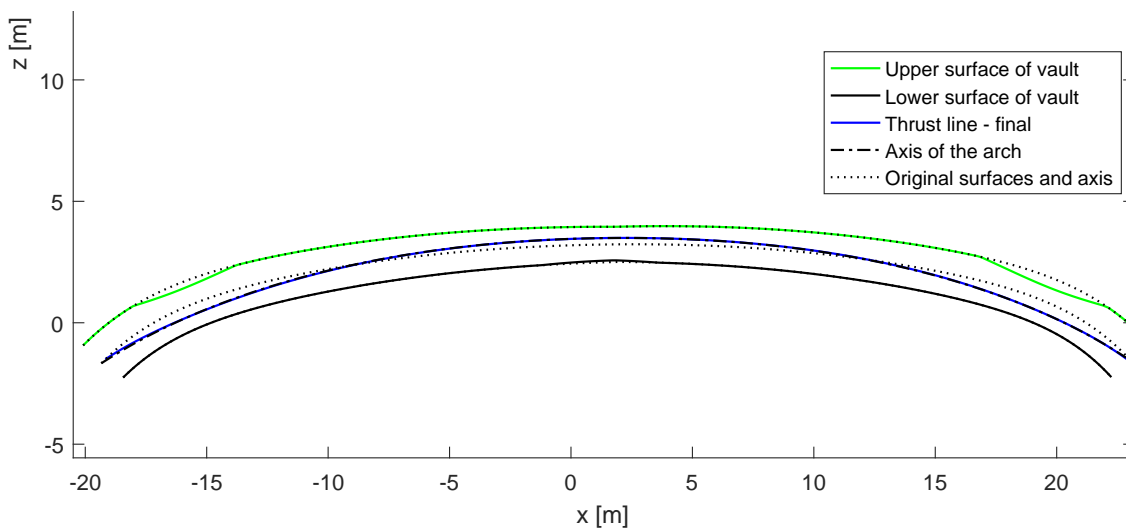
Figure 10.17: Span 4 - final shape of the vault, thrust line. The vault is loaded just with self-weight.

10.6.5 Static load test

Six vehicles of weight 31.6, 31.2, 31.7, 31.5, 31.7, 31.5 t were used for the static load test. The test was carried out according to [ÚN13a] in spans 3, 4, 5, 6. In this article, only results of span 4 are presented. The measured displacements are pretty small compared to the precision of the measurement, which is equal to 0.25 mm. Four functions of transverse vertical displacement are compared in Figure 10.21:

1. linear beam model,

2. linear solid model,

3. "non-linear beam model",

4. "non-linear solid model".

127
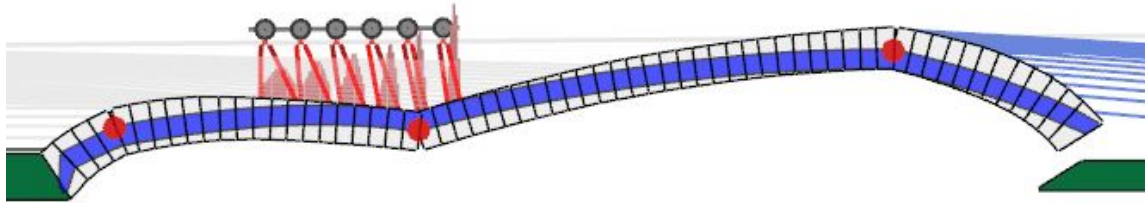
Figure 10.18: Failure mode of span 4.
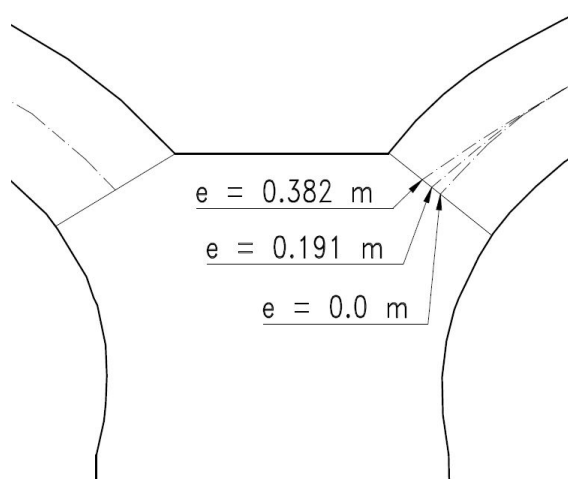
Figure 10.19: Changes in the geometry of the beam axis depending on the eccentricity of the load. The effect on resulting shear force see in Figure 10.20.

Results from the effective width calculation are not presented in the plot because it is evident that it is very conservative – the resulting displacement on the left and right edges would be zero, which is not valid. The function "non-linear beam model" and "non-linear solid model" was created by multiplying the linear result by k_{non}, which was calculated as $k_{non} = w_{non-linear}/w_{linear}$, where $w_{non-linear}$ is displacement from the 2D non-linear model loaded by self-weight and w_{linear} is displacement from the linear solid model loaded by self-weight.

The resulting "non-linear" calculated displacements are in the range of measured displacements +- preciseness (equal to 0.25 mm). The results approve the non-linear behaviour of the bridge.

10.7 Comparison of methods and discussion

10.7.1 Self-weight – the main load

In Figure 10.22 we can see the eccentricity obtained from the linear, non-linear model and the graphical solution (the archive documentation). Eccentricity from the non-linear model is higher, as expected, because tension, which is allowed in the linear model, pushes
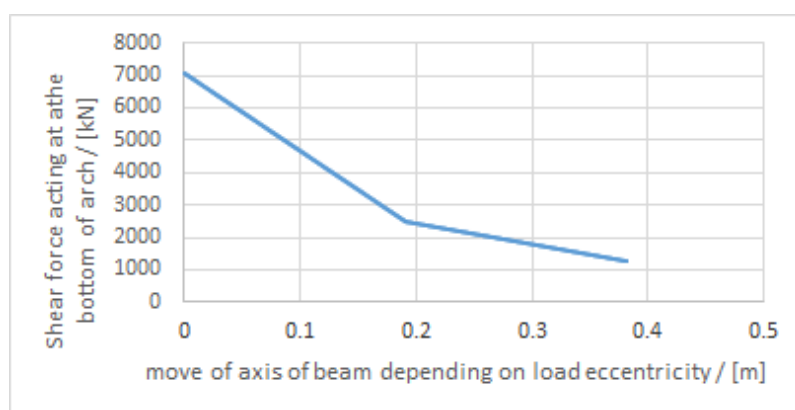
Figure 10.20: Resulting shear force depending on the eccentricity of load $e = M/N$ (in the arch springing). For the eccentricity of the load see Figure 10.19.

the resultant thrust line to the centroid of the cross section. The non-linear analysis is more time-consuming (on the engineer's effort and the computer's effort). Still, the real behaviour of the structure is better described by the non-linear model (see the behaviour of masonry in Figure 10.6). The results from the non-linear model are more non-conservative and are closer to the limit states.

10.7.2 Traffic load and its distribution in transverse direction

The load distribution in the transverse direction was compared on three models – 3D solid, 3D beam, and effective width. The result can be found in Figures 10.13, 10.14 and 10.11. The 3D linear solid model assumes linear behaviour in all directions; it, therefore, gives the most non-conservative results. The most conservative model is the effective width model because it entirely excludes part of the cross section. The real behaviour is somewhere between. The beam model gives results between the two mentioned methods; in author's opinion is, therefore, the most real. The beam model is much simpler, and the stiffness in the transverse direction can be easily changed. The real 3D solid model (which considers non-linear behaviour) is complicated with the fact that we do not know many crucial characteristics of masonry – such as bending and shear stiffness of mortar between the blocks – neither in longitudinal nor in the transverse direction. For this reason, we do not recommend the 3D solid model for the practical calculations; it is also not used for calculating the final results of LCC.

10.7.3 Final results of load carrying capacity

The final results of LCC reflect both the results of modelling the arch itself and modelling of the transverse direction. When using the effective width method, the live load is concentrated to a small strip of the arch, but in the 3D beam model all the beams carry part of the load.

The LimitState:RING in general gives non-conservative results, which was also stated, for example, in [NB17] and [Cob18]. The non-linear model is conservative because of

129
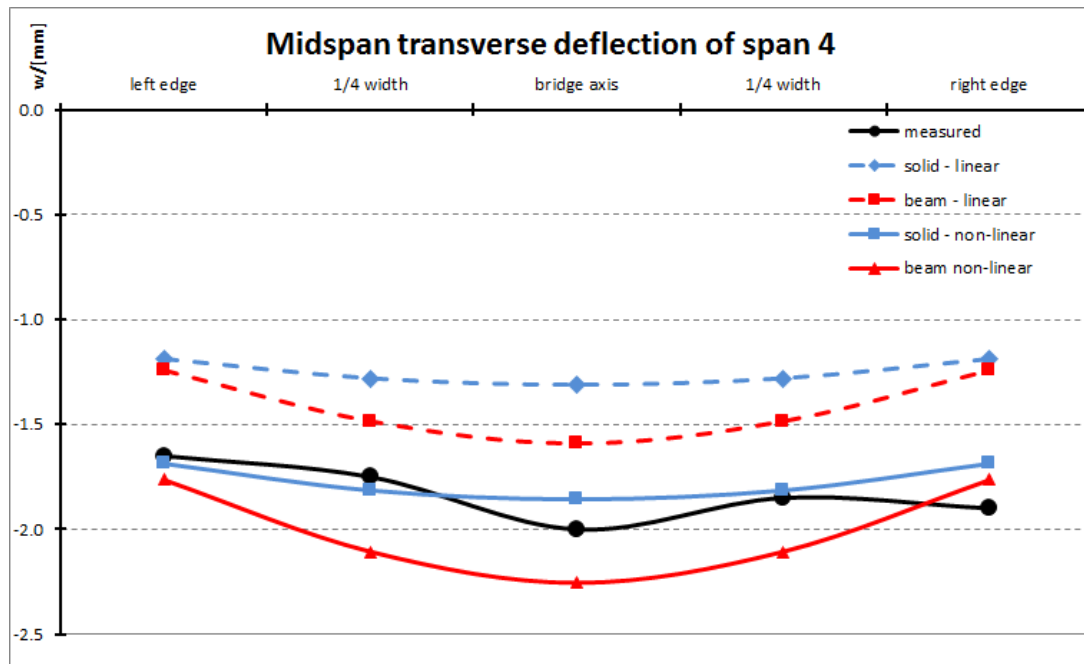
Figure 10.21: Comparison of the calculated displacements with the displacements obtained by the static load test.

Arch model	Transverse model	Vn	Vr	Ve
Linear	3D beam	21	53	104
Non-linear Midas	effective width	32	83	185
Non-linear MVo	effective width	37	92	194
LimitState:RING	effective width	46	105	182

Table 10.1: Resulting LCC

assessing the load distribution in the transverse direction. The linear model gives the most conservative results, because the thrust line is not optimized to find the highest LCC (thrust line is optimized only in the non-linear model).

10.8 Conclusion

Several models of the Legion Bridge were carried out. In the opinion of the author, the most realistic behaviour of arches describes the non-linear model, because it considers the non-linearity, which impacts the calculation the most – negligible strength in tension. The results from modelling are non-conservative in comparison to other methods. Modelling of load distribution in the transverse direction showed that the 3D solid model gives the upper bound (non-conservative), the effective width gives the lower bound (conservative results), and the 3D beam model is somewhere between, which is the most realistic behaviour. However, the use of an effective width is precise enough for small spans (spans of 90 % of stone arch bridges are less than 10 m). Still, it leads to very conservative results for such
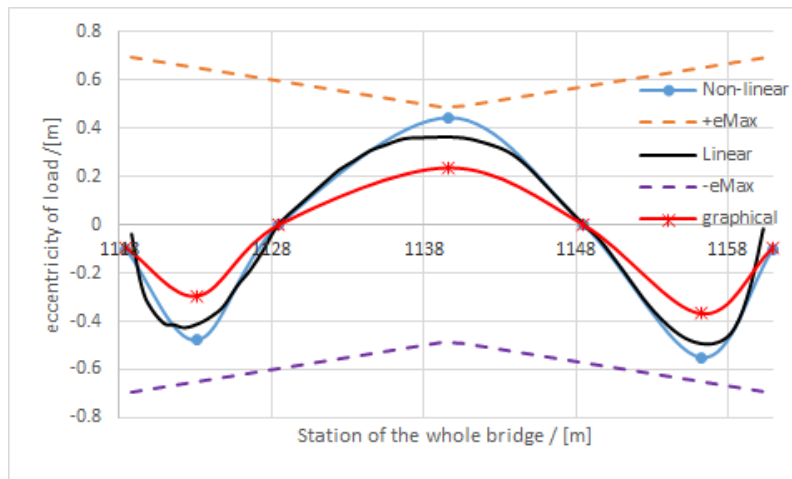
Figure 10.22: Comparison of linear, non-linear and graphical methods for span 4.

a bridge with a very large span (the span of the Legion Bridge is the largest in the Czech Republic).

Verification of shear resistance also showed the importance of considering the material non-linearity. The shear forces resulting from the linear beam model, which does not consider the non-linearity,were shown to be unreal; the structure collapsed even loaded by self-weight. When assessing the shear, we can say that the non-linear model and LimitState:RING model are in good agreement, considering that weight of models of traffic loads (Vn, Vr, Ve) is relatively small in comparison to self-weight.

131

Chapter 11

Load Carrying Capacity of Stone Arch Bridge in Karlovy Vary

The content of this chapter is mainly taken from the article [VD22b].

11.1 Introduction

The load carrying capacity (referred to as LCC) can be explained as the gross weight of a vehicle, which can pass the bridge under specific conditions. For road bridges (which is the case of the Cheb Bridge), three types of LCC are to be assessed – see [ÚN13b] and Section 10.1:

Conditions, that must be fulfilled for the masonry elements, are specified in [HD08] and [PL07]. See the equations for the check in Section 2. This chapter deals with a description and comparison of results from various computational models of vault bridges.

Throughout history, many methods have been used for the modelling of arch bridges; see Section 6.

In this chapter, the following methods described in chapter 11.3 are used:

- Linear beam model according to [Goc78] - which is the most common in practise - was enhanced to 3D,

- Non-linear 2D analysis using planar elements - the similar model was described in [BDS08],

- LimitState:RING (see below),

- Non-linear 2D analysis using beam elements – this method was proposed by [SF14] and used, for example, in [ZPTP20]. These models use a non-linear stress-strain diagram but do not consider the geometry change by the opening of the cracks. The method, which considers the geometry change due to the non-linear behaviour of the material and takes into account also the second-order effects, was introduced by [VD17] for slender columns. This concept was used for arch bridges in [VD18] for the first time. In this thesis, it is called the "MVo code".

In this thesis, the Rigid-body method is used for the verification of the ULS - ultimate limit state according to [PL07] and the non-linear analysis is used for the verification of the SLS according to [HD08]. The linear stress-strain diagram is used for the SLS; "inelastic strains are associated with permanent deformations of the arch which is allowed in the ULS design, the safety assessment of a masonry bridge at the SLS should avoid any inelastic strain to develop in the structure" [BM07]. Masonry is considered to be suitably homogenized, and the basic material of bricks and stones is considered to be isotropic according to the current standard. See the details of homogenization in Section 1.

The opening of cracks, which might occur, is modelled by an appropriate stress-strain diagram, which is in this chapter linear for the compression and zero for the tension (at the SLS check) because the joints cannot transfer tension.

The used analysis methods are simplified compared with the complicated 3D non-linear models. These simplified methods are proposed for practical verification, in which the structural engineer does not know all the input parameters of the 3D non-linear model. The real tensile strength in the structure or the real friction between the masonry arch and the fill are examples of parameters that cannot be stated by the real diagnostic survey. The same applies to the biaxial stress tests of spandrel walls – for such testing, large samples must be taken. Basically, the whole spandrel wall must be tested destructively; see the example of such a test in [FFMS19]. As an input for this calculation, destructive and non-destructive tests were carried out. See the non-destructive testing methods in [OG09] and destructive testing method in [FFMS19].

▪ 11.2 Diagnostic survey

This chapter gives a summary of the diagnostics of the bridge which was available: [ssro20].

▪ 11.2.1 Brief description, history

The bridge was constructed in 1869. It is located between the "Namesti Republiky" square and "Sokolovska" in the historic city of Karlovy Vary, Czech Republic. The span of all five arches is 17.5 m, sagitta 2.25 m ("sagitta" is also in literature referred to as "rise" of arch intrados). The width of the arch is 6.88 m; the thickness of the arch varies from 1.1 m (springing) to 0.79 m (midspan). The thickness of the spandrel walls is 0.73 m. The height of the piers is 5.5 m. See the simplified view of the longitudinal section of the bridge in Figure 11.7. At the beginning of the 20th century, the bridge was widened by a steel cantilever. In the 1980s, the corrosion of the steel structure caused a collapse of the widening. In 1986, reconstruction was done by adding reinforced concrete panels (see the cross section of the bridge in Figure 11.9). These slabs were added across the entire width and length of the bridge. The substructure is massive, made of granite blocks on a surface. The piers and abutments are filled with compact weak masonry. The foundation of the bridge is lain on wooden piles.

The diagnostic survey proved this description. Today, the bridge administrator plans to renew the bridge; the original historical arrangement of the bridge should be restored.

(a) : The mortar in the joints of the substructure is missing up to 200 mm deep.

(b) : The salt leaching and deposits on the intrados of the vault (black because of SO_4^{2-}.)

Figure 11.1: The most important defects of the bridge.

11.2.2 Detailed bridge inspection

The bridge inspection does not have a numerical output, but it is an important method of the diagnostic survey. Detailed visual inspection of the bridge can quantify defects, assess quality of materials, bring classification of structural state, and set the scope of works of the diagnostic survey. The two most severe defects can be seen in Figure 11.1a and 11.1b.

11.2.3 Core sampling

The core samples were carried out according to [ssro20]:

- Through the pier vertically (thickness of the pavement, as well as the foundation of the bridge, were investigated),

- through the abutment horizontally,

- through the arch.

See the compressive strengths, which were obtained by testing, in Table 11.1.

compressive strength of the masonry element cylinder / [MPa]	compressive strength of the mortar cylinder / [MPa]
68.5	20
75.2	15.9
63	22.1
70.4	10
59.2	
91.7	
117	
79.7	
94.1	
48.2	

Table 11.1: The compressive strength of the core samples

According to [PL07], the characteristic compressive strength should be calculated according to Equation 1.2, for the Cheb Bridge, we obtained values of:

- $\alpha_m = 0.7$ for usual mortar,

- $\beta = 0.3$ for usual mortar,

- $K_z = 0.45$ for blocks of natural stone,

- $f_b = 76.7$ MPa (mean value),

- $f_m = 17$ MPa (mean value).

The resulting masonry characteristic compressive strength f_k was 19.3 MPa. The design compressive strength was calculated according to Equation 1.3, for the case of the Cheb Bridge, the following factors were used:

- $\gamma_{M1} = 2.0$ is the basic value of safety factor, value for clay masonry elements,

- $\gamma_{M2} = 1.1$ for the level of brickwork,

- $\gamma_{M3} = 1.2$ for the considered moisture around 60 %,

- $\gamma_{M4} = 1.1$ for the case of local cracks in the stone blocks.

The final design compressive strength of masonry f_d was 6.64 MPa, which is quite a high value compared to other vault bridges in the Czech Republic.

▪ 11.2.4 Temperature, geodetic survey

The temperature of the air in the shade, arch intrados (number 2) and extrados (number 1) was measured – see the positions of temperature gauges in Figure 11.9. See the measured temperature in Figure 11.2:
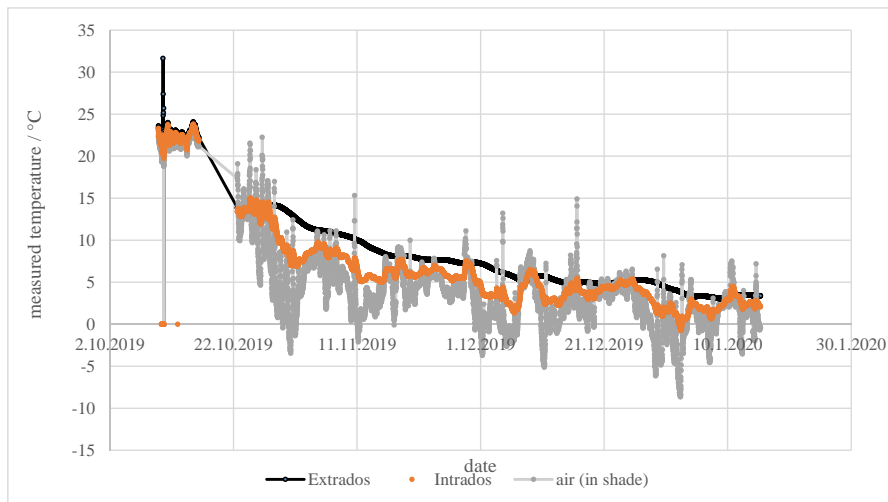
Figure 11.2: The temperature measured.

A detailed topographical survey of the whole bridge was carried out. Eight points on the bridge cornice were measured in four time periods. These points were fixed in the chosen midspans and on the support axes. Based on these measurements, which were carried out during different (and measured) air and bridge temperatures, the dependence of the bridge deformation due to a temperature change was plotted in Figure 11.3:
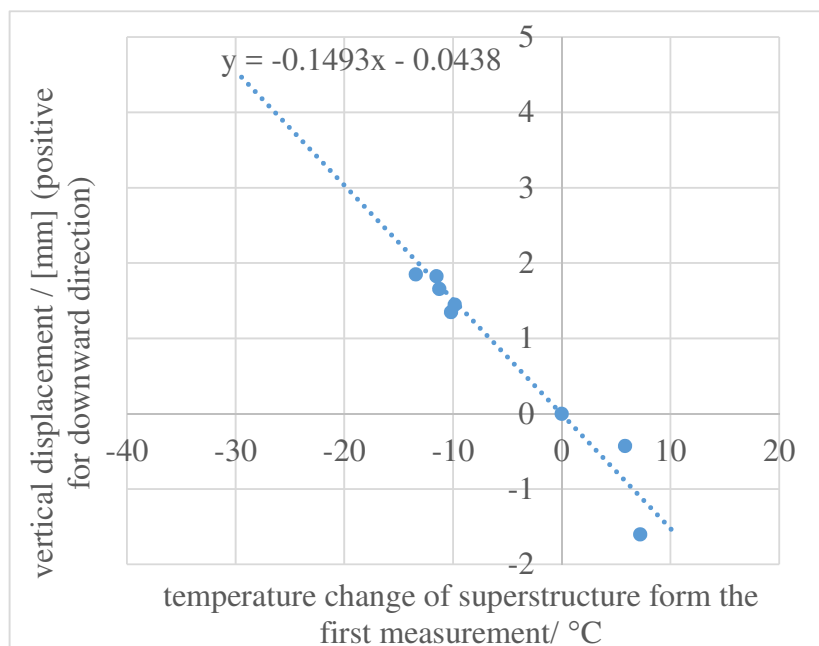
Figure 11.3: The vertical displacement of the arch top in dependence on the temperature of the superstructure.

The vertical displacement of the arch midspan was determined as the difference between the deformation of the arc top and the deformation of the pillar. For the plot, the least

square method was used. The linear function was used for the approximation due to the measurement and calculation of the Legion Bridge – see Figure 8.11 and [VD19]. In the 2D non-linear model, the coefficient of thermal expansion was determined by the previous plot; its value was 5e-06 1/°C. The change of temperature has been considered in two ways in the following models:

- Uniform temperature change – the value of the temperature change considered was taken from the measurement – the value in the middle of the cross section height, calculated as an average value from the arch extrados and intrados. The difference between extrados and intrados was not greater than 5 ° C.

- Linear temperature gradient - only the linear beam model was loaded by the linear temperature change. The value of the temperature considered was taken from the current standard because this value is larger. The period of measuring the temperature was not long enough to show the maximal temperature gradient, which can occur.

11.2.5 Modulus of elasticity

The modulus of elasticity used for granite is $E_m = 28.607$ GPa, which is the value of modulus of elasticity of granite from the experimental tests of the substructure of the Legion Bridge [VD19]. According to [oR17], the modulus of elasticity of masonry is lower due to the fact that the modulus of elasticity of granite blocks is combined with the impact of the mortar:

$$E_{cm} = 5000 + 300f_b = 24125 MPa. \tag{11.1}$$

In the case of the bridge in Karlovy Vary, the original lime mortar was supplemented (partially) with cement mortar within the reconstruction in 1986, [SSZ85]. Therefore, the following value of modulus of elasticity of masonry with the lime-cement mortar is used according to [oR17]:

$$E_{Lcm} = 0.8E_{cm} = 19300 MPa, \tag{11.2}$$

where:

- E_m – mean value of granite modulus of elasticity,
- E_{cm} – mean value of the modulus of elasticity of masonry with joints made of cement mortar,
- E_{Lcm} – mean value of the modulus of elasticity of masonry with joints made of lime-cement mortar.

11.3 Methods of modelling

One of the significant differences between all modelling methods is dealing with the backfill impact on an arch bridge. In general, the backfill impacts the bridge in several ways

described in Figure 7.8. In this section, the following methods are compared (and their ways of modelling the backfill are explained).

- Linear beam model,

- Non-linear 2D analysis using planar elements,

- LimitState:RING,

- Non-linear 2D analysis using beam elements.

The backfill properties were known from few samples; the real composition of all parts of the backfill and reinforced concrete slabs, which cover the entire bridge, is unknown and therefore also the real load dispersion is unknown. All the methods deal with this problem and in a different manner. The linear model contains the slab modelled by beam elements of real material and dimensions. The remaining methods use the effective width concept justified by the position of resultant force of live and dead loads - see Section 11.3.3. Assessing of the effective width uses a conservative idea that axle load distributes through the concrete panel and then backfill, see Figure 11.10. The concrete slab is in the concept of effective width used just as a layer with larger disperse angle.

11.3.1 Beam model with linear behaviour

The model, which represents the arch, backfill, and substructure as a beam, was created in 3D to model the transverse direction as well as the behaviour of the arch in its plane. The view of the model (longitudinal section) is shown in Figure 11.4.
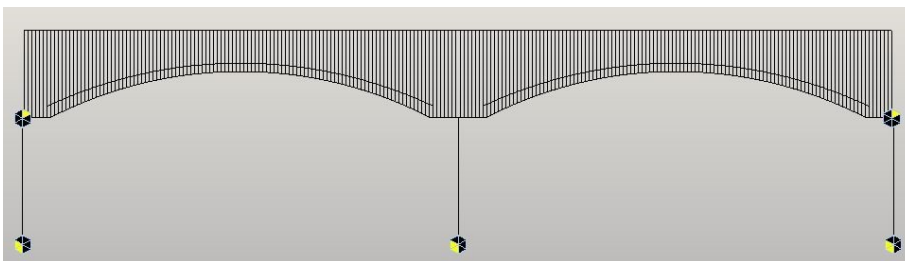
Figure 11.4: The longitudinal section of the beam model.

See the 3D model of the bridge with the real thickness of the elements in Figure 11.5.
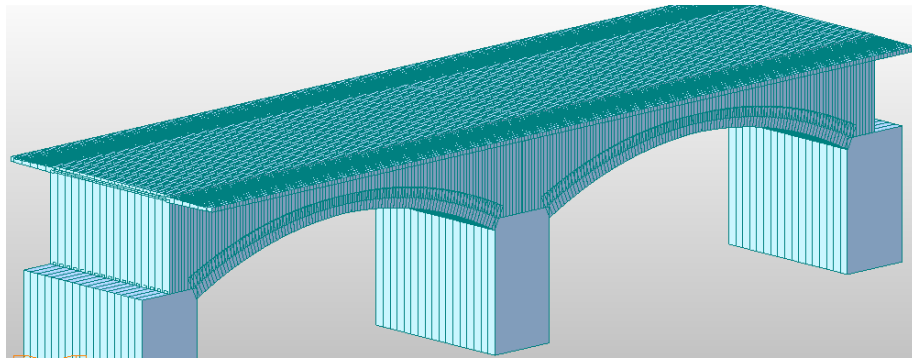
Figure 11.5: The axonometric view of the beam model.

The direction of the backfill beams limits the modelling of the backfill in this type of model. The arch is not loaded by earth horizontal pressure, which is not true. The horizontal stiffness of the backfill is also not modelled. On the other hand, the value of the horizontal pressure and backfill stiffness is much smaller than the value of the vertical one, at least for such arches of low ratio v/L.

The arch and the pier have been modelled by their axis, and they have real dimensions. All the materials are considered to behave linearly in both tension and compression. The specific weight of the masonry and the backfill was taken from the diagnostic survey, as well as the strength of the masonry. The supports are considered infinitely stiff in all models; no uneven settlement of the supports is considered. The model can be used to check the ULS and SLS; the internal forces obtained can be directly compared with the resistance of the structure.

▪ 11.3.2 2D non-linear model using plane-stress elements in program Midas

Midas software was chosen for this analysis. The non-linearity is modelled in the joints between the masonry blocks by the use of non-linear elastic links. The backfill is modelled by the elastic elements. In this way, the dispersion of the concentrated load is modelled as well as the impact of self-weight of the backfill and horizontal earth pressure. The modulus of elasticity of backfill is considered 100 MPa (was taken from the diagnostic survey – the average value), which is much smaller than the modulus of elasticity of masonry - 19.3 GPa. The found backfill soil is compacted sand with the debris. Since this 2D model was proposed for the modelling of the behaviour of the bridge in the SLS (the usual daily loading of the bridge), the structure deformations must remain small; the stresses should not exceed a certain value; excessive crushing cannot occur. Therefore, the stress-strain diagram used is zero in tension and linear for the compression. It is also justified by the verification that the acting stress is less than allowable stress. The fill is considered to be joined to the arch, especially because the SLS is checked by this model. Another approach can be seen in [GF16] where the author used contact elements at the interface between the masonry and fill with an isotropic Coulomb friction model; this allows the material to 'stick' and then 'slide' when the shear stress exceeds the limiting frictional stress. The passive earth pressure, which might act in the ULS, will not activate in the SLS. For assessing the width of the structure, the effective width was used; see the following section. See the model view

in Figure 11.6; the detail of model of similar bridge see in Fig. 10.7.
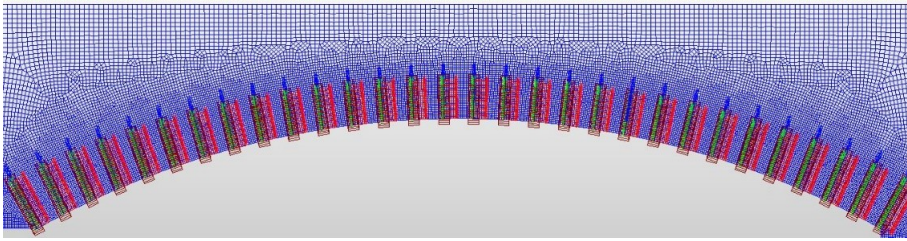
Figure 11.6: The longitudinal section of the 2D non-linear model.

The model can be used in general also for the ULS, as can be seen in [Knu17] and others. The disadvantage is that the real stress-strain diagram is hard (almost impossible) to obtain, and the current standard [PL07] does not recommend any diagram.

■ 11.3.3   2D rigid-body model using the program LimitState:RING

LimitState:RING is a program for the assessment of the LCC of a vault in the longitudinal section, including all the impacts of the backfill, such as the dispersion of a concentrated load (see in Figure 7.8 and 10.8). The method is described in Section 7.1.2. Considering the crushing always decreases the LCC. In this chapter, the value of f_d was considered (see Section 11.2.3). See the model view in Figure 11.7.
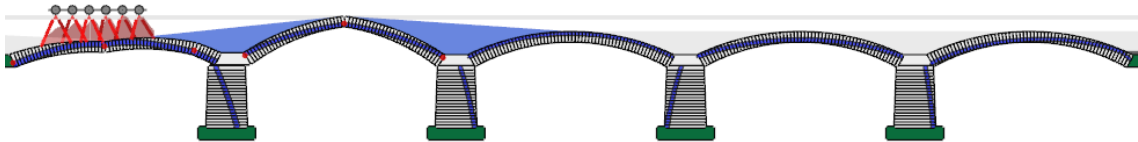
Figure 11.7: 2D model at collapse load.

The input parameters of the calculation are the following: masonry unit weight $25.9 \, \text{kN/m}^3$, backfill weight $18 \, \text{kN/m}^3$, coefficient of friction 0.4, angle of internal friction of the soil 30 °, cohesion 0 kPa, disperse angle see in Figure 11.9. This software does not handle the temperature loading.

This program and the 2D non-linear analysis assume that the width of the structure that carries the load is assessed from the effective-width calculation. It comes from the idea that in a transverse direction, the point or axle load disperses in the same way as in a longitudinal direction (see Figure 11.9). This simplified method is used in many standards. Usually, this method is applied at the arch top (where the height of the backfill is minimal), and the effective width is considered constant for the entire length of the arch (the classical model, see Figure 11.8). In the calculation, it is considered that only the effective part of the arch carries the live load. For this reason, this method of modelling the load dispersion in the transverse direction is conservative. It considers that the blocks of masonry have neither bending nor shear bearing capacity in the transverse direction.

The basic approaches to considering load spread according to [Har06], can be seen in Figure 11.8.
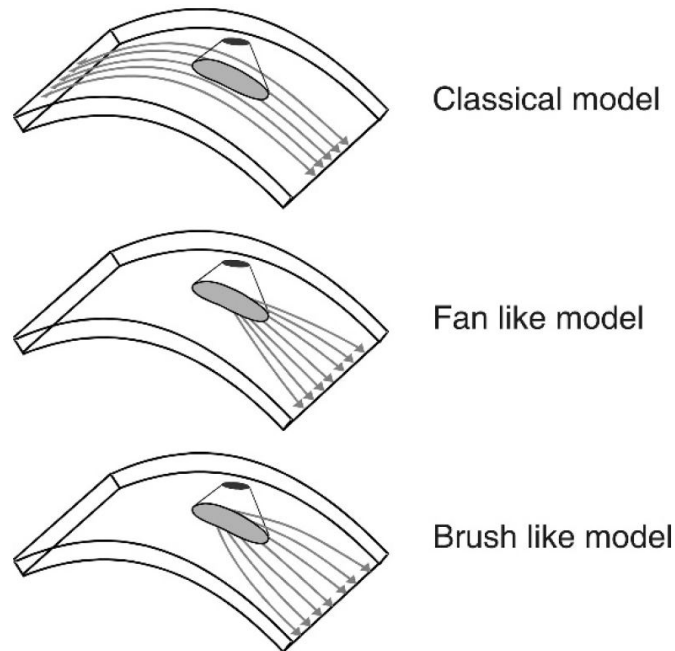
Figure 11.8: Ways of assessing the effective width.

For a determination of the effective width of the Cheb Bridge graphically see Figure 11.9 and 11.10. The "classical" model according to Figure 11.8 was used.
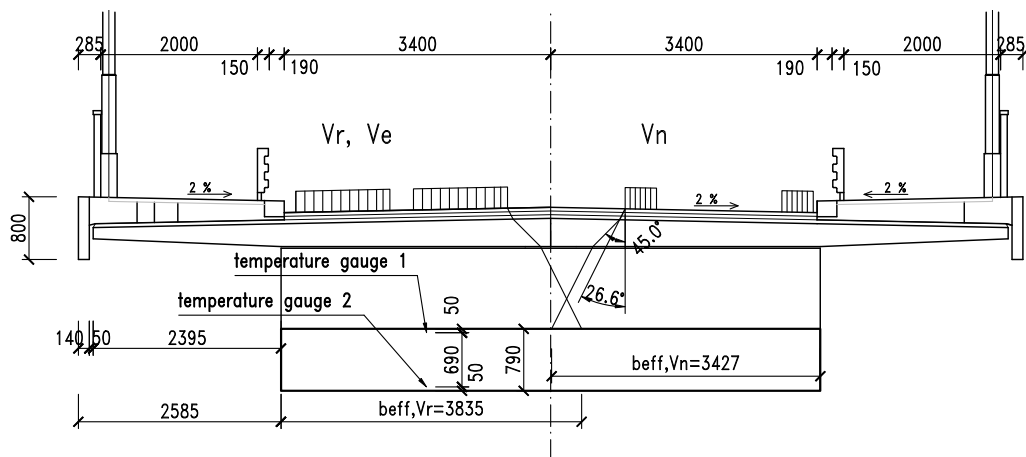
Figure 11.9: Assessing the effective width - cross section of the bridge.

To use the effective width concept, the resultant force of the live load and the dead load must be in the middle of the studied width b_{eff}. Since both the resultant force of the live load and the resultant force of the dead load of the structure have eccentricity to the axis of the effective width (and not the same), the resulting stress diagram of the studied width b_{eff} has, for example of Vn, the trapezoidal shape, see Figure 11.10.

142
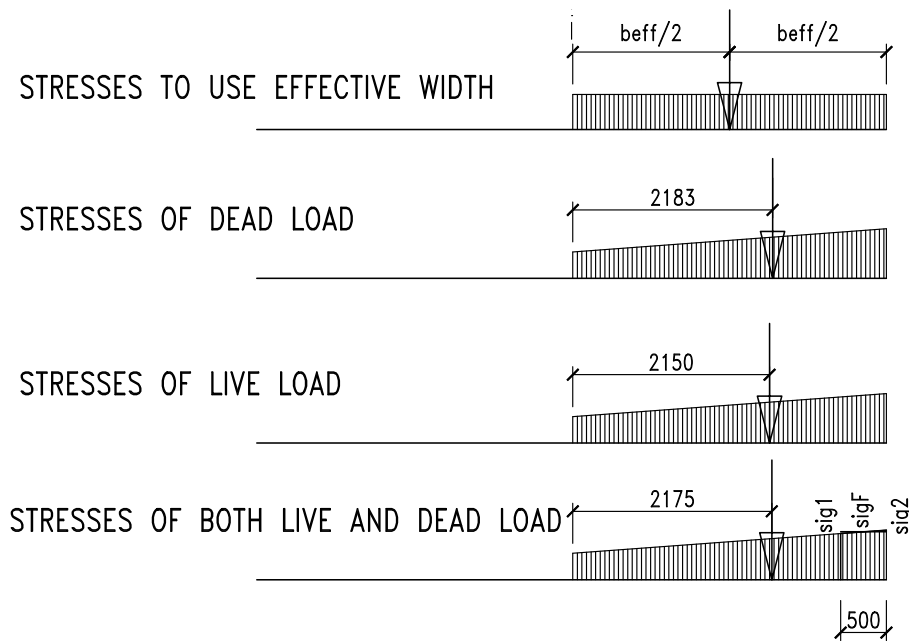
Figure 11.10: Stress diagram of the bridge cross section.

The calculation is based on the spacing of the wheels of the load model. The effective width b_{eff} considered for assessing the LCC Vn is 3.427 m, for Vr and Ve is 3.835 m, the final effective width strip was taken 0.5 m and the stress $sigF$ considered for the assessment was taken as average stress in the strip of the width 0.5 m, i.e., $sigF = (sig1 + sig2)/2$.

11.3.4 2D non-linear model using beam elements

For analysing the masonry arch bridges, the MATLAB® code was developed – the MVo code. It is described in Section 8.1.2. Compared to non-linear analysis using Midas and its plane-stress elements, the advantage of this model is that user input is less time-consuming, and the calculation is variable and versatile. In this model, the arch is represented by the beams in its axis. The number of beams, in which the arch is divided, can be chosen; usually, around 256 or 512 elements are used. The tensioned part of the cross section is excluded from the calculation, resulting in a changed geometry and stiffness of the beam.

11.4 Results of modelling

11.4.1 Linear beam model

In Figure 11.11, eccentricities of the load are compared from the linear model (shortcut "lin"). The structure is loaded by:

- sw – self-weight,
- uc – uniform temperature change – cooling,

143

- uh – uniform temperature change – heating,

- lc – linear temperature change – cooling,

- lh – linear temperature change – heating.
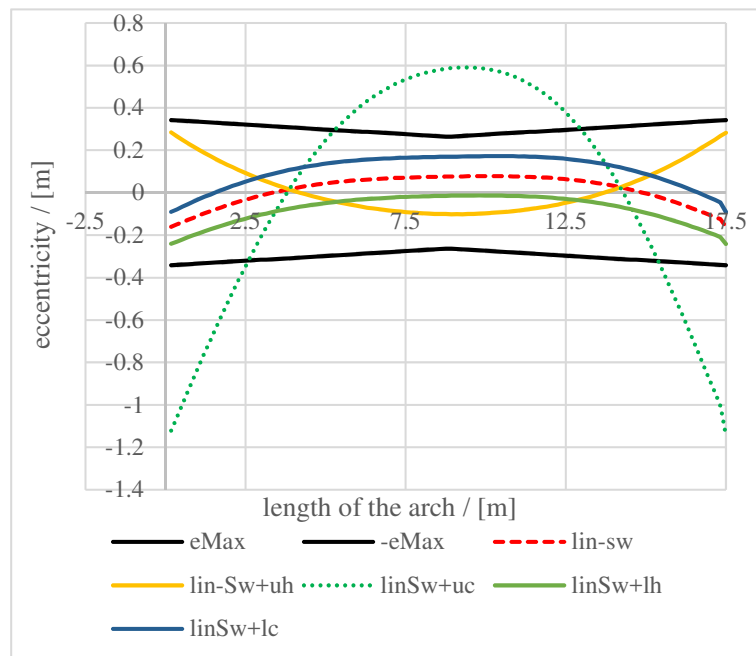
Figure 11.11: Eccentricities from the self-weight and temperature loading of a linear beam model.

See the results of the bending moments in the transverse direction in Figure 11.12.
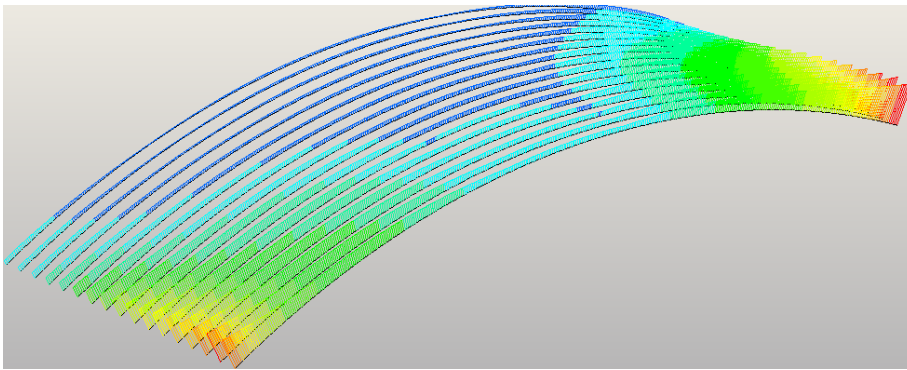
Figure 11.12: Bending moments Mmin (minimal) for the load case Vr (position of Vr is at the right edge of the bridge).

The diagram of the bending moments shows that all the strips of the vault carry some part of a live load. This fact has also been proven by the static load test of the Legion Bridge [VD19], see also Section 10.6.5.

■ 11.4.2 2D non-linear model in Midas

The stress distribution is non-linear, see Figures 11.13, 11.14a, 11.15 and 11.14b. Only at the midspan, the stress distribution is almost linear for example of self-weight load. It can be seen that at $L/4$ and springing, the stress distribution from the traffic load nearly satisfies the criterion of maximal permitted eccentricity according to Equation 2.4 (almost one-half of the cross section height is compressed), which shows the desirable shape of the arch. In combination with self-weight, the criterion of maximal eccentricity is fulfilled easily. The maximal load (LCC), for which the eccentricity of the resultant force is equal to maximal eccentricity allowed, is sought iteratively. See the LCC result comparison in Section 11.4.5.
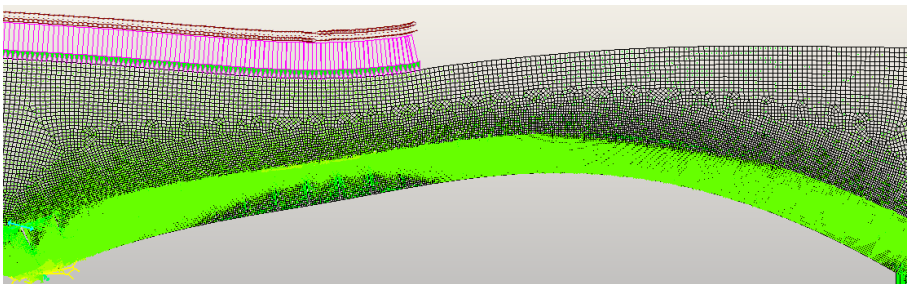
Figure 11.13: Graphical output of arch stresses – load case "tr4".

Legend – in figures, the following denotation is used:

- tr – means the traffic load alone, the maximum of the load model Vn, Vr, Ve is considered,

- N $\hat{}$ – means a non-linear combination,

145
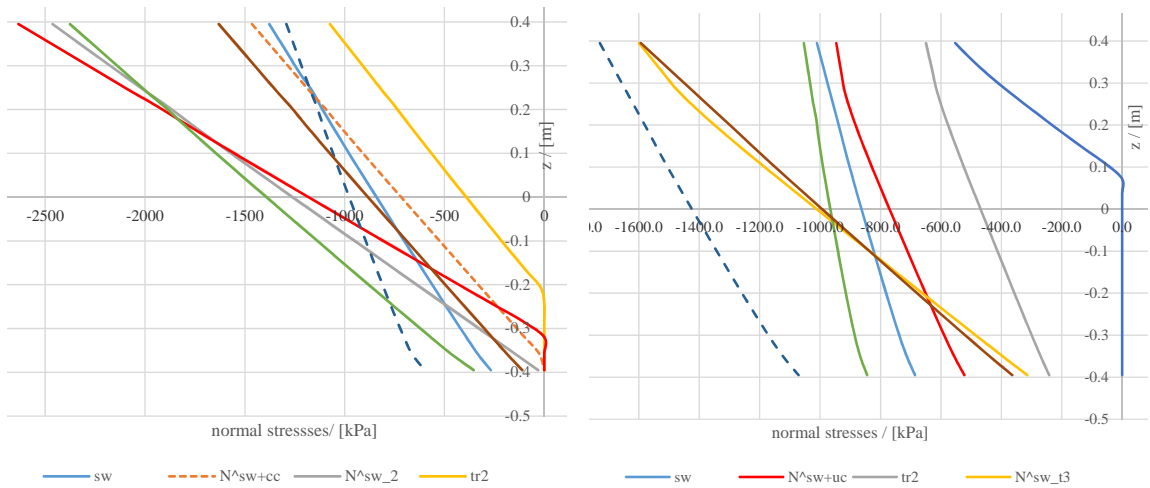
(a) : Stresses at the arch midspan.

(b) : Stress at L/4.

Figure 11.14: Resulting stress in dependence on the height of the cross section.

- uc – means uniform cooling of the structure,

- uh – means uniform heating of the structure (usually a positive effect for the stress and eccentricity),

- number means the position of moveable traffic load.

146
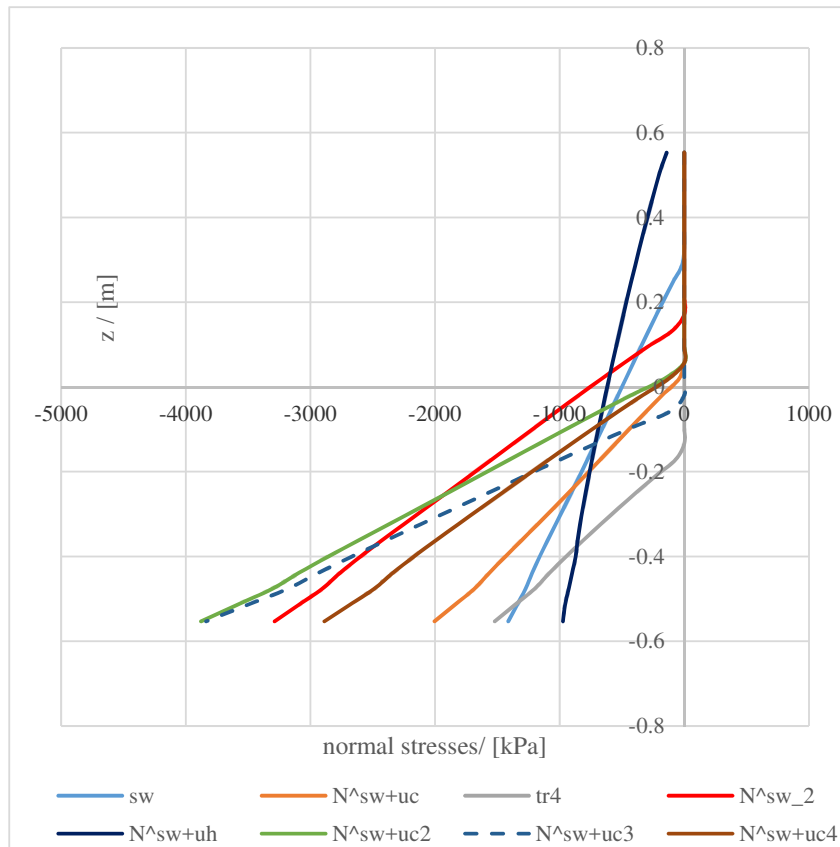
Figure 11.15: Stresses at the arch springing.

11.4.3   Results of non-linear model using beam elements

As an output of the MVo coding, internal forces and deformations are shown in Figure 11.16. The arch is loaded only by self-weight. The dash-dotted line is axis of the arch. Units are metres and it is relevant only for the axis of the arch. The blue lines representing the deformation and internal forces are illustrative; only the shape of the curve is relevant.
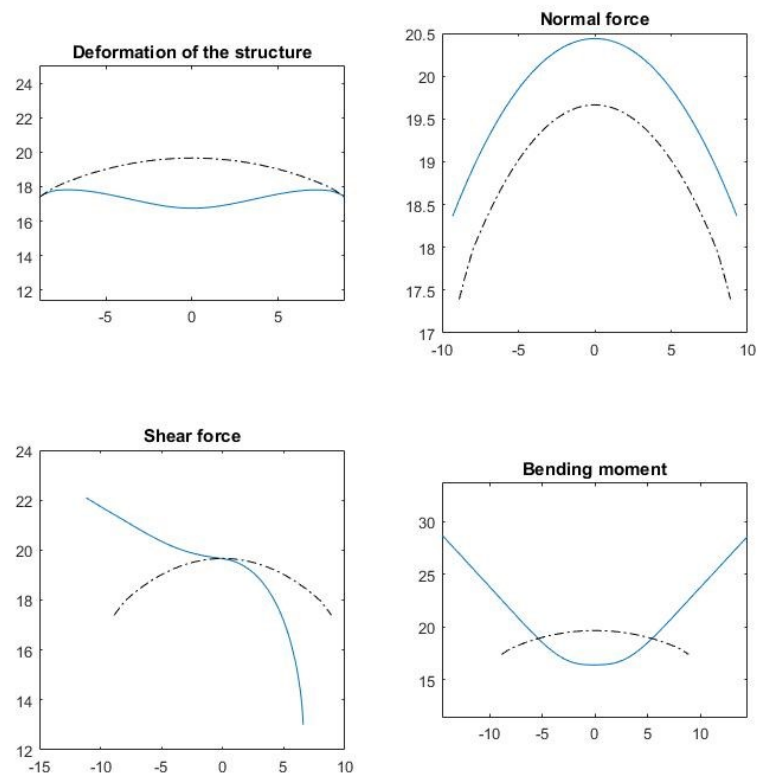
Figure 11.16: Internal forces and deformations from the MVo code.

The final shape of the cross section, which reflects the excluded tensioned parts of the cross section, was plotted in Figure 11.17:
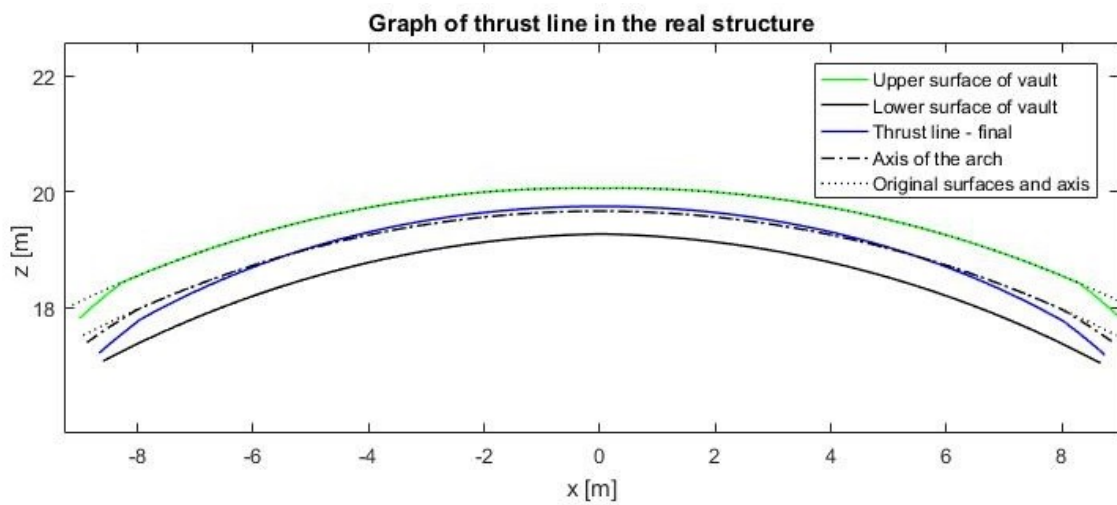
Figure 11.17: Final thrust line and shape of the arch from the MVo code.

11.4.4 Comparison of linear beam model, non-linear beam model, and 2D non-linear model

In the following plots – Figures 11.18, and 11.19 – eccentricities of the load are compared from the linear beam model (shortcut "lin"), the non-linear model in Midas (shortcut "non-linM"), and the non-linear beam model (shortcut "non-linB"). The structure is loaded by self-weight (sw), uniform temperature change – cooling (uc), and traffic load (tr). Traffic load means the maximum of load models Vn, Vr, Ve.
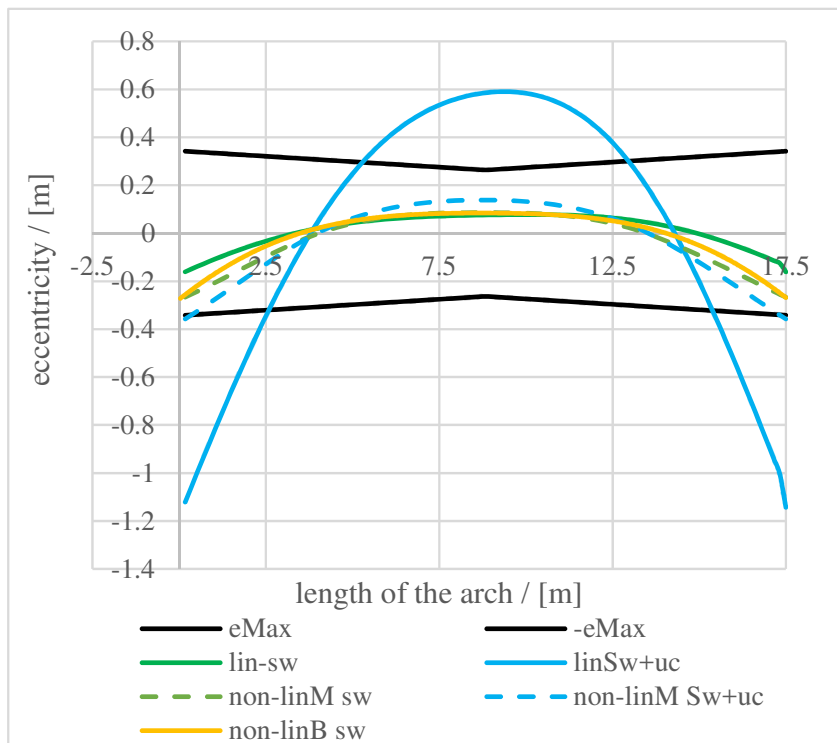
Figure 11.18: Load eccentricities from the linear and non-linear model. $eMax$ is the maximal eccentricity due to the SLS criteria.
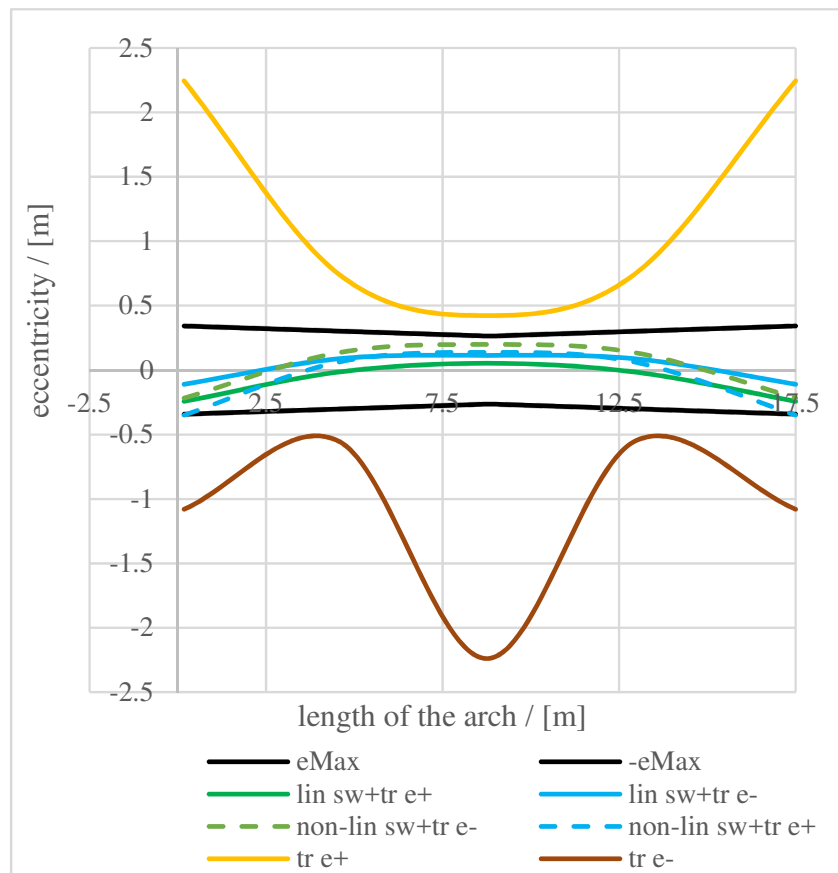
Figure 11.19: Load eccentricities from the linear and non-linear model. $e+$ means the eccentricity from the minimal negative moment, $e-$ means the maximal positive bending moment.

Even when the lower modulus of elasticity is considered, the bending moments from the temperature change from the linear model are so high that the eccentricity exceeds the SLS conditions, the eccentricity of the load is larger than half of the height of the cross section, the thrust line out of the cross section, which means a collapse of the structure; this is not true.

The maximal stress criterion is not considered; it is not decisive. The maximal ratio V/N (shear force from the load over normal force from the load) is around 0.1-0.2 from the beam model and 0.15-0.26 from the non-linear model. This shows that the criterion, that the ratio should be less than 0.4, is satisfied easily. However, the result values are quite different.

■ **11.4.5   Result summary**

The final LCC see in the table 11.2:

	Type of analysis	Vn - normal	Vr - exclusive	Ve - exceptional
1)	2D Non-linear model in Midas	41	126.0	215
2)	3D beam linear model	33	68	144
3)	2D Non-linear beam model	39	119	191
4)	LimitState:RING	69	170	217

Table 11.2: Comparison of all the methods used.

11.4.6 Discussion

The LCC from the 3D beam model was assessed by neglecting the temperature effect. Temperature loading of the linear beam model results in theoretical collapse of the structure, which does not reflect the real behaviour of the structure. Therefore, this model is not suitable for modelling of temperature load. The LimitState:RING software does not handle temperature loading, which seems to be reasonable. It was shown that the crack opening significantly decreases the temperature effects. In the collapse state, the cracks are open wide.

The behaviour of the linear beam model loaded by a traffic load and a self-weight is different from that of the 2D non-linear model. It is caused by an opening crack and changes in stiffness and geometry (mainly in the arch springing), proven by the non-linear model. This causes different bending moments in the arch midspan – higher compared to the non-linear model. Consequently, the linear model gives the lowest LCC. The thrust line is not optimised, the critical point of the arch does not move with the increasing load. This impact is not included in the linear model. Even in the linear model, the tension occurs, and the crack (joint between the blocks) should open, but it is not allowed. The linear model might be used just to assess the load distribution in the transverse direction.

In the transverse direction, the load distribution is solved in two ways – the beam model shows that all arch parts carry some part of the live load. The effective width calculation results in leaving out large parts of the vault; for the mentioned example of load position and wheel spacing of the model, around one-half of the vault was left out. These are two extreme cases; the true behaviour must be somewhere between. From all of these models, the maximal ratio V/N (shear force over normal force) is 0.26. However, the result values are quite different from the beam and the non-linear model. Since it was proven that the linear model is not suitable, the values from the non-linear are closer to the real behaviour. The ratio 0.26 is low, which shows that the arch shape is desirable.

The results of the LCC assessment obtained by the program LimitState:RING are the highest. It is used for ULS assessment. It is evident that movement of the thrust line from $H/3$, where H is the height of the cross section to $H/2$ (the maximal eccentricity in the SLS is $H/3$, collapse occurs when the thrust line reaches $H/2$), is caused by a much higher permitted traffic load. A significant increase of the LCC is also caused by the fact that after the thrust line reaches $H/2$ at one point, the hinge is created, and the loading continues until the four hinges are activated to create a moveable mechanism. That is why the LCC calculated by the program LimitState:RING is much higher than the one calculated by the other methods. In the standards, which admits the method of LimitState:RING, much higher coefficients are recommended, and then the SLS criteria must not be assessed

(see, for example, [fRB19]).

The discussed methods are used for arch bridges of a large span; many calculation methods are limited by the maximal span, which is similar to the span of the Cheb Bridge. It was shown that the methods examined, usually used for the assessment of small-span bridges, could also be used for the large-span bridges.

■ 11.4.7 **Conclusions**

The results of the modelling of the arches of the Cheb Bridge were compared. The simple, real-time methods, which can be used in practical bridge assessment, were used. The fully non-linear 3D analysis demands real tensile strength in the structure, biaxial stress diagram of masonry, and the real friction between the masonry arch and the fill, which are examples of parameters that the real diagnostic survey cannot state; these parameters are also hardly derivable from other parameters. It is also a problem of the current standards – values of these parameters, such as non-linear stress-strain diagram, are not provided and no recommendation is given. The second problem of the standard is that the ULS is verified by a fully rigid-plastic check, being an unlikely collapse mode of the Cheb Bridge, which has such a high strength of the granite blocks of the arch.

It was shown that the linear model, which is still the most used model, is not suitable for the vault modelling, especially for the assessment of longitudinal direction; the collapse caused by the usual temperature loading is not real. The model allows high tension between the masonry block, which is impossible (150 year old bridge). The linear model is the most conservative; the resulting LCC is the lowest. In the non-linear models, the cracks in the arch can open, which means a redistribution of internal forces away from the critical arch point. The iterative search for the state of cracks is how the thrust line is "optimized". Consequently, the non-linear model gives much better results and higher LCC. The non-linear model should be used. The only benefit of the 3D linear beam model is the possibility of investigation of the load distribution in the transverse direction. It shows the maximal load distribution in all arch parts; the effective width method is conservative and gives the minimal load distribution. For the practical calculations, the author of this thesis recommends using the LimitState:RING for the ULS criteria and the non-linear calculation for the SLS. For this calculation, considering the linear stress distribution for compression and neglecting the tensile strength is recommended and required by the current standard [PL07]. The LCC from the LimitState:RING is the highest; the collapse load must consume much more energy than just the opening of crack up to one-half of the cross section height, even when using a different (ULS) set of partial safety factors.

The temperature loading of the non-linear planar elements increases the pressure from the self-weight 1.7-2.7 times. The increase in the linear beam model is about 3-6 times. Therefore, the effects of the temperature loading of the linear model are about two times higher than the effect from the non-linear model. The linear model should not be used for temperature loading.

Chapter 12

Results of experiments according to [Lim20]

In appendix G of the publication [Lim20], the behaviour of vaults loaded by a force (which is close to an axle load) was investigated; 15 experiments were performed and the results of the LimitState:RING program were compared with the real collapse load. The result can be seen in the table 12.1. The ratio of the collapse load from the LimitState:RING software over the real experimental collapse load was on average 94.1 %, i.e. the real collapse load was mostly slightly higher than the collapse load by the software (when all the safety coefficients are equal to one). The agreement of the two mentioned results is very good.

experiment according to + description	sample No.	RING / mean experimental result [%]
appendix G.1 laboratory full scale	sample 1	82
	sample 2	80
	sample 3	100
appendix G.2 laboratory small scale	sample 1	93
	sample 2	94
	sample 3	96
	sample 4	104
	sample 5	95
	sample 6	103
appendix G.3 laboratory full scale	sample 1	97
	sample 2	104
appendix G.4 field test	sample 1	81
	sample 2	100
	sample 3	92
	sample 4	90

average	94.1
minimum	80
maximum	104
coefficient of variation	8.2

Table 12.1: Results of experiments.

Part V

Discussion and conclusions

A new algorithm was created for handling the slender masonry elements. It is based on a beam model with material and geometric non-linear behaviour. The code was used for calculating the bearing capacity of masonry columns and vaults.

Columns

The newly proposed method was implemented in Matlab, and a study of resistance of various columns was carried out. Then, the results of the mathematical modelling were compared with the experimental program. The behaviour of the columns in the experimental program was linear until the collapse, this behaviour fits with the computation methods; comparison of behaviour of slender masonry columns with six various stress-strain diagrams is quite similar until the collapse. The rigid-plastic model is an exception; it was stated as inappropriate (because of assumption of infinite rotation of the cross section and unreal height of the compressed area of the cross section).

The methods and results found in the literature were also considered and used for the evaluation of the new method; methods found in the literature are mostly very conservative (multiplying 2 reduction factors of requiring the whole cross section to be compressed). According to the results of methods used, it was stated that the rigid-plastic check (used, for example, in the current standard – Eurocodes) is not suitable for the slender masonry columns, especially the ones loaded in 2 planes; the rigid-plastic check is suitable only for new masonry structures with very small slenderness. The results of the loading capacity of columns obtained by the calculation according to the standards are mainly conservative.

On the basis of the previous sections, new recommendations for the assessment of columns were made: Second-order analysis should obviously be used; linear stress-strain diagram can be used for compression (tensile strength neglected). The compressed area of the cross section should be at least one-half of the total area of the cross section, even for the case of biaxial bending. The 3D effect can be neglected only if one of the bending moments M_y and M_z is much lower than the other.

Vault bridges

The results of the arch bridge modelling were compared with each other; limited comparison with experiments was also carried out. Simple, real-time methods, which can be used in practical bridge assessment, were used. The fully non-linear 3D analysis demands many parameters which are almost impossible to obtain, even with the diagnostic survey. The real tensile strength in the structure, the real stress-strain diagram, the biaxial stress diagram of the masonry, the fracture energy, and the real friction between the masonry arch and the fill are examples of parameters that the real diagnostic survey cannot state; these parameters are also hardly derivable from other parameters.

In the case study and also for the case of two assessed bridges of a large span, the LCC values from the Rigid block analysis were the highest. The Rigid block analysis (evaluating the collapse load) results are up to two times higher than the results of the MVo code (diagram linear for the compression and zero for tension used for the SLS). The reason is

that the collapse load must consume much more energy than just the opening of the crack up to one half of the cross section height, even when using a different (ULS) set of partial safety factors. A significant increase of the LCC is caused also by the fact that after the thrust line reaches $H/2$ at one point, the hinge is created, and the loading continues until the four hinges are activated to create a moveable mechanism.

The linear beam model gives the lowest LCC, and the non-linear model gives mostly values of LCC between the two above-mentioned methods.

The linear calculation gives very conservative results; LCC is usually from two to three times lower than from the non-linear model. This is because the non-linear model can change its geometry to minimize the bending moments in the critical points, and the only boundary conditions for the geometry of the arch are the extrados and intrados of the assessed arch. The iterative search for the crack state is how the thrust line is "optimized" and controlled as one of the crucial safety conditions. Consequently, the effect of redistribution of internal forces and the crack opening increases the final LCC.

Finally, it was shown that the linear model, which is still the most used model, is not suitable for vault modelling, especially for the assessment of longitudinal direction; the collapse caused by usual temperature loading is not real. When comparing the effects of temperature loading of a non-linear model of planar elements and the linear beam model, we find out that the stress of the linear model is 2-3 times higher than the non-linear model. Therefore, the linear model should not be used for modelling of temperature loading. The model allows for high tension between the masonry block, which is not possible. Loading by self-weight showed non-conservative results and loading by the axle load showed conservative results.

The experiments that were carried out to assess the behaviour of vaults loaded by a force (which is close to an axle load) until the collapse showed very good agreement with the LimitState:RING results.

Verification of shear resistance also showed the importance of considering the material non-linearity. The shear forces resulting from the linear beam model, which does not consider the non-linearity, showed to be unreal; for example elliptical structures collapse even loaded by self-weight. From the point of view of the shear, the non-linear model and the Rigid block analysis model agree well. It is also essential to know the accurate angle between the joints and the vault surface.

The coefficient of friction between blocks is not important (decisive) for circular vaults, but other shapes, especially ellipse and ogive, are very sensitive to the coefficient of friction. For example, the Eurocode significantly underestimates the value of the friction coefficient (with recommended value of $\approx 0.4/2=2$), especially the LCC of elliptic shape vaults would be very low according to the Eurocode. The value of the coefficient of friction from the literature is between 0.6 and 0.7.

Modelling of the load distribution in the transverse direction, which was compared with the static load test, showed that the 3D solid model gives an upper bound (non-conservative), the effective width gives the lower bound (conservative results), and the 3D beam model is somewhere between. Using effective width is precise enough for small spans (spans of 90 % of masonry arch bridges are lower than 10 m) but leads to very conservative results for a bridge with a very large span (30 - 40 m). The non-linear model of longitudinal direction

was in the best agreement with the result of the test.

The positive effect of spandrel walls on LCC was neglected in all models. The cracks, which occurred on all the spandrel walls of the Legion Bridge, are caused by the temperature loading. This was shown on the 3D solid linear model. The fact that the spandrel walls are cracked and their stiffness decreases rapidly is the reason for neglecting the effect of spandrel walls on LCC.

The most sensitive input parameters for the calculation of LCC are the masonry strength and the thickness of the vault. Masonry strength is important, especially for vaults of low sagitta (rise), for which the crushing of masonry can be decisive failure mode.

The modulus of elasticity, the considered change of temperature, and the coefficient of thermal expansion are three parameters, which work together on the final stresses in the structure. The final resulting stresses caused by the temperature load might be so high as to cause a collapse of the vault in case of the wrong choice of model parameters. Therefore, the parameters for the calculation are also very sensitive.

The depth of the backfill, the soil angle of internal friction, the effective width of a vault, and the shape of a vault are medium-sensitive parameters. The longitudinal slope of the backfill, the specific weight of the masonry, the specific weight of backfill, and the cohesion of the backfill are parameters, which have a low impact on the final LCC.

Comparing the sensitivity to change of the input parameter in the SLS and the ULS gives very similar results, even though the methods used were different. This comparison was provided for all key parameters, which were proven to be the most sensitive. The comparison of analysis using Scia software with 2D planar elements with the MVo results showed good agreement except for small arch spans, where the behaviour of backfill significantly affects the final LCC. The soil model used was completely different. For this reason, further study of the backfill behaviour should be conducted with advanced methods explicitly designed for soil behaviour.

The finding that the behaviour of slender masonry columns with various stress-strain diagrams is quite similar, except for the rigid-plastic model (which was stated as inappropriate) also fits for the vault bridges. Plastic check of the ULS controls normal stress in the cross section of unreal compressed area height, and it does not fit the real collapse mechanism (the collapse occurred in vast majority by forming the 4-hinges mechanism). For the practical calculations, the author of this thesis recommends using Rigid block analysis (such as LimitState:RING software) for the ULS criteria and non-linear analysis for the SLS. For SLS assessment, we recommend considering linear stress distribution for compression and neglecting the tensile strength, which is also required by the current standard. The compressed area of the cross section should be at least one-half of the total area of the cross section. Second-order analysis should be used only for the case of vault bridges with a large span and a low ratio of rise over the span length; otherwise, the second-order effects can be neglected.

It can be stated that the current standards are insufficient for assessment of slender masonry structures. The main problems are insufficient recommendation on the use of the stress-strain diagram, which is not provided, and no recommendation is given even on the topic of calculation methods. Another example is verification of the ULS by a fully rigid-plastic check, which is not valid.

Appendices

Appendix **A**

Index

163

Appendix B

Bibliography

[AB10]   A. Audenaert and J. Beke, *A comparison between 2D-models for masonry arch bridge assessment*, Proceedings of the 3rd WSEAS international conference on Engineering mechanics, structures, engineering geology, July 2010, pp. 251–256.

[AFSP08]   A. Audenaert, P. Fanning, L. Sobczak, and H. Peremans, *2-D analysis of arch bridges using an elasto-plastic material model*, Engineering Structures **30** (2008), 845–855.

[Ant95]   A. Anthoine, *Derivation of the in-plane elastic characteristics of masonry through homogenization theory*, International Journal of Solids and Structures **32** (1995), no. 2, 137–163.

[AP10]   N. Augenti and F. Parisi, *Constitutive models for tuff masonry under uniaxial compression*, Journal of Materials in Civil Engineering **22** (2010), no. 11, 113–120.

[BC10]   Z. P. Bažant and L. Cedolin, *Stability of structures; elastic, inelastic fracture and damage theories*, World Scientific Publishing Co. Pte. Ltd., 2010.

[BdFG01]   A. Brencich, U de Francesco, and L. Gambarotta, *Elastic no tensile resistant-plastic analysis of masonry arch bridges as an extension of Castiglianos method*, 9th Canadian masonry symposium (2001), 56–68.

[BDS08]   M. Betti, G. A. Drosopoulos, and G. E. Stavroulakis, *Two non-linear finite element models developed for the assessment of failure of masonry arches*, Comptes Rendus Mécanique **336** (2008), no. 1, 42 – 53, Duality, inverse problems and nonlinear problems in solid mechanics.

[BM07]   A. Brencich and R. Morbiducci, *Masonry arches: Historical rules and modern mechanics*, International Journal of Architectural Heritage **1** (2007), 165–189.

[Boe15]   I. Boem, *Enhancement of the seismic performances of historic masonry buildings through glass fiber - reinforced mortar*, Universita degli studi di Trieste, 2015.

[BRR99]   S. B. Briccoli, G. Ranocchiai, and L. Rovero, *A micromechanical model for linear homogenization of brick masonry*, Materials and Structures **32** (1999), 22–30.

[BSI05]   BSI, *5628-1:2005 Code of practice for the use of masonry, Part 1: Structural use of unreinforced masonry*, Standard, British Standards Institution, December 2005.

[CA72]   W. F. Chen and T. Atsuta, *Strength of eccentrically loaded walls*, International Journal of Solids and Structures **9** (1972), no. 10, 142–148.

[Cai57]   J. Cais, *The eccentrical loading of columns in accordance with new standards*, Inženýrské stavby **1** (1957), no. 5, 56–72.

[CMAI18]   C. M. Chisari, L. Macorini, C. Amadio, and B. Izzuddin, *Identification of mesoscale model parameters for brick-masonry*, International Journal of Solids and Structures **146** (2018), 224–240.

[Cob18]   M. Cobley, *An investigation into the variance between Archie-M and Limit-State:RING in the assessment of masonry arches*, Anglia Ruskin University, 2018.

[Das18]   B. Das, *Principles of foundation engineering*, Cengage, 2018.

[Dra13]   M. Drahorád, *Load–bearing capacity of masonry arch bridges*, International Conference Engineering Mechanics, vol. 19, Institute of Thermomechanics of the Czech Academy of Sciences, v. v. i., 2013, pp. 33–34.

[Dra14]   M. Drahorád, *The guide to use of software LimitState:Ring for employees of SŽDC*, SŽDC, 2014.

[Esh57]   J. D. Eshelby, *The determination of the elastic field of an ellipsoidal inclusion, and related problems*, Proceedings of the Royal Society of London. Series A, Mathematical and Physical Sciences, vol. 241, Royal Society, aug 1957, pp. 376–396 (21 pages).

[Fö17]   V. Förster, *Load-bearing capacity of slender unreinforced masonry compression members under biaxial bending*, Mauerwerk **21** (2017), no. 5, 320–331.

[FAT03]   T. Ford, C. Augarde, and S. Tuxford, *Modelling masonry arch bridges using commercial finite element software*, 9th International Conference on Civil and Structural Engineering Computing, September 2003, pp. 125–138.

[FF80]   R. Frisch-Fay, *Buckling of masonry pier under its own weight*, International Journal of Solids and Structures **16** (1980), no. 5, 445–450.

[FFMS19]   F. Ferretti, B. Ferracuti, C. Mazzotti, and M. Savoia, *Destructive and minor destructive tests on masonry buildings: Experimental results and comparison between shear failure criteria*, Construction and Building Materials **199** (2019), 12 – 29.

[fRB19]   Design Manual for Roads and Bridges, *CS 454 assessment of highway bridges and structures, revision 0*, Standard, Highway Structures and Bridges; Inspection and Assessment, December 2019.

[fS07]   European Committee for Standardization, *EN 1992–1–1 - Design of concrete structures*, Standard, ÚNMZ, May 2007.

[FSB17]   T. Forgács, V. Sarhosis, and K. Bagi, *Minimum thickness of semi-circular skewed masonry arches*, Engineering Structures **140** (6/2017), 317–336.

[GDE85]   E. Gazzola, R. Drysdale, and A. Essawy, *Bending of concrete masonry walls at different angles to the bed joints*, Proceedings 3 th North American Masonry Conference, Arlington, Texas, USA **27** (1985), 125–132.

[GF16]   N. Gibbons and P. J. Fanning, *Progressive cracking of masonry arch bridges*, Bridge Engineering **169** (2016), no. 2, 93 – 112.

[Gil01]   M. Gilbert, *Ring: A 2D rigid-block analysis program for masonry arch bridges*, ARCH01: 3rd International Arch Bridges Conference, January 2001, pp. 459–464.

[Gil07]   M. Gilbert, *Limit analysis applied to masonry arch bridges: State-of-the-art and recent developments*, Conference: 5th International Arch Bridges Conference, January 2007, pp. 13–28.

[GM94]   M. Gilbert and C. Melbourne, *Rigid block analysis of masonry structures*, The structural engineer **72** (1994), 356–361.

[Goc78]   R. Gocht, *Untersuchungen zum tragverhalten rekonstruierter eisenbahnge-wölbebrücken*, Hochschule für Verkehrswesen "Friedrich List" Dresden, 1978.

[Han03]   L. Z. Hansen, *Stability of masonry columns*, Danmarks tekniske universitet, 2003.

[Har06]   W. J. Harvey, *Some problems with arch bridge assessment and potential solutions*, Structural Engineer **84** (2006), 45–50.

[HD08]   V. Hrdoušek and M. Drahorád, *ČSN P 73 6213 - Design of masonry road bridges*, Standard, ÚNMZ, March 2008.

[HD17]   V. Honzík and M. Drahorád, *The behaviour of masonry columns loaded eccentrically*, Stavebnictví **1** (2017), no. 4, 31–38.

[Hey95]   J. Heyman, *The stone skeleton: Structural engineering of masonry architecture*, Cambridge University Press, 1995.

[Hey98]   J. Heyman, *Structural analysis - historical approach*, Cambridge University Press, 1998.

[HK01]   A. W. Hendry and F. M. Khalaf, *Masonry wall construction*, Spon press, USA and Canada, 2001.

[HS95]   B. Harvey and F. W. Smith, *British practice in arch bridge assessment*, Fourth international bridge engineering conference **1** (1995), 91–99.

[ifs80]   Czech institute for standardization, *ČSN 73 1101 – Design of masonry structures*, Standard, ÚNMZ, May 1980.

167

[ifs95]   Czech institute for standardization, *ČSN 73 0202 - Geometry accuracy in building. General requirements*, Standard, ÚNMZ, March 1995.

[IPI19]   Klokner Institute, Pontex, and Inset, *Diagnostics of Legion bridge*, 2019.

[Jä13]   W. Jäger, *Mauerwerk-kalender 2012, schwerpunkt: Eurocode 6*, Ernst und Sohn, 2013.

[Klo16a]   J. Klouda, *The behaviour of masonry columns loaded eccentrically, part 1 and 2*, Stavebnictví **1** (2016), no. 8, 56–72.

[Klo16b]   J. Klouda, *En 772-1 - Methods of test for masonry units, Part 1: Determination of compressive strength*, Standard, ÚNMZ, January 2016.

[Knu17]   J. Knudtsen, *Comparison of modelling approaches to analysis of masonry arch bridges*, Czech Technical University in Prague, 2017.

[KRJ07]   B. H. Kaushik, C. D. Rai, and S. K. Jain, *Stress-strain characteristics of clay brick masonry under uniaxial compression*, Journal of Materials in Civil Engineering **19** (2007), no. 9, 35–47.

[Kyu01]   L. Kyungwoo, *Post-buckling of uniform cantilever column under a combined load*, International Journal of Non-Linear Mechanics **36** (2001), no. 5, 813–816.

[Laf17]   M. Laffineur, *Optimization of a computational model for the restoration of the intrados of the Charles Bridge (Prague)*, CTU in Prague, 2017.

[Lep14]   M. Lepš, *Linear stability and theory of II. order*, Department of mechanics, vol. Mech.fsv.cvut.cz, 2014.

[Lim20]   LimitState, *LimitState:RING Manual*, Tech. report, LimitState, 2020.

[Lip98]   E. Lipanská, *Historic vaults*, El Consult, 1998.

[LLM93]   M. Papia L. La Mendola, *Stability of masonry piers under their own weight and eccentric load*, Journal of Structural Engineering ASCE **119** (1993), no. 6, 1678–1693.

[LMTZ07]   P. Lourenco, G. Milani, A. Tralli, and A. Zucchini, *Analysis of masonry structures: Review of and recent trends in homogenization techniques*, Canadian Journal of Civil Engineering **34** (2007), 1443–1457.

[Lou02]   P. Lourenco, *Computations on historic masonry structures*, Progress in Structural Engineering and Materials **4** (2002), 301 – 319.

[Lou13]   P. Lourenço, *Computational strategies for masonry structures : multi-scale modelling, dynamics, engineering applications and other challenges*, Congreso de Métodos Numéricos en Ingeniería; Bilbao, España, jun 2013.

[LSS04]   M. Lu, A. Schultz, and H. Stolarski, *Analysis of the influence of tensile strength on the stability of eccentrically compressed slender unreinforced masonry walls under lateral loads*, Journal of Structural Engineering - ASCE **130** (2004), 254–261.

[MGF14]   G. Minafo, C. Giacchino, and M. Fossetti, *M. stability analysis of clay brick masonry columns: numerical aspects and modelling strategies*, Materials and structures **1** (2014), no. 28, 102–114.

[MI11]   L. Macorini and B. Izzuddin, *A non-linear interface element for 3D mesoscale analysis of brick-masonry structures*, International Journal for Numerical Methods in Engineering **85** (2011), 1584 – 1608.

[MID19]   MIDAS, *Midas user manual*, Tech. report, MIDAS Information Technology, 2019.

[ML12]   G. Milani and P. B. Lourenco, *3D non-linear behaviour of masonry arch bridges*, Computers and Structures **110-111** (2012), 133–150.

[MLGB13] J. Milosevic, M. Lopes, A. Gago, and R. Bento, *Testing and modelling the diagonal tension strength of rubble stone masonry panels*, Engineering Structures **52** (2013), 581–591.

[MLT06]   G. Milani, P. Lourenco, and A. Tralli, *Homogenization approach for the limit analysis of out-of-plane loaded masonry walls*, Journal of Structural Engineering - ASCE **132** (2006), 202–209.

[MR75]   R. M. McMeeking and J. R. Rice, *Finite-element formulations for problems of large elastic-plastic deformation*, International Journal of Solids and Structures **11** (1975), no. 5, 601–616.

[ms13]   The masonry society, *TMS 402/ACI 530/ASCE 5 – building code requirements for masonry structures*, Standard, The masonry society, December 2013.

[MSS05]   L. Mu, A. E. Schultz, and H. K. Stolarski, *Application of the arc-length method for the stability analysis of solid unreinforced masonry walls under lateral loads*, Engineering Structures **27** (2005), no. 6, 909–919.

[Mur08]   I. Mura, *Stability of nonlinear masonry members under combined load*, Computers and Structures **86** (2008), no. 15–16, 1579–1593.

[MW10]   C. Melbourne and J. Wang, *Mechanics of MEXE method for masonry arch bridge assessment*, Proceedings of the ICE - Engineering and Computational Mechanics **163** (2010), 187–202.

[ÚN05a]   ÚNMZ, *EN 1991-2 - Traffic loads on bridges*, Standard, ÚNMZ, June 2005.

[ÚN05b]   ÚNMZ, *ČSN EN 1990 - Basis of structural design*, Standard, ÚNMZ, December 2005.

[ÚN05c]   ÚNMZ, *ČSN ISO 13822: Bases for design of structures - Assessment of existing structures*, Standard, ÚNMZ, March 2005.

[ÚN13a]   ÚNMZ, *ČSN 73 6209 – Static load tests of bridges*, Standard, ÚNMZ, March 2013.

[ÚN13b] ÚNMZ, *ČSN 73 6222 - Load bearing capacity of road bridges*, Standard, ÚNMZ, March 2013.

[ÚN14] ÚNMZ, *ČSN 73 0038: Assessment of existing structures - supplementary guidance*, Standard, ÚNMZ, December 2014.

[NB17] L. Nobile and V. Bartolomeo, *Comparison between available assessment methods of historical masonry arches*, International journal of mathematical models and methods in applied sciences **11** (2017), 61–67.

[Nem20] Nemetschek, *Scia engineer manual*, Tech. report, Scia, 2020.

[Och02] J. A. Ochsendorf, *Collapse of masonry structures*, University of Cambridge, 2002.

[OET16] R.S. Olivito, M. Esposito, and N. Totaro., *Experimental investigation for the friction evaluation in the masonry structures*, International Journal of Masonry Research and Innovation **1** (2016), no. 1, 27–47.

[OG09] Z. Orban and M. Gutermann, *Assessment of masonry arch railway bridges using non-destructive in-situ testing methods*, Engineering Structures **31** (2009), no. 10, 2287 – 2298.

[Ohl86] A. Ohler, *Zur berechnung der druckfestigkeit von mauerwerk unter berücksichtigung der mehrachsigen spannungszustände in stein und mörtel*, Bautechnik **5** (1986), 163–169.

[oR11] International Union of Railways, *UIC 778-3 - Recommendations for the inspection, assessment and maintenance of masonry arch bridges (czech version of irs 70778-3*, April 2011.

[oR17] International Union of Railways, *IRS 70778-3 - Recommendations for the inspection, assessment and maintenance of masonry arch bridges*, December 2017.

[Orb07] Z. Orban, *UIC project on assessment, inspection and maintenance of masonry arch railway bridges*, EU, 2007.

[PeD07] M. Posch, P. Řeřicha, and M. Drahorád, *Modeling of masonry arch bridges - method of determination of load capacity of masonry arch bridges*, National Conference with International Participation: Engineering mechanics, may 2007.

[PG09] D. Proske and P. Gelder, *Safety of historical stone arch bridges*, Springer, 2009.

[PL07] D. Pume and K. Lorenz, *EN 1996–1–1 - Design of masonry structures*, Standard, ÚNMZ, May 2007.

[RKR⁺19] F. Rehman, S. A. Khan, S. U. Rehman, M. S. Khan, S. Mughal, S. Ahmad, and M. A. Aman, *Finite element analysis of brick masonry*, 2nd Pak-Turk International Conference on "Emerging Technologies in the field of Sciences and Engineering", March 2019.

[RLP16] G. Ramaglia, G. P. Lignola, and A. Prota, *Collapse analysis of slender masonry barrel vaults*, Engineering Structures **117** (2016), 86–100.

[SŽ15] SŽDC, *Systematic directive for determination of load carrying capacity of bridges*, 2015.

[Sad05] M. H. Sadd, *Elasticity: Theory, applications and numerics*, Elsevier Butterworth-Heinemann, 2005.

[Sar71] M. Sargin, *Stress–strain relationship for concrete and analysis of structural concrete sections*, Cohn MZ, Solid Mechanics Division, University of Waterloo (1971), 89–101.

[SAS17] R. Serpieri, M. Albarella, and E. Sacco, *A 3D microstructured cohesive-frictional interface model and its rational calibration for the analysis of masonry panels*, International Journal of Solids and Structures **122-123** (2017), 110–127.

[SF14] S. De Santis and G. Felice, *A fibre beam-based approach for the evaluation of the seismic capacity of masonry arches*, Earthquake Engineering and Structural Dynamics **43** (2014), 112–120.

[SFL19] V. Sarhosis, T. Forgács, and J. V. Lemos, *A discrete approach for modelling backfill material in masonry arch bridges*, Computers and Structures **224** (2019), 106108.

[SMC95] C. Southcombe, I. May, and V. Chong, *The behaviour of brickwork panels with openings under lateral load*, Proc., 4 th Int. Masonry Conf. Proc. Brit. Mas. Soc., London, UK **1** (1995), 105–110.

[Som11] M. Somr, *Numerical simulation of Cocciopesto-based masonry structures*, Master thesis, 2011.

[SR84] F. Sawko and M. A. Rouf, *On the stiffness properties of masonry*, Proceedings of the Institution of Civil Engineers **77** (1984), no. 1, 1–12.

[SSF16] V. Sarhosis, S. De Santis, and G. Felice, *A review of experimental investigations and assessment methods for masonry arch bridges*, Structure and Infrastructure Engineering **12** (2016), 1439–1464.

[ssro20] Pontex, spol. s r. o., *Diagnostic survey of Cheb bridge in Karlovy Vary*, 2020.

[SSZ85] SSZ a. s., *Project of reconstruction: Rekonstrukce Chebského mostu v Karlových Varech, stupeň JP*, Standard, Stavby silnic a železnic, March 1985.

[SSZ⁺08] J. Sejnoha, M. Sejnoha, J. Zeman, J. Sykora, and J. Vorel, *Mesoscopic study on historic masonry*, Structural engineering and mechanics **30** (2008), 99–117.

[Ste12] B. Stecinsky, *Wall arches of railway bridges*, Roads and Railways **1** (2012), no. 5, 1–15.

[TB77] E. Tesfaye and T. H. Broome, *Effect of weight on stability of masonry walls*, Journal of the Structural Division ASCE **103** (1977), no. 5, 961–970.

[TG61]   S. P. Timoshenko and J.M. Gere, *Theory of elastic stability*, McGraw-Hill., 1961.

[TOB09]   A. R. Tóth, Z. Orbán, and K. Bagi, *Discrete element analysis of a stone masonry arch*, Mechanics Research Communications **36** (2009), no. 4, 469 – 480.

[VD17]   M. Vokál and M. Drahorád, *Non–linear analysis of slender masonry beam*, Sborník vědeckých prací Vysoké školy báňské–Technické univerzity Ostrava. Řada stavební **17** (2017), no. 2, 151–160 (English).

[VD18]   M. Vokál and M. Drahorád, *The load bearing capacity of railway masonry arch bridges*, Transactions of the VŠB – Technical University of Ostrava, Civil Engineering Series **18** (2018), no. 2, 14–22.

[VD19]   M. Vokál and M. Drahorád, *Legion Bridge in Prague - assessment of stone arches*, Transactions of the VŠB – Technical University of Ostrava, Civil Engineering Series **19** (2019), no. 2, 71–80.

[VD20]   M. Vokál and M. Drahorád, *Sensitivity analysis of input parameters for load carrying capacity of masonry arch bridges*, Acta polytechnica **60** (2020), no. 4, 349–358.

[VD21]   M. Vokál and M. Drahorád, *Non-linear analysis of slender masonry column subjected to biaxial bending*, Acta polytechnica **61** (2021), no. 2, 391–405.

[VD22a]   M. Vokál and M. Drahorád, *Load carrying capacity of masonry arch railway bridges at the serviceability limit state*, Acta polytechnica **61** (2022), no. 7, 780–791.

[VD22b]   M. Vokál and M. Drahorád, *Load carrying capacity of stone arch bridge in Karlovy Vary*, Acta polytechnica (hopefully 2022?), ?

[Vok17]   M. Vokál, *Non-linear analysis of slender masonry column*, PhD workshop, vol. 8, 2017, pp. 48–50.

[Vok18]   M. Vokáč, *The graphical solution of thrust line of a vault*, Česká technika, 2018.

[Web99]   W. K. Weber, *Die gewölbte eisenbahnbrücke mit einer Öffnung. begriffserklärungen, analytische fassung der umrisslinien und ein erweitertes hybridverfahren zur berechnung der oberen schranke ihrer grenztragfähigkeit, validiert durch einen großversuch*, Lehrstuhl für Massivbau der Technischen Universität München, 1999.

[WHM13]   J. Wang, B. J. Haynes, and C. Melbourne, *Comparison between the MEXE and Pippard's methods of assessing the load carrying capacity of masonry arch bridges*, 7-th International Conference on Arch Bridges **7** (2013), 53–68.

[Yok71]   F. Y. Yokel, *Stability and load capacity of members with no tensile strength*, Journal of the Structural Division **99** (1971), 788–789.

[ZNSS08]   J. Zeman, J. Novak, M. Sejnoha, and J. Sejnoha, *Pragmatic multi-scale and multi-physics analysis of Charles Bridge in Prague*, Engineering Structures **30** (2008), 3365–3376.

[ZPTP20]   P. Zampieri, S. Perboni, C. Tetougueni, and C. Pellegrino, *Different approaches to assess the seismic capacity of masonry bridges by non-linear static analysis*, Frontiers in Built Environment **6** (2020), 124–134.

Zápis o ODBORNÉ ROZPRAVĚ
v rámci studijního bloku doktorského studia

Doktorand: MAREK VOKÁL   Datum konání rozpravy: 18.1.2018

Studijní obor: KONSTRUKCE A DOPRAVNÍ STAVBY

Název odborné studie: NELINEÁRNÍ ANALÝZA ŠTÍHLÝCH ZDĚNÝCH KONSTRUKCÍ

Složení komise: předseda komise* (nesmí být školitel) VLADIMÍR KŘÍSTEK

vedoucí školicího pracoviště   ALENA KOHOUTKOVÁ

školitel   ALENA KOHOUTKOVÁ

školitel specialista (pokud je stanoven)

oponent   IVA BROUKALOVÁ

případní další členové   MICHAL DRAHORÁD

Výsledek odborné rozpravy:

☒ SOUHLAS se závěry odborné studie a pokračováním studia

☐ NESOUHLAS se závěry studie s povinností jejího přepracování

Zdůvodnění:

Termín opakované rozpravy:

Definitivní téma disertační práce:

NELINEÁRNÍ ANALÝZA ŠTÍHLÝCH ZDĚNÝCH KONSTRUKČNÍCH PRVKŮ

Podpis předsedy komise:

Podpisy členů komise:

---

* zpravidla předseda ORO, nebo jím jmenovaný předsedající ze členů ORO

Pozn. *Předseda komise zajistí doručení tohoto zápisu včetně posudku oponenta na oddělení VaV nejpozději sedmý den po konání rozpravy*